A Simple and Versatile Pathway for the Synthesis of Visible Light Photoreactive Nanoparticles

Peer-reviewed author version

Delafresnaye, Laura; ZAQUEN, Neomy; Kuchel, Rhiannon P.; Blinco, James P.; Zetterlund, Per B. & Barner-Kowollik, Christopher (2018) A Simple and Versatile Pathway for the Synthesis of Visible Light Photoreactive Nanoparticles. In: ADVANCED FUNCTIONAL MATERIALS, 28(23) (Art N° 1800342).

DOI: 10.1002/adfm.201800342
Handle: http://hdl.handle.net/1942/26164

Advanced Functional Materials

A Simple and Versatile Pathway for the Synthesis of Visible Light Photoreactive Nanoparticles

--Manuscript Draft--

Manuscript Number:	adfm.201800342R1
Full Title:	A Simple and Versatile Pathway for the Synthesis of Visible Light Photoreactive Nanoparticles
Article Type:	Full Paper
Section/Category:	
Keywords:	Miniemulsion; Tetrazole Driven Photochemistry; Profluorescent Particles; Visible Light Ligation; Biomolecule Tagging
Corresponding Author:	Christopher Barner-Kowollik, Prof. Queensland University of Technology (QUT) Brisbane, AUSTRALIA
Additional Information:	
Question	**Response**
Please submit a plain text version of your cover letter here. **If you are submitting a revision of your manuscript, please do not overwrite your original cover letter. There is an opportunity for you to provide your responses to the reviewers later; please do not add them here**.	Dear Dr. Ritterbusch, Thank you very much for sending us the reviewers' comments on the above manuscript. Our detailed point-by-point reply as well as the revised version of the manuscript is attached. I look forward to hearing from you. Kindest regards from Brisbane Christopher Barner-Kowollik
Do you or any of your co-authors have a conflict of interest to declare?	No. The authors declare no conflict of interest.
Corresponding Author Secondary Information:	
Corresponding Author's Institution:	Queensland University of Technology (QUT)
Corresponding Author's Secondary Institution:	
First Author:	Laura Delafresnaye, Dr.
First Author Secondary Information:	
Order of Authors:	Laura Delafresnaye, Dr.
	Neomy Zaquen, Dr.
	Rhiannon Kuchel, Dr.
	James Blinco, Dr.
	Per Zetterlund, Prof.
	Christopher Barner-Kowollik, Prof.
Order of Authors Secondary Information:	
Abstract:	We herein pioneer the design of visible and UV-B light reactive nanoparticles via radical polymerization in aqueous heterogeneous media based on methyl methacrylate (MMA) and unique acrylates bearing tetrazole functionalities in a simple and straightforward two step reaction. Stable colloidal nanoparticles with an average diameter of 150 nm and inherent tetrazole functionality (varying from 2.5 to 10 wt.% relative to MMA) were prepared via one-pot miniemulsion polymerization. In a

	subsequent step, fluorescent pyrazoline moieties serving as linkage points were generated on the nanoparticles by either photo-induced nitrile imine-mediated tetrazole-ene cycloaddition (NITEC) or nitrile imine carboxylic acid ligation (NICAL) in water, thus enabling the particles as fluorescent tracers. Through in-depth molecular surface analysis, we demonstrate that the photoreactive nanoparticles undergo ligation to a variety of substrates bearing functionalities including maleimides, acrylates or carboxylic acids, illustrating the versatility of the particle modification process. Critically, the unique ability of the photo-reactive nanoparticles to be activated with visible light allows for their decoration with UV light sensitive molecules. Herein, we exemplify the ligation of folic acid - a vitamin prone to degradation under UV light - to the photoreactive nanoparticles using visible light, demonstrating the synthetic power of our photoreactive fluorescent nanoparticle platform technology.

WILEY-VCH

DOI: 10.1002/ ((please add manuscript number))
Article type: Full Paper

A Simple and Versatile Pathway for the Synthesis of Visible Light Photoreactive Nanoparticles

Laura Delafresnaye, Neomy Zaquen, Rhiannon P. Kuchel, James P. Blinco, Per B. Zetterlund and Christopher Barner-Kowollik**

Dr. L. Delafresnaye, Dr. J. P. Blinco, Prof. Dr. C. Barner-Kowollik
School of Chemistry, Physics and Mechanical Engineering, Queensland University of Technolog (QUT), 2 George St, Brisbane, QLD 4000, Australia.
Email: christopher.barnerkowollik@qut.edu.au

Dr. N. Zaquen, Prof. P. B. Zetterlund
Centre for Advanced Macromolecular Design, School of Chemical Engineering, The University of New South Wales, High Street Gate 2, 2033 Kensington, Sydney, NSW Australia.
Email: p.zetterlund@unsw.edu.au

Dr. R. Kuchel
Electron Microscope Unit
The University of New South Wales, High Street Gate 2, 2033 Kensington,
Sydney, NSW Australia.

Dr. N. Zaquen
Australian Centre for Nanomedicine, The University of New South Wales, High Street Gate 2, 2033 Kensington, Sydney, NSW Australia.
Polymer Reaction Design Group, Institute for Materials Research (IMO-IMOMEC), Universiteit Hasselt, Agoralaan Building D, B-3590 Diepenbeek, Belgium.

Prof. Dr. C. Barner-Kowollik, Dr. J. P. Blinco
Macromolecular Architectures, Institut für Technische Chemie und Polymerchemie, Karlsruhe Institute of Technology (KIT), Engesserstr. 18, 76131 Karlsruhe, Germany.
Institut für Biologische Grenzflächen, Karlsruhe Institute of Technology (KIT), Hermann-von-Helmholtz-Platz 1, 76344 Eggenstein-Leopoldshafen, Germany.

Keywords: Miniemulsion, Tetrazole Driven Photochemistry, Profluorescent Particles, Visible Light Ligation, Biomolecule Tagging

Abstract

We herein pioneer the design of visible (415 nm) and UV-B light (300 nm) reactive nanoparticles via radical polymerization in aqueous heterogeneous media based on methyl methacrylate (MMA) and unique acrylates bearing tetrazole functionalities in a simple and straightforward two step reaction. Stable colloidal nanoparticles with an average diameter of 150 nm and inherent tetrazole functionality (varying from 2.5 to 10 wt.% relative to MMA) were prepared via one-pot miniemulsion polymerization. In a subsequent step, fluorescent pyrazoline moieties serving as linkage points were generated on the nanoparticles by either photo-induced nitrile imine-mediated tetrazole-ene cycloaddition (NITEC) or nitrile imine carboxylic acid ligation (NICAL) in water, thus enabling the particles as fluorescent tracers. Through in-depth molecular surface analysis, we demonstrate that the photoreactive nanoparticles undergo ligation to a variety of substrates bearing functionalities including maleimides, acrylates or carboxylic acids, illustrating the versatility of the particle modification process. Critically, the unique ability of the photo-reactive nanoparticles to be activated with visible light allows for their decoration with UV light sensitive molecules. Herein, we exemplify the ligation of folic acid – a vitamin prone to degradation under UV light – to the photoreactive nanoparticles using visible light, demonstrating the synthetic power of our photoreactive fluorescent nanoparticle platform technology.

1. Introduction

The demand for polymeric nanoparticles (PNPs) has recently seen rapid growth due to their extensive use in biomedical applications, mostly as imaging agents.[1] The fate of PNPs in organisms is usually visualised by fluorescent markers, which can be encapsulated, coated/grafted on the PNPs surface or even integrated within the polymer nanoparticle. Significant efforts have been directed to improve current fluorescent-based materials.[2-4] Substantial advances have also been made in the area of inorganic semiconductor nanoparticles,

known as quantum dots (QD), the use of fluorescent dyes as well as conjugated polymers.[5-10] Although promising at first, QDs still show signs of cytotoxicity, even though significant efforts to reduce their toxicity through encapsulation or surface modification have been made. The use of organic fluorescent dyes is an alternative approach to impart fluorescence onto a particle system, however, most current generation dyes undergo photo-bleaching over time.[11] The use of conjugated materials is an attractive tool to design inherently fluorescent nanoparticles, but the synthesis process is tedious and can be time consuming.[12, 13]

Light-driven processes have received significant attention due to their spatial-, temporal- and energy-gated nature,[14-16] making them powerful tools for surface modification on 2D and 3D substrates,[17] biomedicine,[18] drug release,[19, 20] or even photocontrol of biological systems.[21] Light thus constitutes a versatile – and mild – means for polymer formation, surface modification, precision bond cleavage, (de)protection or cross-linking reactions.[22-25] Light-driven reactions for the surface functionalization of PNPs are attractive, yet some issues remain. A key challenge is the inherent optical opacity of the PNPs in suspension, which reduces the penetration depth of the light. The nature and size of the colloidal particles as well as the irradiation conditions influence the reaction efficiency as well as the spatio-temporal precision. Our team jointly with the Bowman group functionalized polymeric microparticles with an average diameter of 4.1 µm in a methanol/THF mixture via nitrile imine mediated tetrazole-ene cycloaddition (NITEC) under UV light.[26] Using either UV[27] or visible[28] light, tetrazoles form nitrile imines, which are highly reactive 1,3-dipoles capable of ligating a vast array of dipolarophile moieties (*e.g.* alkene, acids, thiols, alcohols). Critically, tetrazoles are profluorescent entities, affording highly fluorescent species, *e.g.* pyrazolines upon reaction with alkenes. The mild reaction conditions, absence of catalysts and the resulting broad (visible light) fluorescence makes the NITEC reaction a versatile synthetic tool.[29, 30] Interestingly, only a limited number of studies report the surface functionalization of PNPs by photochemical processes in water. Recently, the UV light-induced folding of water-soluble single chain

nanoparticles (SCNPs) in water has been reported by our team.[31] Fluorescent SCNPs smaller than 5 nm were synthesized via NITEC or nitrile imine mediated carboxylic acid ligation (NICAL) reactions. Herein, we introduce a simple, powerful and rapid method for the preparation of *inherently* photoreactive nanoparticles in the important 100-200 nm range using two tetrazole-based ligation chemistries (NITEC and NICAL) in water. Our SCNP platform technology thus enables the generation of functional fluorescent PNPs, decorated with a wide range of ene and carboxylic acid species. Importantly, we broaden the scope of fluorescent PNPs to biological applications by designing visible light reactive nanoparticles, as many substances – such as proteins or other biological molecules – are sensitive to high energy, UV-light and tend to degrade under irradiation.

The main scaffold for our light reactive PNPs is poly(methyl methacrylate) (PMMA), a well-studied polymer that has been used in a wide range of fields and is routinely employed in the (mini)emulsion realm.[32] Thus, tetrazole-functional monomers were copolymerized with MMA for the aqueous miniemulsion based synthesis of the UV and visible light reactive nanoparticles. Initially, random copolymers consisting of MMA and tetrazole-based acrylates were synthesized via radical polymerization in aqueous miniemulsion in which the tetrazole monomer (UV or visible light) as well as its content (2.5 to 10 wt% relative to MMA) were varied. Subsequently, post-modification with functional variable ene and acid substrates of the random copolymer based nanoparticles via NITEC or NICAL resulted in functional fluorescent PNPs.

2. Results and Discussion

2.1. Miniemulsion polymerization

We base our photoreactive nanoparticles on two new tetrazole (Tz) monomers: one capable of UV light-induced cycloaddition (abbr. **Tz-UV**, **Figure 1**, methoxy phenyl moiety) and the second one able to undergo a visible light-induced cycloaddition (abbr. **Tz-Vis**, pyrene moiety).

Both were synthesized according to literature procedures for the tetrazole entities (refer to Figure S1 to Figure S9) leading to the UV reactive Tz-UV[33] and visible light reactive Tz-Vis[28, 34] monomers, respectively.

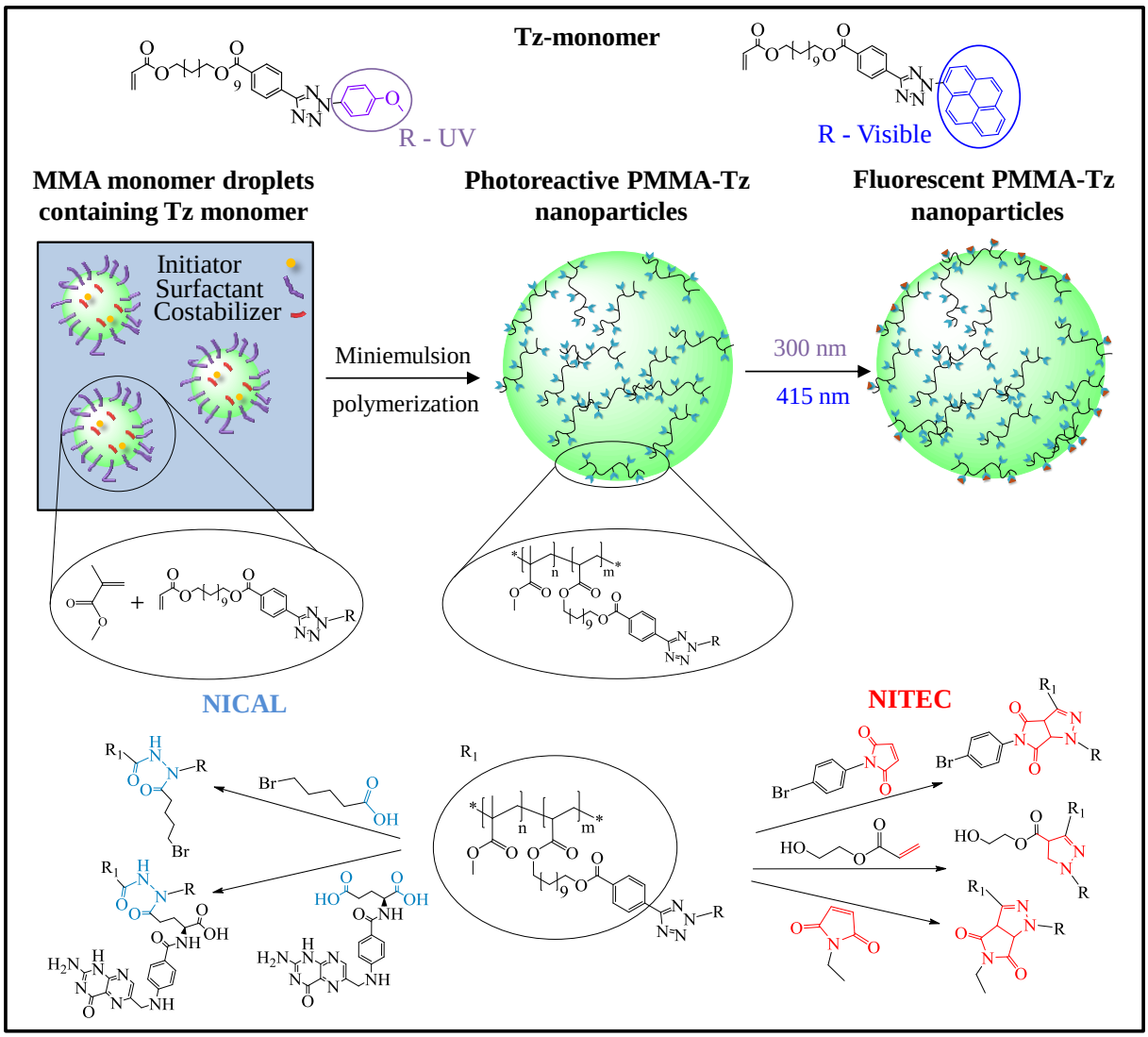

Figure 1. Synthetic route for the formation of fluorescent PMMA-Tz nanoparticles via a miniemulsion approach, affording both visible and UV light reactive PMMA-Tz nanoparticles.

The miniemulsions were generated by ultrasonication of a mixture of the oil and water phases. In order to confirm that the Tz-monomers were able to withstand this treatment, each monomer was dissolved in a THF/MeOH mixture (3/2 v/v%; *i.e.* a homogeneous system) and subjected to high shear energy via ultrasonication (amplitude of 50 % for 10 min) following the same protocol as that used for generation of miniemulsions. Electrospray Ionization Mass Spectrometry (ESI-MS; Figure S12, Figure S27, Table S1, Table S8) and ^{1}H NMR (Figure S13

and Figure S28) clearly demonstrate the stability of both **Tz-UV** and **Tz-Vis** towards high shear energy forces.

As noted above, MMA was selected as co-monomer for the synthesis of photoreactive nanoparticles. A variety of random copolymers – featuring a tetrazole monomer content varying from 2.5 wt% (abbreviated with **UV1** / **Vis1** in **Table 1** respectively), 5.0 wt % (abbreviated with **UV2** / **Vis2** in Table 1 respectively), 7.5 wt% (abbreviated with **UV3** / **Vis3** in Table 1 respectively) up to 10 wt% (abbreviated with **UV4** / **Vis4** in Table 1 respectively) relative to the MMA content – were synthesized via radical polymerization in miniemulsion targeting a 10 wt% solids content (abbreviated PMMA-Tz, refer to Figure 1). Pure PMMA nanoparticles were also synthesized to function as control substrates, which all analysis of the PMMA-Tz nanoparticles are compared to. 1,2-Dichloroethane (11 wt% rel. to MMA) was used to solubilize the tetrazole moiety in the dispersed phase since the Tz-monomers have limited solubility in the MMA/hexadecane mixture.

Table 1. Miniemulsion polymerization recipes with varying Tz contents

Dispersed Phase	Continuous Phase	Control	UV1/Vis1	UV2/Vis2	UV3/Vis3	UV4/Vis4
		Amount in gram				
MMA[a]		0.9	0.9	0.9	0.9	0.9
Tetrazole[b]		0	0.0225	0.045	0.0675	0.09
Hexadecane[c]		0.072	0.072	0.072	0.072	0.072
1,2-Dichloroethane[d]		0.1	0.1	0.1	0.1	0.1
AIBN[e]		0.00018	0.00018	0.00018	0.00019	0.00019
	Water	10	10	10	10	10
	SDS[f]	0.086	0.088	0.089	0.091	0.093

[a] 9 wt% relative to water; [b] 2.5 wt% to 10 wt% relative to monomer; [c] 8 wt% relative to monomer; [d] 11 wt% relative to MMA
[e] total concentration of 0.01 mol L^{-1} relative to the organic phase; [f] 8 wt% relative to the organic phase

After stirring both the continuous and dispersed phases separately, the dispersed phase was added to the continuous phase and successful droplet formation took place by exposing the coarse emulsion to ultrasonication (Table S2 and Table S9). Subsequently, polymerization at 70 °C for 24 h led to the successful formation of PMMA-Tz particles. In order for the droplet volume to not contract due to partitioning effects, 1,2-dichloroethane saturated water was used

for measuring the droplet diameter.[32] Dynamic light scattering (DLS) (Figure S14, Figure S29, Table S3 and Table S10) demonstrates the presence of droplets and particles in the nanometer range, with a $Z_{average}$ between 115 nm and 167 nm and a polydispersity (*PDI* < 0.4 depending on the amount of Tz monomer added) for the PMMA-Tz PNPs. No clear correlation between the particle size and the amount of Tz monomer was observed. These results are confirmed by visualizing the PNPs by transmission electron microscopy (TEM; **Figure 2,** Figure S23). Spherical particles of close to 100 nm are obtained when low amounts of Tz-UV (< 5 wt% relative to monomer) are incorporated into the polymer chains. PMMA-Tz-Vis PNPs are more difficult to visualize using TEM, most likely due to a reaction of the osmium (used for staining) with the pyrene moiety in the Tz-Vis monomer (Figure S38 and Figure S39). Nevertheless, in each case generally spherical particles can be observed with a size of approximately 100 nm.

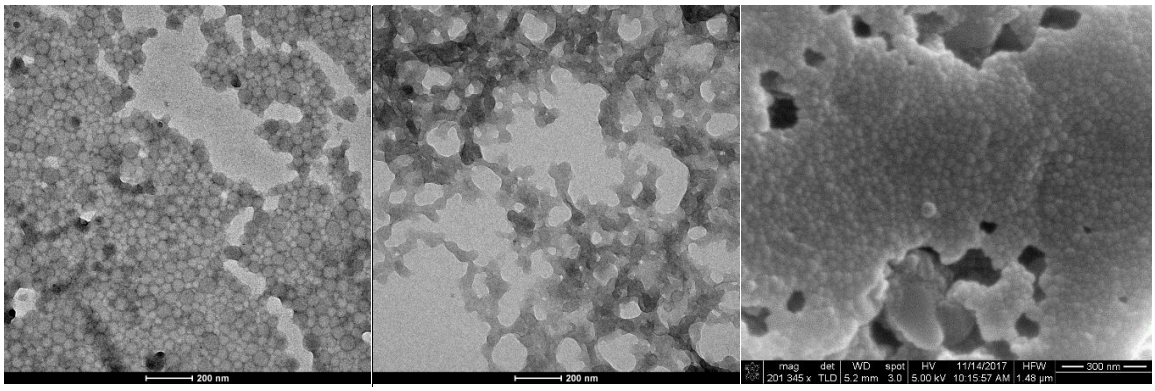

Figure 2. TEM images of PMMA-Tz-UV (2.5 wt%, left) and PMMA-Tz-Vis latexes (2.5 wt%; middle) using 2 wt% osmium vapour (OsO_4) staining. SEM image (right) of PMMA-Tz-Vis dried latex (2.5 wt%; middle) on double sided carbon tape using a 5 nm platinum coating.

Table S4 and Table S7 show that all miniemulsion polymerizations proceeded to high overall monomer conversions of above 90 % after 24 h. Conversions were determined via gravimetric measurements, followed by NMR analysis on the dried latex. As the Tz-monomer is a solid powder, any residual monomer would still be present in the dried latex and thus a signal for the vinylene peaks would be present in the ^{1}H NMR spectra between 5.5 and 6.5 ppm. The ^{1}H NMR spectra as depicted in Figure S21 and S37 unambiguously evidence full conversion of the Tz-monomer. The accompanying size exclusion chromatography (SEC) traces in Figure S17 and

Figure S32 confirm the formation of high molecular weight polymer with M_n values in excess of 250,000 g mol^{-1} in all cases.

An overview of all analytical results including an image of the resulting polymer latex for the PMMA-Tz PNPs using either 10 wt% of Tz-UV or Tz-Vis is given in **Table 2**.

Table 2. Overview of results of PMMA-Tz PNPs using 10 wt% of Tz-UV or Tz-Vis

Analysis	**Tz-UV 10 wt%**		**Tz-Vis 10 wt%**	
$Z_{aver.\ droplet}$ **(nm)**[a]	234 ± 40		89 ± 2	
$Z_{aver.\ particle}$ **(nm)**[a]	167 ± 4		111 ± 6	
$PDI_{particle}$	0.22 ±0.01		0.29 ± 0.03	
Particle size (nm)[b]	100		80	
M_n **(kg mol^{-1})**[c]	330		420	
$Đ$[c]	4.1		3.0	
λ_{abs} **(nm)**[d]	293		348	
λ_{em} **(nm)**[e]	n.a.		432	
Conversion (%)[f]	94		92	

Results obtained by using the following analysis techniques: [a] DLS; [b] TEM; [c] SEC; [d] UV-Vis; [e] Fluorescence Spectroscopy; [f] Gravimetry

The UV-Vis absorbance spectra – collected on a diluted solution of the latex – show the expected absorbance at 293 nm and at 348 nm for the PMMA-Tz-UV and PMMA-Tz-Vis nanoparticles, respectively. PMMA-Tz PNPs lead in both cases to similar absorbance values as for the initial Tz monomer (UV or Vis) itself, indicating the successful incorporation of the Tz-moiety. In addition, the fluorescence spectrum of the PMMA-Tz-Vis nanoparticles reveals a clear emission peak at 432 nm.[35] FT-ATR analysis indicates the presence of the aromatic units (=*C*-*H*- bending in ring between 850 cm^{-1} and 800 cm^{-1} and –*C*=*C*- bending in ring at 1509 cm^{-1}) for both PMMA-Tz copolymers, as well as the vibrations associated with the vinyl ether unit (=*C*-*O*- at 1016 cm^{-1}) in the case of the PMMA-Tz-UV (Figure S16 and Figure S31). Characterization via ^{1}H NMR of the PMMA-Tz-UV (Figure S18 to Figure S21) and PMMA-Tz-Vis (Figure S33 to Figure S36) nanoparticles shows – based on the integration of the aromatics proton resonances (6.75– 8.75 ppm) – the successful incorporation of the Tz moiety

upon varying Tz contents. Unambiguous resonances associated with the Tz-UV units (-OCH_3 at 3.81 ppm; -*O*-*C*=*O*- at 4.30 ppm; -*C*=*C*- between 6.75 and 8.75 ppm) or the Tz-Vis moieties (*O*-*C*=*O*- at 4.30 ppm; *pyrene* –*C*=*C*- between 7.75 and 9 ppm.) as well as the PMMA species (-OCH_3 at 3.62 ppm) can be identified within the ^{1}H NMR spectra. In addition, an image of both latexes after polymerization (Table 2) shows clear differences in colour – white *vs.* pink – when using the Tz-UV or Tz-Vis monomer, respectively.

Quantification of the amount of Tz units present on the surface of the nanoparticles was performed using X-ray photoelectron spectroscopy (XPS) analysis. This powerful technique provides information about the surface composition with an average depth of 5 nm and a detection limit up to 0.1 atom%. The composition of the nanoparticles was thus determined by comparing the nitrogen content at the surface of the PNPs with calculated theoretical values (Equation S1). XPS measurements were performed for the PMMA-only control particles, as well as all PMMA-Tz particles. XPS high resolution scans of nitrogen for the PMMA-Tz-UV are depicted in Figure S24, while the results of PMMA-Tz-Vis are shown in Figure S40. High resolution XPS results of the control PMMA particles are in line with literature results, showing clearly the absence of the N1*s* peak at 400 eV,[36] indicating that the use of AIBN as initiator does not affect the atomic percentage of nitrogen present on the surface of the particles. Thus, any nitrogen signal observed in the PMMA-Tz particles can be directly correlated with the amount of Tz present at the surface of the particles. The N1*s* spectra of the PMMA-Tz particles show a strong signal around 400 eV that can be assigned to the tetrazole species (-*N*=*N*-).[37] The additional weak N1*s* shoulder present around 403 eV is the result of hydrazone or hydrazine formation due to trapped nitrile imines in water.[38-40] A closer inspection of the high resolution XPS scans for nitrogen for both the PMMA-Tz-UV and PMMA-Tz-Vis particles reveals an increase in atomic percentage when increasing the Tz content from 2.5 to 10 wt% as expected. The atomic percentage of nitrogen obtained via XPS can be readily converted into a mole percentage of Tz monomer units (relative to all monomer units) present at the surface (Equation

S1).[41] **Figure 3** shows the mole percentage of Tz units present at the surface estimated via XPS plotted *vs.* the theoretical amount of Tz units present in the entire particle (not just in surface layer).

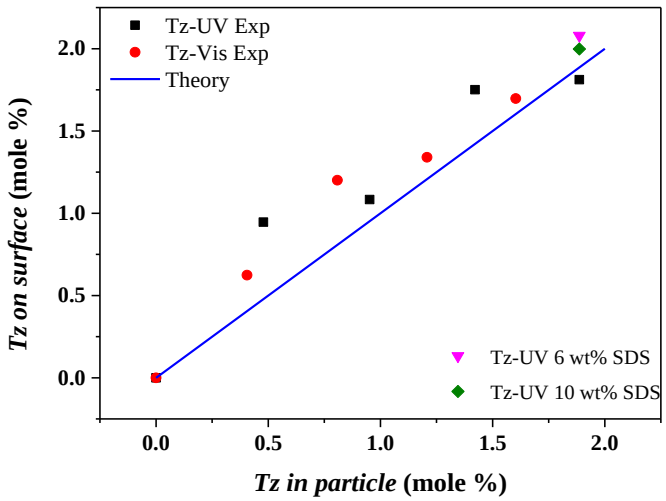

Figure 3. Relationship between the amount of Tz monomer units (mole %) present on the surface *vs.* the amount present in the particle overall. The surface content is calculated from the atomic % of nitrogen present on the surface according to XPS results, neglecting the presence of AIBN on the surface. The latter assumption was also made calculating the theoretical amount of Tz present in the particles overall. The blue line represents the situation where the surface composition is the same as the overall composition, *i.e.* the Tz monomer is evenly distributed throughout the particle.

The XPS data in Figure 3 demonstrate that on the basis of full monomer conversion of both monomers (the monomer conversions were in excess of 90% in all cases), the surface concentration (as mol%) of Tz monomer is approximately equal to the overall Tz monomer concentration within the particles.

The influence of the amount of the surfactant sodium dodecyl sulphate (SDS) used on the mole percentage of Tz-UV present at the surface of the particles was subsequently investigated. Three miniemulsion polymerizations were conducted with either 6, 8 (standard reaction conditions) or 10 wt% of SDS relative to the organic phase and 10 wt% of Tz-UV. DLS results of both the droplets (Table S5) as well as the particles after polymerization (Table S6) confirm the successful formation of the PMMA-Tz-UV PNPs. PNPs synthesized with 8 wt% of SDS led to

the smallest particle sizes ($Z_{average}$ of 167 nm), while an increase in SDS content up to 10 wt% resulted in unexpected larger particles of 524 nm. At this high concentration of surfactant, the observed increase in particle size is likely due to an increase in ionic strength of the aqueous phase. Smaller particles are highly desirable for these systems, as the NITEC reaction used in the second step is a light mediated reaction, which is sensitive to light scattering of large entities. In all cases, conversion of 94% or higher as well as high molecular weights are obtained for each latex (Table S7 and Figure S25). XPS analysis reveals that there is negligible influence of the amount of SDS used on the presence of Tz at the particle surface (Figure S26 and Figure 3, purple and green symbol).

2.2. NITEC / NICAL reaction

For the NITEC and NICAL driven photochemical ligation onto the photoreactive PNPs, two maleimides, *i.e.* N(-4-bromophenyl)-maleimide (N-BPM), N-ethyl maleimide (NEM), an acrylate (2-hydroxyethyl acrylate - HEA), an acid (5-bromovaleric acid - BVA) and a biomolecule of interest, *i.e.* folic acid, were selected, as shown in Figure 1. Stoichiometric conditions were used according to the initial loading of Tz. A series of samples were placed into a photoreactor and irradiated with 6 UV-B lamps (λ_{max} = 300 nm) or 3×3W Blue LED (λ_{max} = 415 nm) for the UV and visible nanoparticles, respectively (Figure S10 and Figure S11). The samples were stirred and maintained at ambient temperature during the entire experiment.

2.2.1. UV-B light

Without any purification, N-BPM was introduced in the latex and the mixture was subsequently irradiated under UV-B light. Within a few minutes of irradiation, the PMMA-Tz-UV latex rapidly turned from milky white to different shades of yellow as the reaction time was increased to 120 min (**Figure 4A**). The colloidal dispersion as well as the particles size remained stable

as confirmed by DLS ($Z_{average\ t=0\ min}$ = 160 nm (*PDI* = 0.18) / $Z_{average\ t=120\ min}$ = 158 nm (*PDI* = 0.21).

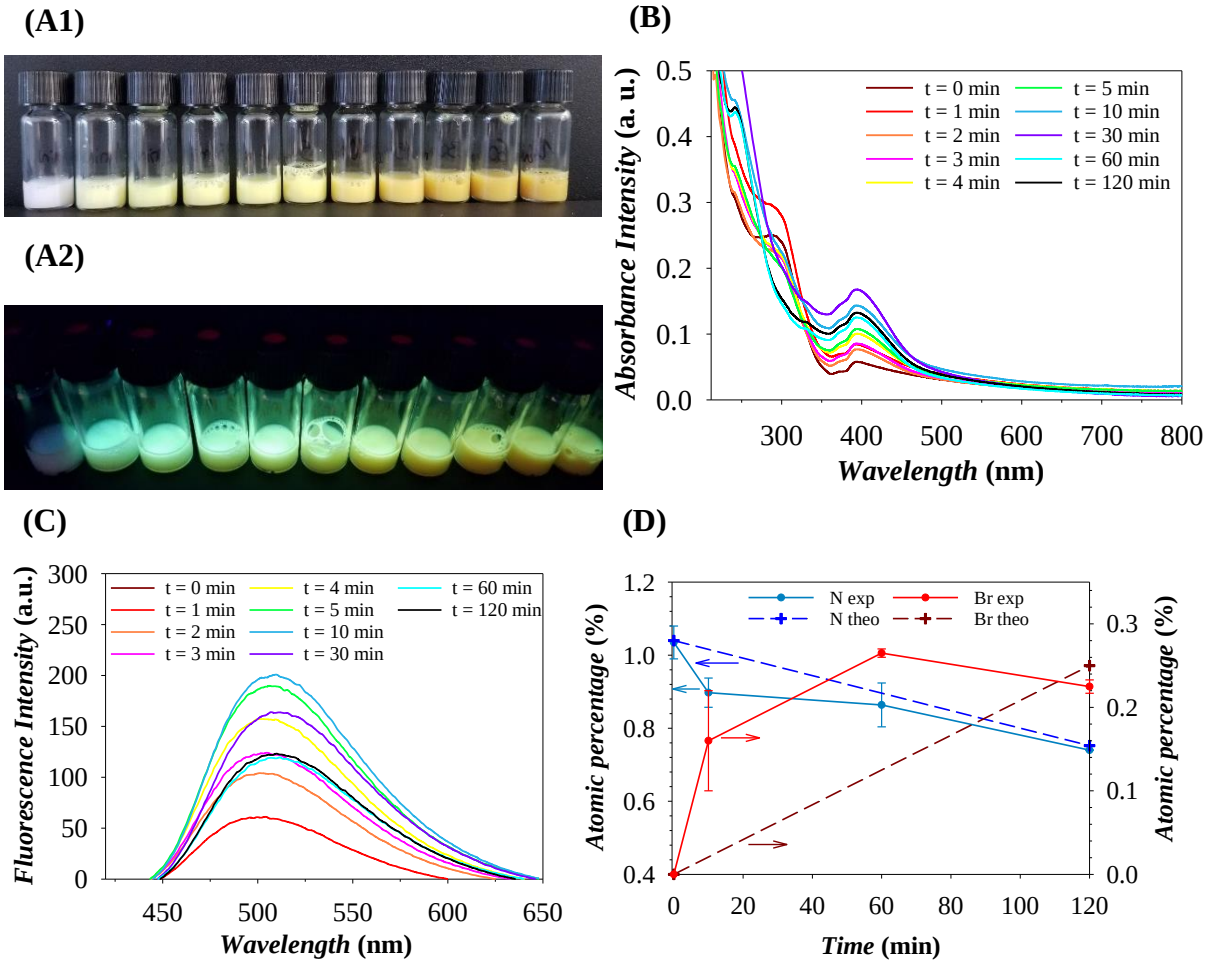

Figure 4. (A) Photographs of the PMMA-Tz-UV (10 wt%, UV4) latex after the NITEC reaction with N-BPM at different reaction times (from left to right: 0, 1, 2, 3, 4, 5, 10, 30, 60 and 120 min) under white light (A1) and under a hand-held UV lamp (λ_{ex} = 365 nm) (A2). (B) UV-vis absorbance spectra of highly diluted PMMA-Tz-UV (10 wt%, UV4) latex after the NITEC reaction with N-BPM at different reaction times. (C) Fluorescence emission spectra of highly diluted PMMA-Tz-UV (10 wt%, UV4) latex after the NITEC reaction with N-BPM at different reaction times (λ_{ex} = 390 nm). (D) Atomic percentage of nitrogen (left y-axis) and bromine (right y-axis) measured by XPS on the surface of dried copolymer after purification. Theoretical content is also displayed (calculated using Equation S1 and S2).

Upon irradiation with a hand-held 365 nm UV lamp, the unreacted nanoparticles (t = 0 min) exhibit a blue coloration whereas the nanoparticles emitted a blueish-green fluorescence after only one minute of irradiation. **Figure 4B** represents the UV-vis absorbance spectra of a 10 wt% PMMA-Tz-UV latexes after the NITEC reaction with N-BPM, clearly showing that the Tz characteristic absorption band at 290 nm vanished after 30 min of irradiation while two new

bands at 240 and 390 nm corresponding to the pyrazoline adduct appeared simultaneously. As previously mentioned, the PMMA-Tz-UV copolymer does not show any fluorescence, yet the pyrazoline adduct exhibits strong fluorescence. Fluorescence spectroscopy (λ_{ex} = 390 nm) was thus used to monitor the kinetics of the NITEC reaction with N-BPM (**Figure 4C**). An intense emission band at 510 nm appears after only 1 min of irradiation and the intensity continuously increases until 30 min. The fluorescence intensity exhibits a slight decrease and reaches a plateau. Indeed, the cycloadduct can undergo rearomatization,[28, 42] leading to a less fluorescent moiety. ^{1}H NMR spectroscopic analysis of the copolymer at 0, 10 and 120 min was carried out (Figure S41). Unfortunately, the resonances of the cycloadduct protons are expected in the region of 4 ppm and thus in the same chemical shift regime as the methoxy group of the methyl methacrylate, and it is thus not possible to follow the formation of the alkene. Nonetheless, comparison to the initial spectrum of the copolymer reveals several changes in the aromatics resonances that confirm the formation of the pyrazoline cycloadduct. As already reported earlier by us,[31] the resonances for the aromatics peaks are shifted to lower ppm during the course of the reaction. After 10 min of irradiation, a mixture of tetrazole and pyrazole is evidenced by the coexistence of different chemical shifts for the same protons whereas the doublet at 8.3 ppm (protons a) completely disappeared after 120 min of irradiation, suggesting the full activation of all Tz functionalities. Although all tetrazole species appear thus to be activated (including those within the nanoparticles), depending on the polarity and water solubility of the substrate (ene or acid), not all of them will react. For example, when one equivalent of N-BPM is used, some unreacted N-BPM is still present at the end of the reaction. This is directly related to the fact that the Tz moieties inside the PMMA-Tz-UV particles may not be accessible for the NITEC reaction, confining the ligation to surface near regions. Quantitative analysis was further carried out by XP spectroscopy (**Figure 4D**, Figure S42, and Table S12). Prior to the analysis, the latex was centrifuged (14 500 rpm, 5 min) and the precipitate was subsequently washed twice to remove any unreacted N-BPM. Thus, the bromine and nitrogen atomic

percentage measured by XPS is the accurate amount present on the surface of the nanoparticles. Previously, the mole percentage of Tz units relative to all monomer units was calculated based on the experimental atomic percentage of nitrogen in a system with three equations and three variables (Equation S1). Since each reacted tetrazole leads to the loss of 2 nitrogen atoms – the activated tetrazole releases molecular nitrogen gas – the unreacted PNPs contain 4 nitrogen atoms (Tz moiety) and the N-BPM-PNPs contains 3 nitrogen atoms (N_2 is released, yet N-BPM contributes one more nitrogen atom), it is challenging to follow the kinetics using the mole percentage as one equation evolves. It is similarly challenging to calculate the mole percentage of bromine during the course of the reaction since the N-BPM-PNPs gain 1 bromine atom. The theoretical atomic percentage of nitrogen and bromine after complete consumption of N-BPM (1.0 eq.) was thus calculated using the atomic percentage of nitrogen detected on the surface at time 0 and compared to the experimental XPS values (Equation S1 and S2). Bromine was detected from 10 min of irradiation and plateaus at 0.245 atom% – close to the theoretical value of 0.250 atom% – within 60 min (Table S12). Simultaneously, the nitrogen content detected by XPS decreases during the course of the reaction. The experimental value of 0.741 atom%, is close to the theoretical value calculated at 0.752 atom%. The bromine content is close to the detection limit, but the standard deviation is under 0.06, supporting the reliability of the measurements. Based on XPS and fluorescence analysis, we estimate that both the tetrazole activation and the NITEC reaction are complete within 60 min. The same experiments were performed varying the Tz-UV content as well as the reactant type (NEM and HEA) (Figure S43 and Figure S44). Maximum fluorescence intensity is reached within 30 min, followed by a slight decrease of the intensity. As expected, the more Tz-UV in the copolymer, the higher the fluorescence intensity. As discussed above, the reaction occurs preferably at the particles' surface – *i.e.* in the water phase. It is thus worth noting that even if N-BPM is not soluble in water, yet the NITEC reaction can still be carried out, paving the way to a multitude of potential

future reactants. Nonetheless, using a water-soluble compound (*i.e.* HEA or NEM) results in a higher fluorescence intensity than N-BPM.

The PMMA-Tz-UV was subsequently employed for the NICAL reaction with BVA. Similar UV and fluorescence spectra were obtained (Figure S45), except for the emission band which is less intense and shifted to lower wavelength (500 nm) in accordance with literature results.[31] In addition, no decrease of the fluorescence intensity was observed since – instead of a cycloadduct – a carboxamide is formed. The ^{1}H NMR spectrum of the copolymer also highlights the shift of the aromatics peaks to lower ppm, yet the resonance corresponding to the newly formed amine is not visible in $CDCl_2$ (Figure S46). In addition, the peaks corresponding to the alkyl protons of the BVA and the Tz monomer both appear around 1.9 ppm and cannot be discriminated. To unambiguously establish the ligation, a NICAL reaction with trifluoroacetic acid (TFA) was undertaken under the exact same conditions. After 60 min of irradiation, the latex was purified to remove any excess of TFA and subsequently analyzed by ^{1}H and ^{19}F NMR (Figure S47). As previously observed, the peak corresponding to the amine proton does not appear in the ^{1}H NMR spectrum, yet critically, the ^{19}F NMR spectrum clearly reveals the presence of three peaks at -68, -71 and -76 ppm. Comparison with the time 0 min (no fluorine signal detected) confirms that all unreacted TFA was fully removed from the latex and TFA was efficiently ligated to the PMMA-UV-Tz copolymer. XPS results of the PMMA-Tz-UV/BVA (Table S13) revealed that no bromine is detected on the surface of the nanoparticles. However, the analysis clearly shows that within 30 min, the nitrogen content decreases until reaching a plateau value at 0.65 atom%. Based on the nitrogen content detected at time 0, the theoretical value calculated for a full activation is 0.53 atom%. As a result, the activation of the Tz moieties is estimated to be 79 % but it was not possible to determine the conversion of the NICAL reaction with BVA quantitatively. Noting that the NICAL reaction is less efficient than the NITEC process (non-quantitative conversion in the NICAL case), the

bromine content might be below the XPS detection threshold. Therefore, the PMMA-Tz-UV/TFA PNPs – which contain 3 fluorine atom instead of 1 bromine – were analyzed by XPS. In this case, the nitrogen content decreased from 1.00 to 0.49 atom % (full activation) and the fluorine was detected at 0.18 atom%, corresponding to 25 % conversion (Table S14). To summarize, the fluorescence spectroscopy study combined with the unambigeous ^{19}F NMR and XPS studies with TFA underpin the successful ligation. It is interesting to note that the nitrogen decrease is also observed without purifying the nanoparticles (Table S15). Without purification, the (un)reacted BVA as well as the SDS are still present – bromine and sulfur are thus detected – but the nitrogen content decreases significantly. Contrary to the N-BPM, BVA is nitrogen-free and it is easier to monitor its release during the NICAL reaction. Avoiding the purification step led to faster and simpler analysis.

2.2.2. Visible light

Driven by the successful NITEC and NICAL reaction of the PMMA-Tz-UV particles under UV-B light, we expand the portfolio of photoreactive PNPs to the use of visible light. Previously, we designed a tetrazole bearing a pyrene moiety that enables visible light reactions.[28, 34] Herein, the same simple procedure as for the PMMA-Tz-UV nanoparticles was employed. Within a few minutes of irradiation, the pink PMMA-Tz-Vis latex turned orange (blue to yellow under a hand-held 365 nm UV lamp), demonstrating the high and rapid reactivity of the tetrazole (**Figure 5A**).

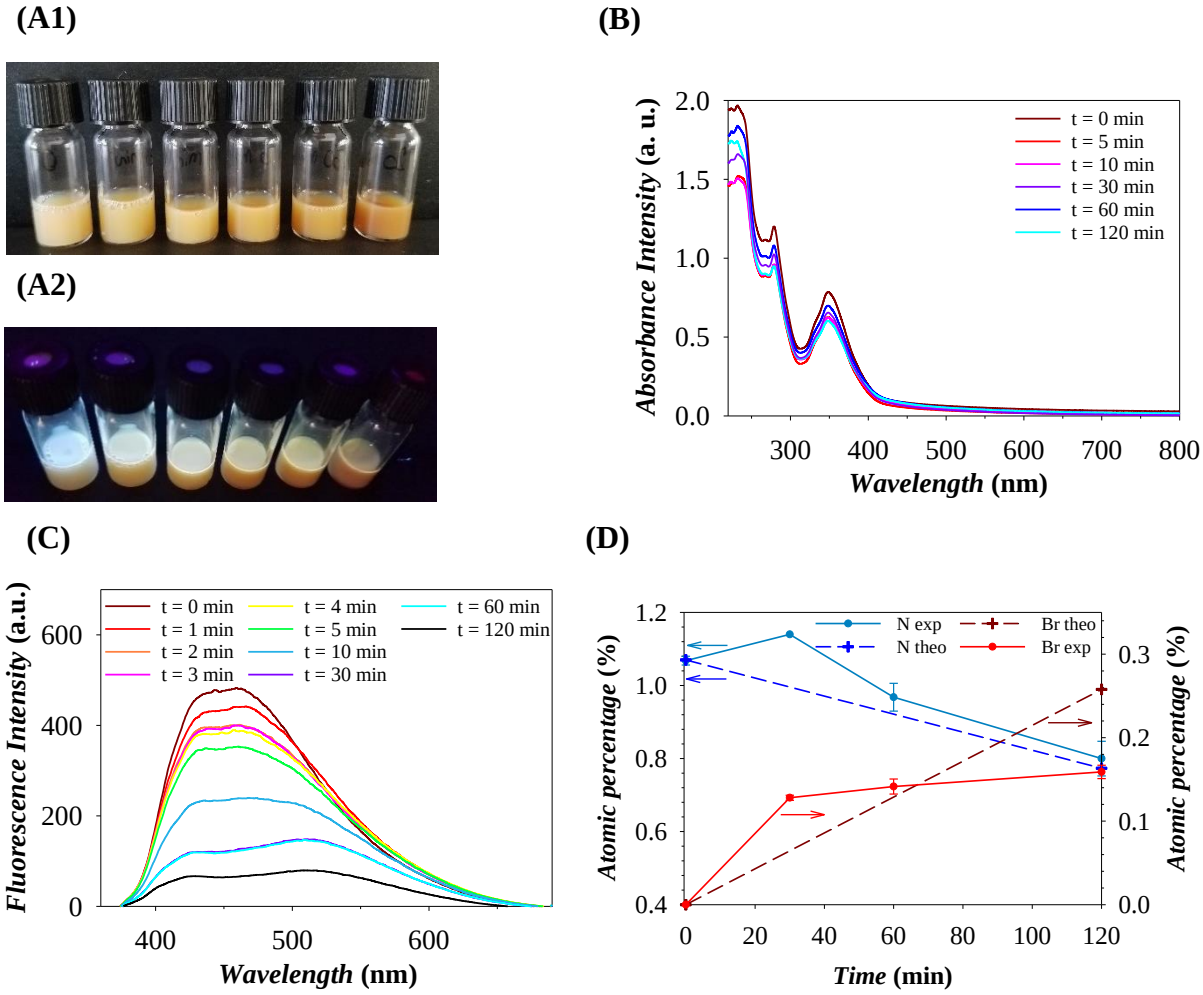

Figure 5. (A) Photographs of the PMMA-Tz-Visible (10 wt%, Vis4) latex after the NITEC reaction with N-BPM at different reaction times (from left to right: 0, 5, 10, 30, 60 and 120 min) under white light (A1) and under a hand-held UV lamp (λ_{ex} = 365 nm) (A2). (B) UV-vis absorbance spectra of highly diluted PMMA-Tz-Vis (10 wt%, Vis4) latex after the NITEC reaction with N-BPM at different reaction times. (C) Fluorescence emission spectra of highly diluted PMMA-Tz-Vis (10 wt%, Vis4) latex after the NITEC reaction with N-BPM at different reaction times (λ_{ex} = 350 nm). (D) Atomic percentage of nitrogen (left y-axis) and bromine (right y-axis) measured by XPS on the surface of the dried copolymer after purification. Theoretical content is also displayed (calculated using Equation S1 and S2).

The colloidal suspension was stable and no notable change in particle size was observed - $Z_{average\ t=0\ min}$= 103 nm (PDI = 0.384) / $Z_{average\ t=120min}$ = 106 nm (*PDI* = 0.373). **Figure 5B** depicts the UV-vis absorbance spectrum of the latex after the NITEC reaction with N-BPM. All spectra overlay, exhibiting the same peak at 232, 279 and 350 nm. Before the reaction, the PMMA-Tz-Vis nanoparticles are highly fluorescent due to the pyrenyl moiety (λ_{ex} = 350 nm) and an intense emission band is detected at 430 nm (**Figure 5C**). During the course of the reaction, the emission peak intensity at 430 nm rapidly decreased due to the change in the aromatic region

(formation of the activated nitrile). Concomitantly, a new band at 515 nm appears after 10 min of irradiation only. A picture of the diluted latex after NITEC reaction (N-BPM, NEM and HEA) clearly shows that the nanoparticles always exhibit a yellow emission under hand-held 365 nm UV lamp, while they initially appeared blue (**Figure 6A**). Contrary to the Tz-UV, the fluorescence of the Tz-Vis does not increase but rather shifts to higher wavelength (510 nm). Lederhose *et al.*[28] also observed that the emission band shifted in a similar manner from 431 to 577 nm after formation of the cycloadduct via the NITEC reaction between the Tz-Vis precursor and a maleimide. ^{1}H NMR spectroscopy of the copolymer also reveals an overall shift from 8.5 to 8 ppm in the aromatic region, yet the individual peaks overlay and broaden the resonance (Figure S48). Even with a COSY acquisition, it is not possible to assign the proton precisely. In addition, XPS analysis of the PMMA-Tz-Vis/N-BPM nanoparticle composition during the course of the reaction demonstrates the decrease of the nitrogen content simultaneously to an increase of the bromine content (**Figure 5D**, Figure S49 and Table S16). The activation of the tetrazole is completed within 120 min, with an experimental value for the nitrogen at 0.80 atom% (theoretical value - 0.77 atom%). The bromine value plateaus at 0.16 atom%, translating to 63 % conversion (theoretical value - 0.26 atom%). NEM and HEA were subsequently employed as well as lower Tz-Vis content (**Figure 6** and Figure S50). All experiments led to the successful cycloaddition with an emission shift to 515 nm. Using PNPs with lower Tz-Vis loading led to lower fluorescent intensities, similarly to the observation made with UV PNPs.

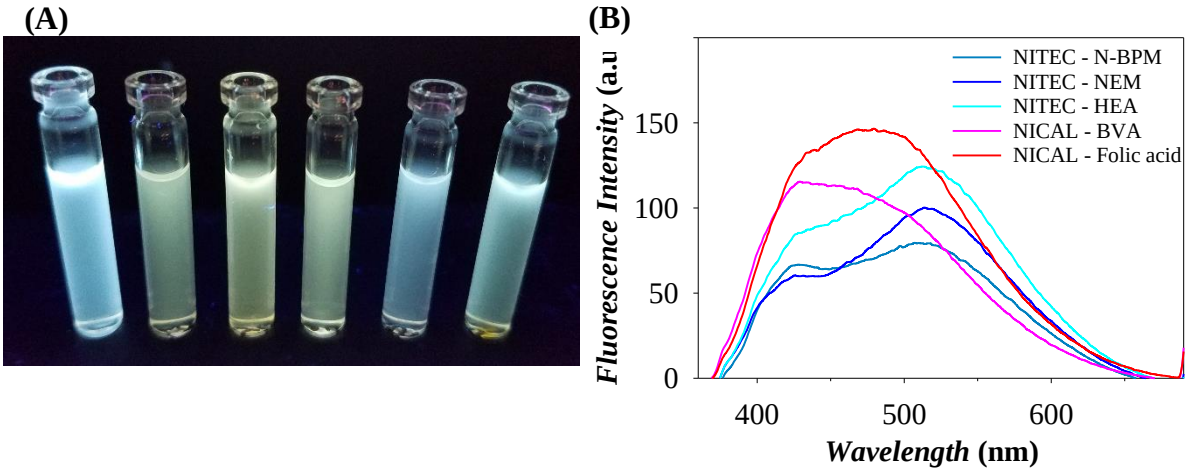

Figure 6. (A) Photographs of diluted PMMA-Tz-Vis (10 wt%, Vis4) latex after the NITEC or NICAL reaction (from left to right: unreacted, NEM, N-BPM, HEA, BVA, folic acid) under a hand-held UV lamp (λ_{ex} = 365 nm). (B) Fluorescence emission spectra of highly diluted PMMA-Tz-Vis (10 wt%, Vis4) latex after the NITEC or NICAL reaction with N-BPM, NEM, HEA, BVA and folic acid after 120 min of irradiation (λ_{ex} = 350 nm).

Finally, the NICAL reaction was undertaken with the visible photoreactive PNPs using BVA under the same conditions. As observed with the UV PNPs, no bromine was detected by XPS but the nitrogen atomic percentage decreasing from 0.94 atom% to 0.73 atom% (Table S17 and Table S18). Since the calculated theoretical value is 0.46 atom%, the activation of the Tz moieties is estimated at 44 %. Surprisingly, the fluorescence intensity decreases in the same manner as the NITEC reaction yet no peak appears at higher wavelength as previously observed (Figure 6). We hypothesize that in the NITEC reaction, the newly formed cycloadduct is fluorescent whereas the NICAL reaction forms a non-fluorescent open-ring carboxamide. To confirm this hypothesis, a model reaction between the Tz-Vis precursor – the Tz-Vis monomer itself is not suitable it contains an acrylate which may react with itself – and BVA was performed in DMF. Close examination of the resulting ^{1}H NMR spectrum demonstrates the ligation of the BVA (**Figure 7**). Indeed, a singlet corresponding to the newly formed secondary amine proton clearly appears at 9.1 ppm, whereas the resonance of initial reactant are shifted to lower ppm. In addition, the fluorescence spectrum of the small molecule exhibits a similar trend to the copolymer, *i.e.* a decrease of the 430 nm peak and no peak around 510 nm. This small

molecule fluorescence test, coupled the XPS analysis, shows that the Tz-Vis PNPs indeed undergoes the NICAL reactions.

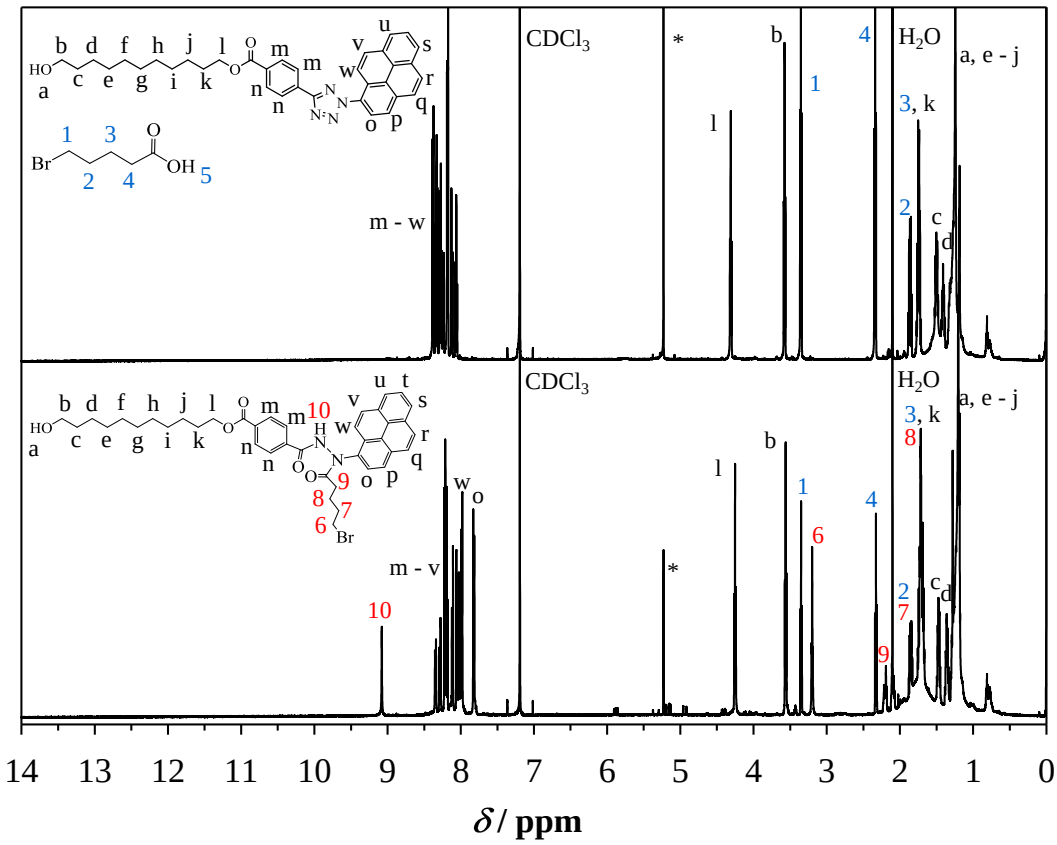

Figure 7. ^{1}H NMR spectrum of the Tz-Vis precursor with BVA before and after 60 min irradiation under visible light with the corresponding labels ($CDCl_3$).

With the demonstrated success of the PMMA-Tz-Vis PNPs to carry out either NITEC or NICAL under visible light, we move to highlight the potential of our photoreactive profluorescent NPs to be functionalized with UV sensitive molecules, which is critical for attaching biological tags during imaging. Specifically, folic acid – a vital vitamin for all living systems – was selected for a proof-of-concept study. Not only is folic acid prone to degradation when exposed to UV light,[43] it is also an excellent candidate for NICAL reactions due to its double carboxylic acid functionality. In a preliminary study, folic acid was exposed to both UV (λ_{max} = 300 nm) and visible light (λ_{max} = 415 nm) for 120 min (**Figure 8** and Figure S51).

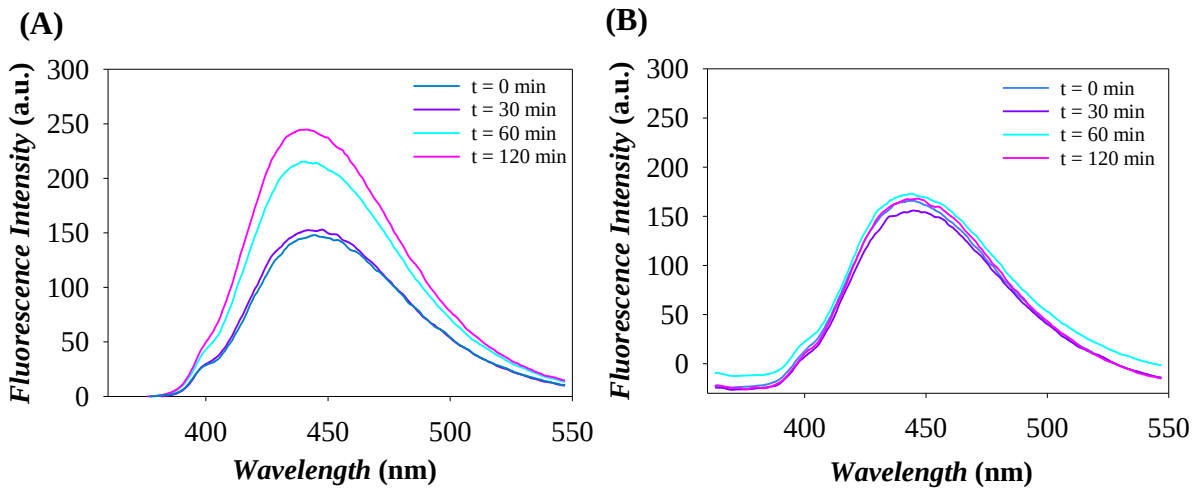

Figure 8. Fluorescence spectra (λ_{ex} = 350 nm) of a folic acid solution (7.2 g L^{-1}) after 120 min irradiation under UV-B light (300 nm) (A) and under visible light (415 nm) (B).

The fluorescence of folic acid is weak but the photoproducts – *p*-aminobenzoyl-$_L$-glutamic acid and 6-formyl pterin – have fluorescent properties.[43] When exposed to UV radiation, the fluorescence intensity increases whereas the same experiment undertaken under visible light proves the photostability of folic acid. Driven by this observation, a NICAL reaction was performed with the PMMA-Tz-Vis latex (as well as with the visible precursor). As previously observed with BVA, the fluorescence intensity decreases over time, for both the latex and the small molecule test reaction. ^{1}H NMR spectrum of the small molecule after reaction with folic acid confirms the formation of the secondary amine (Figure S52). Furthermore, folic acid contains two carboxylic acid groups which can eventually react with the activated nitrile. Due to steric hindrance and evidenced by the ^{1}H NMR spectrum, the proton 1 from the C_5-COOH reacts preferentially (Figure S52). To confirm the folic acid ligation by XPS, nitrogen quantification of nanoparticles before and after reaction with folic acid was undertaken. Folic acid is partially soluble in water and the saturated solution sediments, together with the nanoparticles. It is thus not possible to purify the PNPs by centrifugation and, later on, quantify the ligation. However, the comparison before and after NICAL reaction highlights the nitrogen release ($N(atom\%)_{t=0}$ = 1.71 / $N(atom\%)_{t=120\ min}$ = 1.47), thus indicating successful activation

of the tetrazole.

3. Conclusions

The simple photochemical design of functional fluorescent NPs in aqueous environments for the potential use as imaging agents has been introduced as a platform technology. Specifically, we exploit the profluorescent nature of tetrazoles to establish fluorescent linkages to variable enes and acids during the functionalization of the photoreactive NPs. The particular attractiveness of our approach rests on the wide variety of functional acids and enes that can be used to decorate the NPs, while concomitantly inducing fluorescence during the ligation process. Through careful selection of the chromophore, we designed a tetrazole-based acrylate system reacting either with UV-B (methoxy phenyl moiety) or visible light (pyrenyl moiety). Both Tz monomers were copolymerized with MMA in miniemulsion polymerizations, leading to photoreactive nanoparticles. Stable and spherical colloidal nanoparticles in the 150 nm range were obtained in a fast, robust and reproducible process. The copolymer nanoparticles were further characterized by SEC, ^{1}H NMR, FT-ATR, XPS, UV and fluorescence spectroscopy. Based on these analyses, we demonstrate that the tetrazole monomer concentration at the surface is same as the overall average. Without any purification, the latexes were simply irradiated in the presence of a variety of functional substrates (carboxylic acid, maleimide and acrylate) under UV-B or visible light. Within a few minutes, stable fluorescent nanoparticles were obtained. Full activation of the tetrazole moiety was reached within 120 min for the NITEC reaction whereas the NICAL reaction reached a plateau – 79 % for the UV and 44 % for the visible – within 30 min. Based on the bromine content detected by XPS, the NITEC reaction with N-BPM was quantitative for the UV-PNPs, whereas the conversion reached a plateau at 63 % for the visible PNPs. In terms of fluorescence, the PMMA-Tz-UV nanoparticles emit at 510 nm (λ_{ex} = 390 nm) while the PMMA-Tz-Vis nanoparticles emit at 515 nm (λ_{ex} = 350 nm). In both cases, the higher the Tz content, the stronger the fluorescence. The successful

NITEC or NICAL reactions of PMMA-Tz with insoluble or water-soluble model molecules demonstrate the high potential of our photoreactive nanoparticle materials. Critically, ligation of UV sensitive folic acid under visible light is a step into the realm of attaching biological photosensitive tags onto NPs by photochemical means. We submit that the design of PNP latexes able to react with a variety of alkene and carboxylic acids under visible light opens substantial possibilities tagging UV-sensitive species to nanoparticles. Taking into consideration the higher fluorescence intensity and the full conversion of the PMMA-Tz nanoparticles after NITEC reactions, NITEC is preferred over NICAL. Future variations of the copolymer backbone (*e.g.* film-forming latexes) can potentially extend the field of application of our unique fluorescent NP materials. Clearly, the (visible light) photoreactive PNPs pioneered herein have high potential in materials science, especially in biological tagging applications, where (bio)molecules are sensitive to UV light.

Supporting Information

Supporting Information is available from the Wiley Online Library or from the author.

Acknowledgements

L. Delafresnaye and N. Zaquen contributed equally to this study. C.B.-K. acknowledges the Australian Research Council (ARC) for funding in the form of a Laureate Fellowship underpinning his photochemical research program, as well as the Queensland University of Technology (QUT) for key continued support. The project received additional funding from the European Union's Horizon 2020 research and innovation program under the Marie Skłodowska-Curie grant agreement No 665501 with the research Foundation Flanders (FWO). The XPS data of the latexes after NICAL or NITEC reactions reported herein were obtained at the Central Analytical Research Facility (CARF) operated by the Institute for Future Environments (QUT). Access to CARF is supported by generous funding from the Science and Engineering Faculty (QUT).

Received: ((will be filled in by the editorial staff))
Revised: ((will be filled in by the editorial staff))
Published online: ((will be filled in by the editorial staff))

References

[1] K. Landfester, A. Musyanovych, V. Mailänder, *J. Polym. Sci. A* **2010**, *48*, 493.
[2] F. Su, R. Alam, Q. Mei, Y. Tian, D. R. Meldrum, *PloS one* **2011**, *6*, e24425.
[3] H. Tan, Y. Zhang, M. Wang, Z. Zhang, X. Zhang, A. M. Yong, S. Y. Wong, A. Y.-c. Chang, Z.-K. Chen, X. Li, *Biomaterials* **2012**, *33*, 237.
[4] Y. Tian, W.-C. Wu, C.-Y. Chen, T. Strovas, Y. Li, Y. Jin, F. Su, D. R. Meldrum, A. K.-Y. Jen, *J. Mater. Chem.* **2010**, *20*, 1728.
[5] M. Behrendt, M. G. Sandros, R. A. McKinney, K. McDonald, E. Przybytkowski, M. Tabrizian, D. Maysinger, *Nanomedicine* **2009**, *4*, 747.
[6] Y. Jung, R. J. Hickey, S.-J. Park, *Langmuir* **2010**, *26*, 7540.
[7] D. K. Tiwari, T. Jin, J. Behari, *Int. J. Nanomedicine* **2011**, *6*, 463.
[8] H. Wang, H. H. Wang, V. S. Urban, K. C. Littrell, P. Thiyagarajan, L. Yu, *J. Am. Chem. Soc.* **2000**, *122*, 6855.
[9] W.-C. Wu, H.-H. Chang, *Colloid Polym. Sci.* **2015**, *293*, 453.
[10] W.-C. Wu, C.-Y. Chen, W.-Y. Lee, W.-C. Chen, *Polym.* **2015**, *65*, A1.
[11] M. A. Walling, J. A. Novak, J. R. Shepard, *Int. J. Mol. Sci.* **2009**, *10*, 441.
[12] M. Peters, N. Zaquen, L. D'Olieslaeger, H. Bové, D. Vanderzande, N. Hellings, T. Junkers, A. Ethirajan, *Biomacromolecules* **2016**, *17*, 2562.
[13] N. Zaquen, H. Lu, T. Chang, R. Mamdooh, L. Lutsen, D. Vanderzande, M. Stenzel, T. Junkers, *Biomacromolecules* **2016**, *17*, 4086.
[14] C. Brieke, F. Rohrbach, A. Gottschalk, G. Mayer, A. Heckel, *Angew. Chem. Int. Ed.* **2012**, *51*, 8446.
[15] S. Chatani, C. J. Kloxin, C. N. Bowman, *Polym. Chem.* **2014**, *5*, 2187.
[16] M.-M. Russew, S. Hecht, *Adv. Mater.* **2010**, *22*, 3348.
[17] T. K. Claus, B. Richter, V. Hahn, A. Welle, S. Kayser, M. Wegener, M. Bastmeyer, G. Delaittre, C. Barner-Kowollik, *Angew. Chem. Int. Ed.* **2016**, *55*, 3817.
[18] C. Bao, L. Zhu, Q. Lin, H. Tian, *Adv. Mater.* **2015**, *27*, 1647.
[19] G. Ghosh, M. Minnis, A. A. Ghogare, I. Abramova, K. A. Cengel, T. M. Busch, A. Greer, *J. Phys. Chem. B* **2015**, *119*, 4155.
[20] N. Fomina, J. Sankaranarayanan, A. Almutairi, *Adv. Drug Deliv. Rev.* **2012**, *64*, 1005.
[21] W. Szymański, J. M. Beierle, H. A. V. Kistemaker, W. A. Velema, B. L. Feringa, *Chem. Rev.* **2013**, *113*, 6114.
[22] G. Delaittre, A. S. Goldmann, J. O. Mueller, C. Barner-Kowollik, *Angew. Chem. Int. Ed.* **2015**, *54*, 11388.
[23] T. Junkers, *Eur. Polym. J.* **2015**, *62*, 273.
[24] T. Pauloehrl, G. Delaittre, M. Bruns, M. Meißler, H. G. Börner, M. Bastmeyer, C. Barner-Kowollik, *Angew. Chem. Int. Ed.* **2012**, *51*, 9181.
[25] D. Habault, H. Zhang, Y. Zhao, *Chem. Soc. Rev.* **2013**, *42*, 7244.
[26] C. Wang, M. M. Zieger, A. Schenzel, M. Wegener, J. Willenbacher, C. Barner-Kowollik, C. N. Bowman, *Adv. Funct. Mater.* **2017**, *27*, 1605317.
[27] Y. Wang, C. I. Rivera Vera, Q. Lin, *Org. Lett.* **2007**, *9*, 4155.
[28] P. Lederhose, K. N. Wüst, C. Barner-Kowollik, J. P. Blinco, *Chem. Commun.* **2016**, *52*, 5928.
[29] Y. Wang, W. J. Hu, W. Song, R. K. Lim, Q. Lin, *Org. Lett.* **2008**, *10*, 3725.
[30] W. Song, Y. Wang, J. Qu, M. M. Madden, Q. Lin, *Angew. Chem.* **2008**, *120*, 2874.
[31] C. Heiler, J. T. Offenloch, E. Blasco, C. Barner-Kowollik, *ACS Macro Lett.* **2017**, *6*, 56.
[32] J. M. Asua, *Prog. Polym. Sci.* **2002**, *27*, 1283.
[33] J. O. Mueller, D. Voll, F. G. Schmidt, G. Delaittre, C. Barner-Kowollik, *Chem. Commun.* **2014**, *50*, 15681.

[34] P. Lederhose, D. Abt, A. Welle, R. Mueller, C. Barner-Kowollik, J. P. Blinco, *Chem. Eur. J.*, 10.1002/chem.201705393.
[35] J. Willenbacher, K. N. R. Wuest, J. O. Mueller, M. Kaupp, H.-A. Wagenknecht, C. Barner-Kowollik, *ACS Macro Lett.* **2014**, *3*, 574.
[36] C. Girardeaux, J.-J. Pireaux, *Surf. Sci. Spectra* **1996**, *4*, 134.
[37] E. Szőcs, I. Bako, T. Kosztolanyi, I. Bertoti, E. Kalman, *Electrochim. Acta* **2004**, *49*, 1371.
[38] P. Rouxhet, A. Misselyn-Bauduin, F. Ahimou, M. Genet, Y. Adriaensen, T. Desille, P. Bodson, C. Deroanne, *Surf. Interface Anal.* **2008**, *40*, 718.
[39] H. Meier, W. Heinzelmann, H. Heimgartner, *Chimia* **1980**, *34*, 506.
[40] S.-L. Zheng, Y. Wang, Z. Yu, Q. Lin, P. Coppens, *J. Am. Chem. Soc.* **2009**, *131*, 18036.
[41] F. Jasinski, V. L. Teo, R. P. Kuchel, M. Mballa Mballa, S. C. Thickett, R. H. G. Brinkhuis, W. Weaver, P. B. Zetterlund, *J. Polym. Sci. A* **2017**, *55*, 2513.
[42] J. O. Mueller, F. G. Schmidt, J. P. Blinco, C. Barner-Kowollik, *Angew. Chem. Int. Ed.* **2015**, *54*, 10284.
[43] M. K. Off, A. E. Steindal, A. C. Porojnicu, A. Juzeniene, A. Vorobey, A. Johnsson, J. Moan, *J. Photochem. Photobiol., Part B: Biol.* **2005**, *80*, 47.

List of Figures, Scheme and Tables

Figure 1. Synthetic route for the formation of fluorescent PMMA-Tz nanoparticles via a miniemulsion approach, affording both visible and UV light reactive PMMA-Tz nanoparticles.
Figure 2. TEM images of PMMA-Tz-UV (2.5 wt%, left) and PMMA-Tz-Vis latexes (2.5 wt%; middle) using 2 wt% osmium vapour (OsO_4) staining. SEM image (right) of PMMA-Tz-Vis dried latex (2.5 wt%; middle) on double sided carbon tape using a 5 nm platinum coating.
Figure 3. Relationship between the amount of Tz monomer units (mole %) present on the surface *vs.* the amount present in the particle overall. The surface content is calculated from the atomic % of nitrogen present on the surface according to XPS results, neglecting the presence of AIBN on the surface. The latter assumption was also made calculating the theoretical amount of Tz present in the particles overall. The blue line represents the situation where the surface composition is the same as the overall composition, *i.e.* the Tz monomer is evenly distributed throughout the particle.
Figure 4. (A) Photographs of the PMMA-Tz-UV (10 wt%, UV4) latex after the NITEC reaction with N-BPM at different reaction times (from left to right: 0, 1, 2, 3, 4, 5, 10, 30, 60 and 120 min) under white light (A1) and under a hand-held UV lamp (λ_{ex} = 365 nm) (A2). (B) UV-vis absorbance spectra of highly diluted PMMA-Tz-UV (10 wt%, UV4) latex after the NITEC reaction with N-BPM at different reaction times. (C) Fluorescence emission spectra of highly diluted PMMA-Tz-UV (10 wt%, UV4) latex after the NITEC reaction with N-BPM at different reaction times (λ_{ex} = 390 nm). (D) Atomic percentage of nitrogen (left y-axis) and bromine (right y-axis) measured by XPS on the surface of dried copolymer after purification. Theoretical content is also displayed (calculated using Equation S1 and S2).
Figure 5. (A) Photographs of the PMMA-Tz-Visible (10 wt%, Vis4) latex after the NITEC reaction with N-BPM at different reaction times (from left to right: 0, 5, 10, 30, 60 and 120 min) under white light (A1) and under a hand-held UV lamp (λ_{ex} = 365 nm) (A2). (B) UV-vis absorbance spectra of highly diluted PMMA-Tz-Vis (10 wt%, Vis4) latex after the NITEC reaction with N-BPM at different reaction times. (C) Fluorescence emission spectra of highly diluted PMMA-Tz-Vis (10 wt%, Vis4) latex after the NITEC reaction with N-BPM at different reaction times (λ_{ex} = 350 nm). (D) Atomic percentage of nitrogen (left y-axis) and bromine

(right y-axis) measured by XPS on the surface of the dried copolymer after purification. Theoretical content is also displayed (calculated using Equation S1 and S2).

Figure 6. (A) Photographs of diluted PMMA-Tz-Vis (10 wt%, Vis4) latex after the NITEC or NICAL reaction (from left to right: unreacted, NEM, N-BPM, HEA, BVA, folic acid) under a hand-held UV lamp (λ_{ex} = 365 nm). (B) Fluorescence emission spectra of highly diluted PMMA-Tz-Vis (10 wt%, Vis4) latex after the NITEC or NICAL reaction with N-BPM, NEM, HEA, BVA and folic acid after 120 min of irradiation (λ_{ex} = 350 nm).

Figure 7. ^{1}H NMR spectrum of the Tz-Vis precursor with BVA before and after 60 min irradiation under visible light with the corresponding labels ($CDCl_3$).

Figure 8. Fluorescence spectra (λ_{ex} = 350 nm) of a folic acid solution (7.2 g L^{-1}) after 120 min irradiation under UV-B light (300 nm) (A) and under visible light (415 nm) (B).

Table 1. Miniemulsion polymerization recipes with varying Tz contents

Table 2. Overview of results of PMMA-Tz PNPs using 10 wt% of Tz-UV or Tz-Vis

A Simple and Versatile Pathway for the Synthesis of Visible Light Photoreactive Nanoparticles

Laura Delafresnaye, Neomy Zaquen, Rhiannon P. Kuchel, James P. Blinco, Per B. Zetterlund and Christopher Barner-Kowollik**

Keywords: Miniemulsion, Tetrazole Driven Photochemistry, Profluorescent Particles, Visible Light Ligation, Biomolecule Tagging

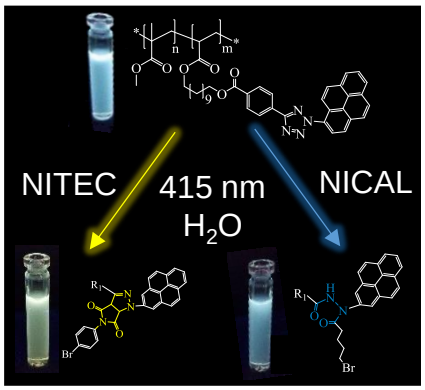

We pioneer a facile and versatile two-step process for the preparation of well-defined functional fluorescent nanoparticles in water. By carefully selecting the chromophore, UV and visible light photoreactive nanoparticles were synthesized by miniemulsion polymerization. Upon visible light irradiation, fluorescent nanoparticles decorated with a wide array of alkene or carboxylic acid moieties become accessible.

Supporting Information

A Simple and Versatile Pathway for the Synthesis of Visible Light Photoreactive Nanoparticles

Laura Delafresnaye, Neomy Zaquen, Rhiannon P. Kuchel, James P. Blinco, Per B. Zetterlund and Christopher Barner-Kowollik**

1. Experimental Section

1.1. Materials

All materials were reagent grade and used as received, unless stated otherwise. Hexadecane (HD, 99% Sigma Aldrich) and 1,2-dichloroethane (98 % Sigma Aldrich) were used as co-solvent. Sodium dodecyl sulfate (SDS; Technical Grade, Ajax Chemicals) was used as anionic surfactant. Deionized (DI) water was produced by a Milli-Q reverse osmosis system and had a resistivity of > 18 $m\Omega \cdot cm^{-1}$. Methyl methacrylate (MMA; > 99 %, Sigma Aldrich) was deinhibited by passing through a column of activated basic alumina (Ajax). The deinhibited monomer was stored in the freezer at -20°C and used within 1 month. 2,2'Azobis(isobutyronitrile) (AIBN, 97%, VWR) was recrystallized twice from methanol.

1.2. Characterization

Nuclear Magnetic Resonance (NMR) Spectrometry: NMR spectra of the copolymers were obtained using a Bruker Avance 400 spectrometer (400 MHz). NMR spectra of the monomers as well as the copolymers after NITEC/NICAL reactions were obtained using a Bruker Avance 600 spectrometer (600 MHz). All chemical shifts are recorded in ppm (δ) relative to tetramethylsilane (δ = 0 ppm), referenced to the chemical shifts of residual solvent resonances (1H). ^{19}F NMR spectra were recorded without proton decoupling using 12 s delay and 128 scans.

The multiplicities were explained using the following abbreviations: s for singlet, d for doublet, t for triplet, m for multiplet and bs for broad signal. The dried samples obtained for gravimetric analysis, was redissolved in deuterated solvent and used for NMR measurements.

Fourier Transform Attenuated Total Reflectance (FT-ATR) Spectroscopy: All measurements are performed on a Bruker IFS 66/S Fourier transform spectrometer equipped with a tungsten halogen lamp, a CaF_2 beam splitter. Spectra were analyzed with OPUS software. The dried samples obtained for gravimetric analysis, were redissolved in deuterated solvent and used for FT-ATR measurements.

Size Exclusion Chromatography (SEC) THF: The molecular weight and polydispersity of synthesized polymers were analyzed via size exclusion chromatography (SEC). A Shimadzu modular system containing a DGU-12A degasser, an LC-10AT pump, an SIL-10AD automatic injector, a CTO-10A column oven and a RID-10A refractive index detector were used. A 50 x 7.8 mm guard column and four 300 x 7.8 mm linear columns (500, 103, 104, 105 Å pore size, 5 μm particle size) were used for analyses. Tetrahydrofuran (THF, HPLC Grade) with a flow rate of 1 mL min^{-1} was used as the mobile phase. The injection volume was 50 μL. The samples were prepared by dissolving 2-3 mg mL^{-1} of the analyte in tetrahydrofuran, followed by filtration through a 0.45 μm filter. The unit was calibrated using commercially available linear PMMA standards (0.5-1000 kDa, Polymer Laboratories). Chromatograms were processed using Cirrus 2.0 software (Polymer Laboratories).

Dynamic Light Scattering (DLS): Particle sizes (the average diameters and size distributions) were determined using a Malvern Zetaplus particle size analyzer (laser, 35mW, λ = 632 nm, angle = 90 °. Samples (1 droplet of latex; approx. 250 mg) were prepared in Milli-Q water for DLS analysis. The count rate was kept in between 100 and 500 kcps, thereby highly diluting the latex samples, leading to almost translucent solutions.

Ultraviolet Visible Spectroscopy (UV-Vis): UV-Vis spectra were recorded on a Varian Cary 300 UV-Vis-NIR spectrophotometer (scan rate 600 nm min^{-1}, continuous run from 200 to 800

nm) equipped with a temperature controller. 1 Droplet of latex (250 mg) was prepared in Milli-Q water for UV Analysis. UV-Vis spectra of the latexes after irradiation were recorded on a Shimadzu UV-2700 spectrophotometer equipped with a CPS-100 electronic temperature control cell positioner. A 50 µL droplet was diluted with a factor of 250 using Milli-Q water.

Fluorescence Intensity: The fluorescence intensities of the latexes were measured using a Cary Eclipse Fluorescence Spectrophotometer (Agilent Technologies). The excitation wavelengths were 293 nm and 348 nm for the latexes prepared with the UV and Visible light monomers, respectively. 1 Droplet of latex (250 mg) was prepared in Milli-Q water for UV Analysis and diluted with a factor of 1000 for fluorescence measurements. After irradiation, the excitation wavelengths used were 390 nm and 350 nm for the latexes prepared with the UV and Visible light monomers, respectively. A 10 µL droplet was diluted with a factor of 250 using Milli-Q water.

Centrifuge. The latexes were purified using a Hettich Universal 320 centrifuge set up with a Hettich fixed angle rotor 24 x 2 mL place. The sample was centrifuged at 14 500 rpm for 5 min and the precipitate was washed and then redispersed with Milli-Q water. This procedure was performed twice.

Gravimetric measurements: Monomer conversions were obtained by gravimetric measurements. After completion of the polymerization, a 2 mL aliquot was transferred to a weighted aluminium tray and reweighted. After drying 2 nights in a vacuum oven at 40 °C, the tray was reweighted and the conversion of monomer was calculated from the difference in weight based on the miniemulsion recipe.

Transmission Electron Microscopy (TEM): A FEI Tecnai G2 20 TEM operating at 200 kV was used to characterise the morphology and shape of the nanoparticles. Samples were prepared by diluting the final latexes in water. 1 drop of the diluted latex was deposited on a Formvar coated copper grid and left to dry for 1 minute. The samples were then stained for 1 h using a vapour

of osmium tetroxide (OsO_4) at 2 wt %. Staining was used to improve the visibility of the particle on the grid.

Scanning Electron Microsopy (SEM): A FEI NOVA NanoSEM 230 SEM at 5 kV and a spot size of 3 was used to characterise the morphology and shape of the nanoparticles. Samples were prepared by depositing the dried latex powder onto double sided carbon tape. The samples were then coated with a 5 nm platinum coating under an angle of 45 °. The coating was used to improve the visibility of the particles on the SEM holder.

Electrospray Ionization Mass Spectrometry (ESI-MS): Samples were run on an Orbitrap LTQ XL ion trap mass spectrometer using a nanospray (nanoelectrospray) ionization source to generate ions from the analyte in solution. The instrument was calibrated with a standard calibration solution (as outlined in the instrument manual) on the day of analysis using direct infusion into the ESI source. The instrument conditions were optimized for sensitivity of the compounds using LC tune software. The analysis was carried out in positive ion mode using the orbitrap FTMS analyser at a resolution of 60 000. Samples, at a concentration of ca. 1 μg mL^{-1} in THF / methanol (3/2 v/v%), were injected into a glass needle and inserted into the nanospray source. Ions generated were measured over the mass range 150 to 2000 Da window. Data was acquired in full scan mode over 30 seconds. Data was analysed using the Qual Browser feature in Xcalibur 2.1.

X-ray Photoelectron Spectroscopy (XPS): XPS samples were prepared by drying the liquid latex in a vacuum oven at 40 °C for 2 nights, immediately after sampling from the reactor vessel. The powder-like material was subsequently casted on Indium foil for XPS analysis. X-Ray Photoelectron Spectroscopy analysis was performed under incident conditions, the X-ray penetration depth being lower than 5 nm (ultrathin layer method). A Kratos Axis ULTRA XPS incorporating a 165 mm hemi-spherical electron energy analyzer was used. The incident radiation was monochromatic A1 X-rays (1486.6 eV) at 225W (15 kV, 15 mA). Survey (wide) scans were taken at analysing pass energy of 160 eV and multiplex (narrow) higher resolution

scans at 20 eV. Survey scans were carried out over 1360-0 eV binding energy range with 1.0 eV steps and a dwell time of 100 ms. Narrow higher resolution scans were run with 0.2 eV steps and 250 ms dwell time. Base pressure in the analysis chamber was 1.0 10^{9} Torr and during sample analysis 1.0 10^{8} Torr. The experimental data were analysed using the software Avantage.

Atomic percentage calculations

The theoretical atomic percentage were calculated from the mole number of each reactant. Water and AIBN were excluded from the calculation. Hydrogen atoms were also excluded from calculation since it is not detected by XPS. Nitrogen and bromine atomic percentage were calculated as follows:

$$Nitrogen\ Atomic\ \% = \frac{x\ T_z}{a\ MMA + b\ T_z + c\ SDS + d\ Br} \times 100 \qquad \text{Equation S1}$$

$$Bromine\ Atomic\ \% = \frac{y\ Br}{a\ MMA + b\ T_z + c\ SDS + d\ Br} \times 100 \qquad \text{Equation S2}$$

Where x and y are the number of nitrogen and bromine and a, b, c and d refer to the number of heavy atoms (*i.e.* detected by XPS) in MMA, Tz monomer, SDS and the Br-reactant (BPM or BVA), respectively. For clarification, those values are reported in the table below.

Value	PMMA-Tz-UV	PMMA-Tz-Vis	PMMA-Tz-UV-BPM	PMMA-Tz-UV-BVA	PMMA-Tz-Vis-BPM	PMMA-Tz-Vis-BVA
x	4	4	3	2	3	2
y	0	0	1	1	1	1
a	7	7	7	7	7	7
b	38	46	38	38	46	46
c	17	17	17 / 0 [a]	17 / 0 [a]	17 / 0 [a]	17 / 0 [a]
d	0	0	14	8	14	8

[a] When the nanoparticles are washed, no SDS is present on the surface so the SDS content is removed from calculation.

The experimental mole percentage of nitrogen at the nanoparticles surface after polymerization was calculated using the experimental XPS results. 3 equations with 3 unknowns were established and solved with the software *Wolfram Mathematica*:

X = Tz mole fraction at the surface
Y = SDS mole fraction at the surface
Z = MMA mole fraction at the surface

$$X + Y + Z = 1$$

$$S(A\%) = \frac{Y}{7\,Z + 38 \text{ or } 46\,X + 17\,Y}$$

$$N(A\%) = \frac{4\,X}{7\,Z + 38 \text{ or } 46\,X + 17\,Y}$$

1.3. Synthesis of UV light tetrazole monomer

Synthesis of 11-hydroxyundecyl (E)-4-((2-tosylhydrazineylidene)methyl)benzoate

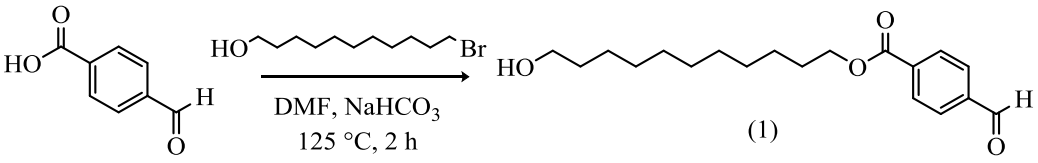

Scheme S1. Reaction scheme for the synthesis of 11-hydroxyundecyl 4-formylbenzoate

4.60 g formylbenzoic acid (30.6 mmol, 1.0 eq.), 5.14 g sodium hydrogen carbonate (61.2 mmol, 2.0 eq.) and 10.0 g 11-bromoundecan-1-ol (39.8 mmol, 1.3 eq.) were dissolved in 40 mL of DMF. The mixture was heated to 125 °C for 2 h and then cooled down to ambient temperature. The salt was filtered out and 200 mL ethyl acetate were added. The crude reaction mixture was then washed 3 times with brine (40 mL) and the organic layer was dried over magnesium sulphate. The solvent was evaporated under reduced pressure and the obtained white paste was used without further purification (8.80 g, yield 89.7%).

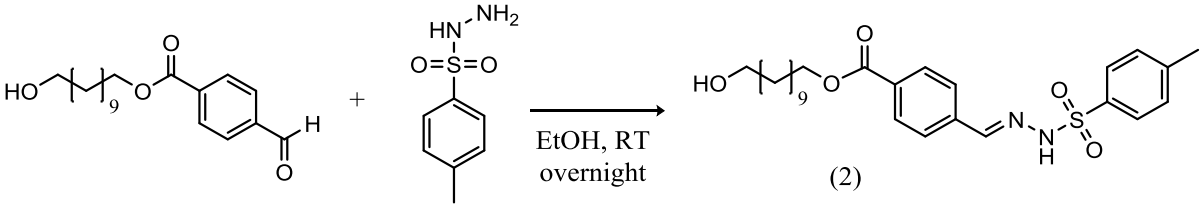

Scheme S2. Reaction scheme for the synthesis of 11-hydroxyundecyl (E)-4-((2-tosylhydrazineylidene)methyl)benzoate.

Compound (**1**) (8.80 g, 27.4 mmol, 1.0 eq.) was dissolved in 80 mL ethanol and 5.63 g p-toluenesulfonylhydrazide (30.2 mmol, 1.1 eq.) was added to the solution and stirred overnight. Subsequently, ethanol was evaporated under reduced pressure and the obtained white paste was dried under high vacuum. ^{1}H NMR (600 MHz , DMSO-d_6) δ [ppm] = 11.71 (s, 1 H), 8.30 (s, 1 H), 7.97 – 7.94 (m, 2 H), 7.78 – 7.76 (m, 2 H), 7.71 – 7.68 (m, 2 H), 7.43 – 7.40 (m, 2 H), 4.38 – 4.32 (m, 2 H), 4.27 – 4.25 (m, 2 H), 3.47 – 3.44 (m, 2 H), 2.36 (s, 3H), 1.72 – 1.67 (m, 2 H), 1.41 – 1.35 (m, 2 H), 1.32 -1.24 (m, 14 H); ^{13}C NMR (151 MHz , DMSO-d_6) δ [ppm] = 165.7, 145.9, 144.0, 138.45, 136.5, 130.2, 129.9, 128.1, 127.7, 65.3, 61.2, 56.5, 33.3, 29.6, 29.4, 29.1, 28.6, 25.9, 21.5 (Figure S1 and Figure S2).

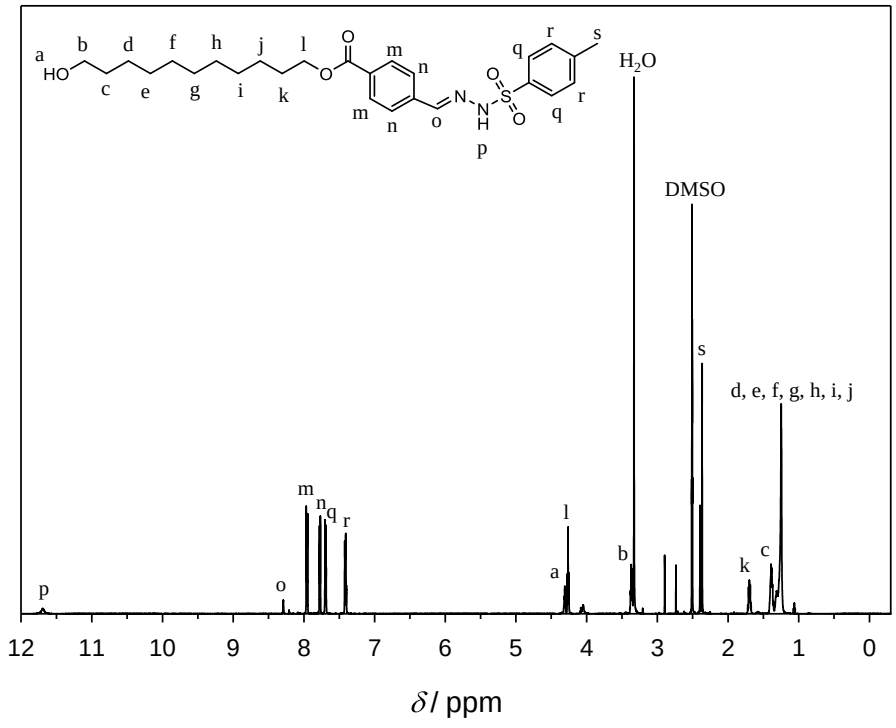

Figure S1. ^{1}H NMR spectrum (600 MHz, 256 scans, DMSO-d_6) of 11-hydroxyundecyl (E)-4-((2-tosylhydrazineylidene)methyl) benzoate (2) : δ 11.69 (s, 1H), 8.01 – 7.90 (m, 2H), 7.82 – 7.75 (m, 1H), 7.69 (dd, J = 8.4, 1.8 Hz, 2H), 7.41 (dd, J = 8.1, 6.2 Hz, 2H), 4.43 – 4.20 (m, 3H), 3.44 (dt, J = 10.6, 5.3 Hz, 1H), 3.37 (dd, J = 7.2, 3.2 Hz, 8H), 2.38 (d, J = 18.8 Hz, 3H), 1.69 (q, J = 6.9 Hz, 1H), 1.38 (h, J = 7.3, 6.8 Hz, 3H), 1.34 – 1.19 (m, 9H), 1.06 (t, J = 7.0 Hz, 2H).

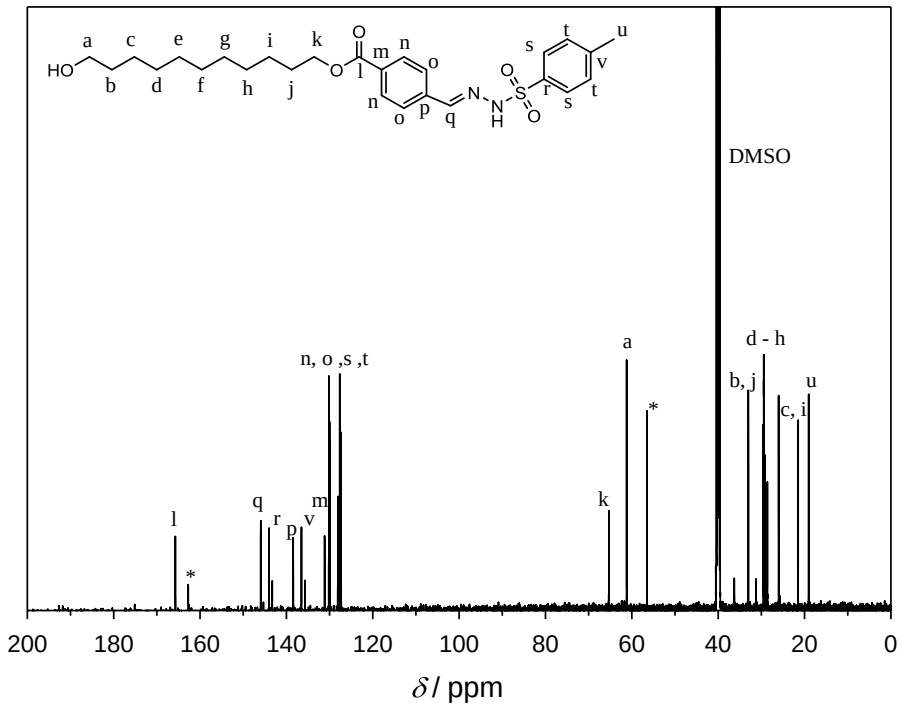

Figure S2. ^{13}C NMR spectrum (600 MHz, 1024 scans, DMSO-d_6) of 11-hydroxyundecyl (E)-4-((2-tosylhydrazineylidene)methyl)benzoate (2).

Synthesis of 11-hydroxyundecyl 4-(2-(4-methoxyphenyl)-2H-tetrazol-5-yl)benzoate (Tz-UV precursor)

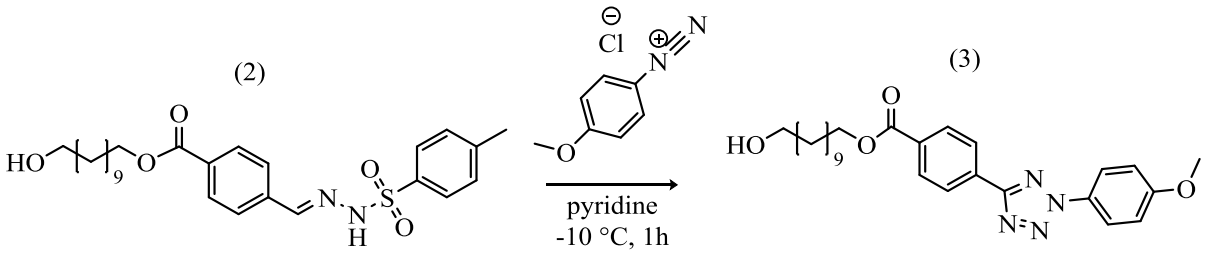

Scheme S3. Reaction scheme for the synthesis of 11-hydroxyundecyl 4-(2-(4-methoxyphenyl)2H-tetrazol-5-yl)benzoate).

2.0 g p-anisidine (16.3 mmol, 1.0 equiv.) was dissolved in 40 mL of a solvent mixture of HCl/water/ethanol (1:3:3). Subsequently, 1.12 g sodium nitrite (16.3 mmol, 1.00 equiv.) was dissolved in a second round bottom flask in 7 mL of solvent mixture of ethanol and water (1:1). The solutions were slowly combined and stirred for 10 minutes at 0 °C. 8.0 g of compound (**2**) (16.4 mmol, 1.0 equiv.) was dissolved in 80 mL of pyridine and cooled to -10 °C. The prepared diazonium salt was then slowly added. After complete addition, the solution was stirred at 0 °C for 1 h and 3 h at ambient temperature. The red solution was precipitated into 1 L of a 1 M

hydrochloric solution. The raw product was recrystallized three times from a mixture cyclohexane/ethyl acetate (10/1). After drying under high vacuum, compound (**3**) was obtained as a pink solid (2.81 g, yield 37 %). ^{1}H NMR (600 MHz , DMSO-d_6) δ [ppm] = 8.27-8.26 (d, 2 H), 8.13-8.12 (d, 2 H), 8.07 – 8.05 (d, 2 H), 7.22 – 7.19 (d, 2 H), 4.34 – 4.32 (t, 1 H), 4.29 – 4.27 (t, 2 H), 3.86 (s, 3H), 3.36 – 3.38 (m, 2H), 1.73 – 1.68 (m, 2 H), 1.41 – 1.36 (m, 4 H), 1.33 -1.32 (m, 2 H), 1.27 - 1.23 (m, 10 H); ^{13}C NMR (151 MHz , DMSO-d_6) δ [ppm] = 165.6,163.8, 160.9, 132.0, 131.1, 130.5, 129.9, 127.3, 122.1, 115.6, 65.5, 61.2, 56.2, 33.0, 29.57, 29.5, 29.5, 29.4, 29.2, 28.6, 26.0, 25.9 (Figure S3 and Figure S4).

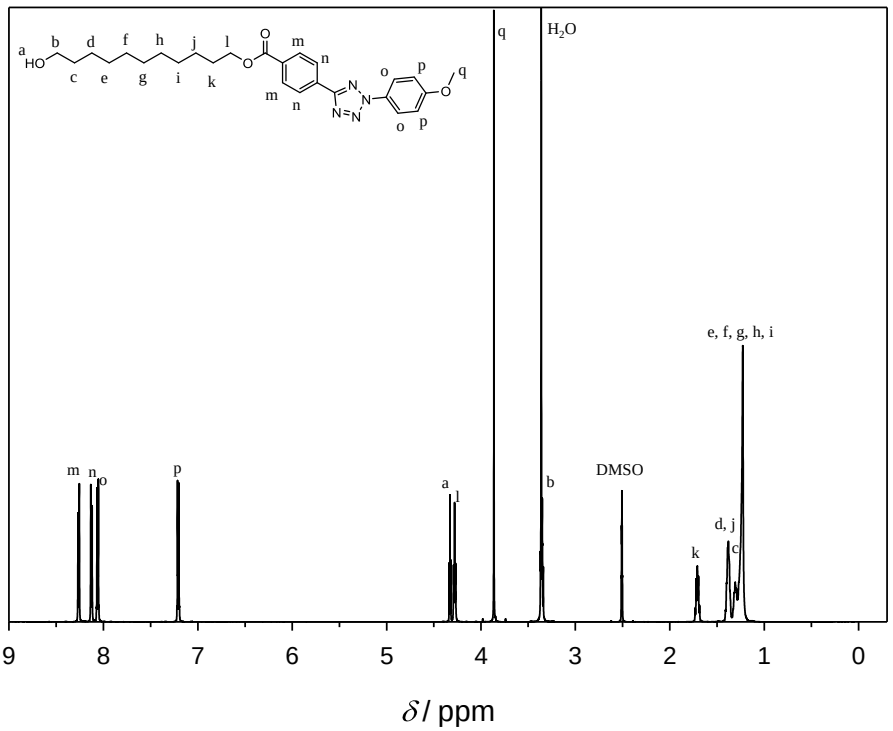

Figure S3. ^{1}H NMR spectrum (600 MHz, 256 scans, DMSO-d_6) of 11-hydroxyundecyl 4-(2-(4-methoxyphenyl)-2H-tetrazol-5-yl)benzoate (Tz-UV precursor, 3): δ 8.29 – 8.24 (m, 1H), 8.15 – 8.10 (m, 1H), 8.09 – 8.03 (m, 1H), 7.24 – 7.18 (m, 1H), 4.35 – 4.25 (m, 2H), 3.86 (s, 2H), 3.39 – 3.32 (m, 1H), 1.71 (p, *J* = 6.8 Hz, 1H), 1.43 – 1.34 (m, 3H), 1.31 (s, 1H), 1.27 – 1.21 (m, 6H).

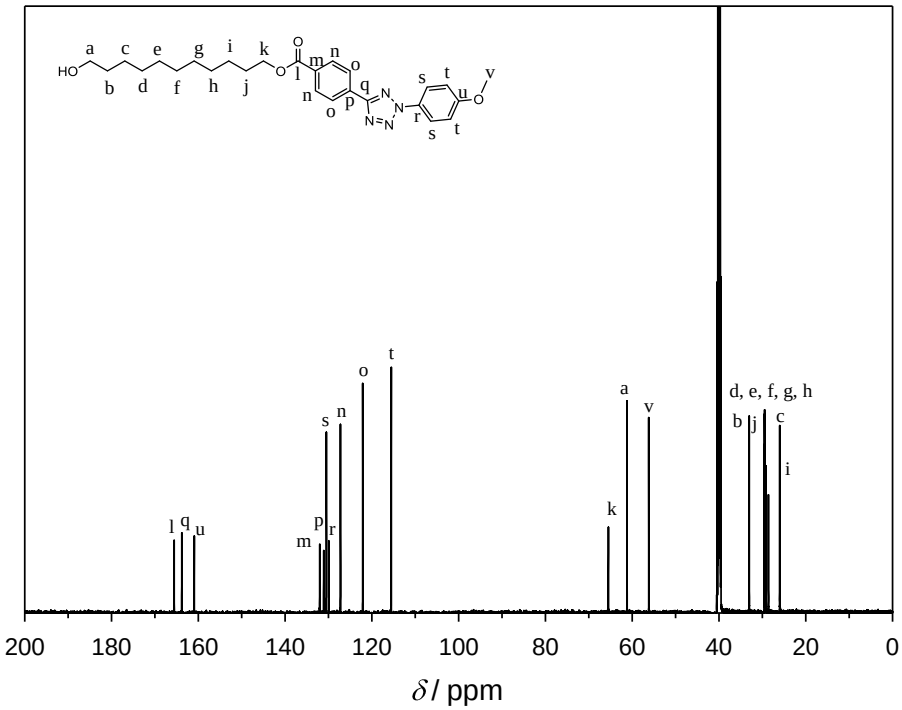

Figure S4. ^{13}C NMR spectrum (600 MHz, 1024 scans, DMSO-d_6)of 11-hydroxyundecyl 4-(2-(4-methoxyphenyl)-2H-tetrazol-5-yl)benzoate (Tz-UV precursor, 3).

Synthesis of 11-(acryloyloxy)undecyl 4-(2-(4-methoxyphenyl)-2H-tetrazol-5-yl)benzoate (Tz-UV monomer)

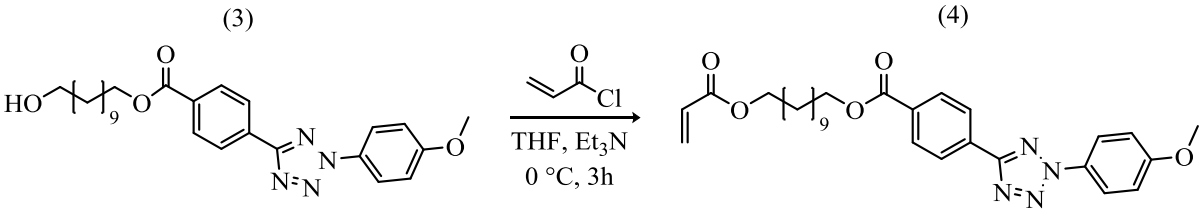

Scheme S4. General reaction scheme of the synthesis of 11-(acryloyloxy)undecyl 4-(2-(4-methoxyphenyl)-2H-tetrazol-5-yl)benzoate (Tz-UV monomer).

In a flame dried schlenk flask, 2.81 g (6.03 mmol, 1.0 eq.) compound (**3**) and 10 mL (71.69 mmol, 11.89 eq.) triethylamine were dissolved in 150 mL of dry THF and subsequently cooled to 0 °C. 6 mL (73.58 mmol, 12.2 eq.) acryloyl chloride was slowly added under an inert atmosphere. The reaction was stirred for three hours at 0°C and then over night at ambient temperature. The salt was filtered out and the solvent was evaporated under reduced pressure. The crude product was purified by flash chromatography (silica gel, cyclohexane/ethyl acetate, 95/5 v/v) to obtain 1.00 g of a yellowish powder (yield 32 %). ^{1}H NMR (600 MHz , $CDCl_3$) δ [ppm] = 8.26-8.25 (d, 2 H), 8.13-8.11 (d, 2 H), 8.07 – 8.04 (d, 2 H), 7.02 – 7.00 (d, 2 H), 6.34 – 6.31 (d, 1 H), 6.07 - 6.03 (m, 1 H), 5.75 – 5.73 (d, 1H), 4.30 – 4.28 (t, 2 H), 4.09 – 4.07 (t, 2 H), 3.84 (s, 3H), 1.75 – 1.71 (m, 2 H), 1.62 – 1.58 (m, 2 H), 1.42 -1.37 (m, 2 H), 1.30 - 1.23 (m, 12 H); ^{13}C NMR (151 MHz , $CDCl_3$) δ [ppm] = 166.6, 166.1, 160.7, 132.1, 131.3, 130.4, 130.2, 128.7, 126.9, 121.5, 114.8, 65.5, 64.7, 55.7, 29.5, 29.3, 29.3, 28.7, 28.6, 26.1, 25.9; HRMS $[M+Na]^+$ m/z: calcd for $C_{29}H_{36}N_4O_5$, Na^+ 543.2592 found 543.2580 (Figure S5 and Figure S6).

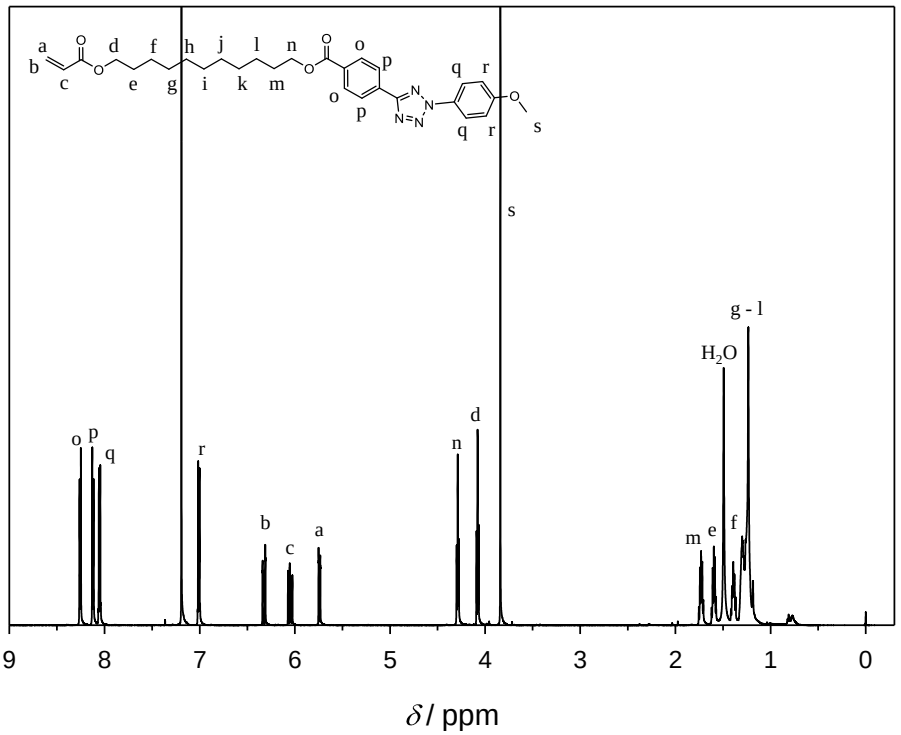

Figure S5. ^{1}H NMR spectrum (600 MHz, 256 scans, $CDCl_3$) of 11-(acryloyloxy)undecyl 4-(2-(4-methoxyphenyl)-2H-tetrazol-5-yl)benzoate (Tz-UV monomer, **4**): δ 8.26 (dd, *J* = 7.8, 1.1 Hz, 3H), 8.15 – 8.09 (m, 4H), 8.10 – 8.02 (m, 4H), 7.19 (s, 3H), 7.03 – 6.98 (m, 3H), 6.32 (ddd, *J* = 17.3, 1.5, 0.7 Hz, 2H), 6.05 (ddd, *J* = 17.2, 10.4, 0.7 Hz, 2H), 5.74 (ddd, *J* = 10.4, 1.5, 0.7 Hz, 2H), 4.29 (t, *J* = 6.7 Hz, 4H), 4.08 (td, *J* = 6.8, 0.7 Hz, 4H), 3.84 (d, *J* = 0.7 Hz, 5H), 1.72 (q, *J* = 7.1 Hz, 4H), 1.59 (q, *J* = 7.0 Hz, 4H), 1.49 (s, 11H), 1.39 (q, *J* = 7.7 Hz, 4H), 1.29 (d, *J* = 4.7 Hz, 4H), 1.19 (s, 1H), 0.77 (s, 2H).

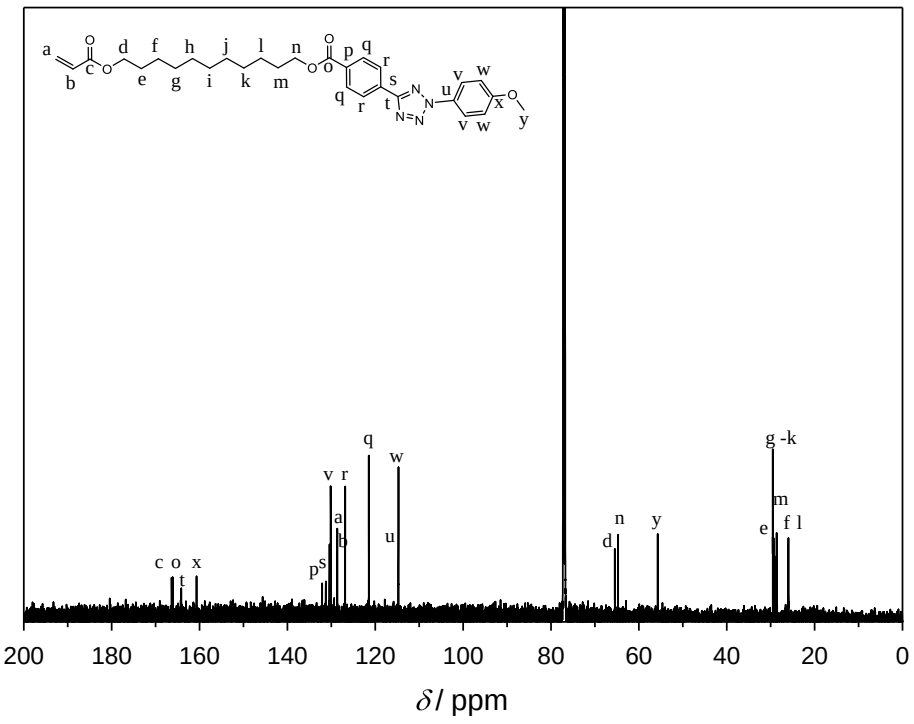

Figure S6. ^{13}C NMR spectrum (600 MHz, 1024 scans, $CDCl_3$) of 11-(acryloyloxy)undecyl 4-(2-(4-methoxyphenyl)-2H-tetrazol-5-yl)benzoate (Tz-UV monomer, 4).

1.4. Synthesis of Visible light tetrazole monomer

Synthesis of 11-hydroxyundecyl 4-(2-(pyren-1-yl)-2H-tetrazol-5-yl)benzoate (Tz-Vis precursor)

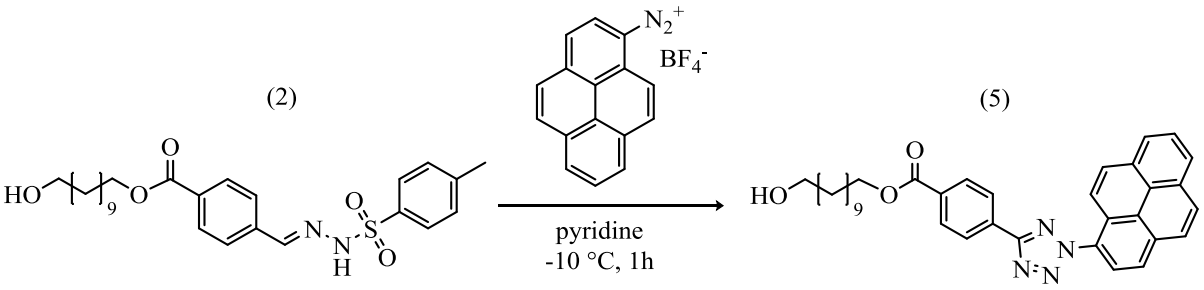

Scheme S5. General reaction scheme of the synthesis of 11-hydroxyundecyl 4-(2-(pyren-1-yl)-2H-tetrazol-5-yl)benzoate (Tz-Vis precursor).

0.258 g 1-aminopyrene (1.19 mmol, 1.0 equiv.) was dissolved in 30 mL THF and cooled to -21°C under an argon atmosphere. In a second round bottom flask 1.07 g sodium tetrafluoroborate (9.76 mmol, 8.1 eq.) was dissolved in 10.5 mL tetrafluoroboric acid (50 wt%) and in 4.5 mL water under an argon atmosphere. This solution was slowly added to the aminopyrene solution and stirred for 20 min at -21°C. Subsequently, 97.0 mg sodium nitrite (1.41 mmol, 1.21 equiv.) was dissolved in a third round bottom flask in 2 mL water. The sodium nitrite solution was slowly combined to form an orange precipitate. The reaction mixture was stirred for another 20 minutes at -21°C. In parallel, 0.7 g compound (**2**) (1.43 mmol, 1.3 eq.) was dissolved in 20 mL pyridine and cooled to 0 °C. The orange diazonium salt formed previously was collected and added to the pyridine solution. The combined reaction mixture was stirred for 1 h and then precipitated into 100 mL of a 1 M hydrochloric acid solution. The raw product was recrystallized once from acetonitrile. After drying under high vacuum, compound (**5**) was obtained as a brown solid (232 mg, yield 35%). ^{1}H NMR (600 MHz , $CDCl_3$) δ [ppm] = 8.35 – 7.99 (m, 13 H), 4.32 – 4.28 (t, 2 H), 3.54 – 3.57 (t, 2 H), 1.75 – 1.70 (m, 2 H), 1.54 – 1.46 (m, 2 H), 1.40 -1.36 (m, 2 H), 1.32 – 1.17 (m, 13 H); ^{13}C NMR (151 MHz , $CDCl_3$) δ [ppm] = 166.1, 165.6, 132.8, 132.3, 131.1, 131.0, 130.5, 130.3, 130.1, 130.1, 129.4, 129.0,

127.1, 127.0, 126.9, 126.7, 126.3, 125.1, 124.9, 124.8, 124.0, 122.7, 121.4, 65.5, 63.1, 32.8, 29.6, 29.5, 29.4, 29.3, 28.7, 26.1, 25.8 (Figure S7 and Figure S8).

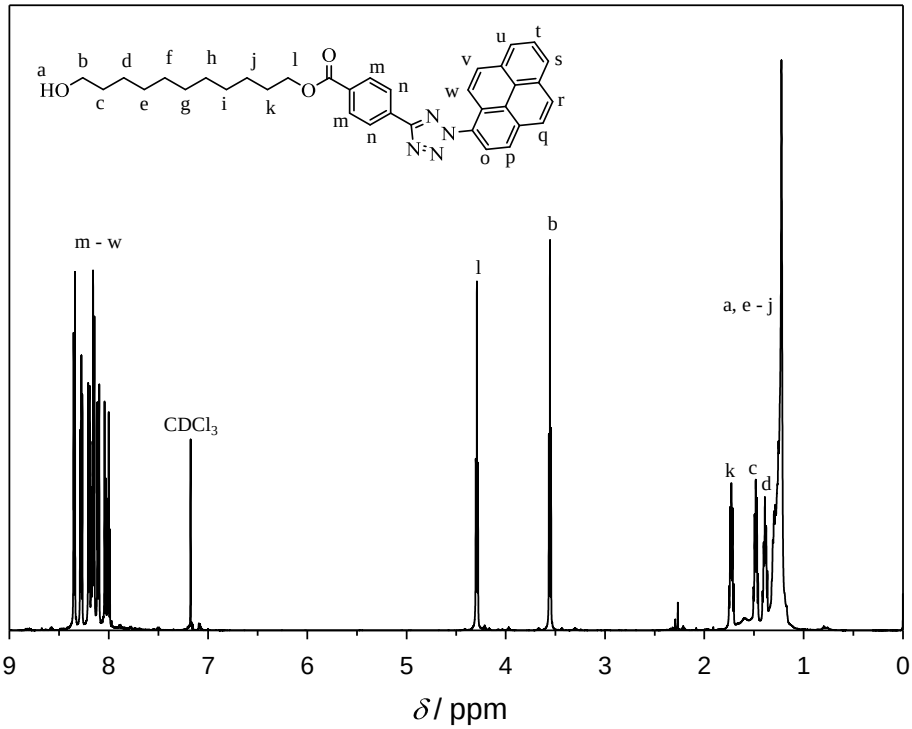

Figure S7. ^{1}H NMR spectrum (600 MHz, 256 scans, $CDCl_3$) of 11-hydroxyundecyl 4-(2-(pyren-1-yl)-2H-tetrazol-5-yl)benzoate (Tz-Vis precursor, 5): δ 8.37 – 8.31 (m, 2H), 8.28 (dd, *J* = 8.7, 5.1 Hz, 2H), 8.25 – 8.08 (m, 6H), 8.07 – 7.97 (m, 2H), 4.29 (t, *J* = 6.7 Hz, 2H), 3.55 (t, *J* = 6.6 Hz, 2H), 1.73 (p, *J* = 6.8 Hz, 2H), 1.48 (dt, *J* = 8.1, 6.5 Hz, 2H), 1.43 – 1.35 (m, 2H), 1.28 (s, 1H), 1.33 – 1.24 (m, 1H), 1.22 (s, 4H), 1.22 (s, 1H).

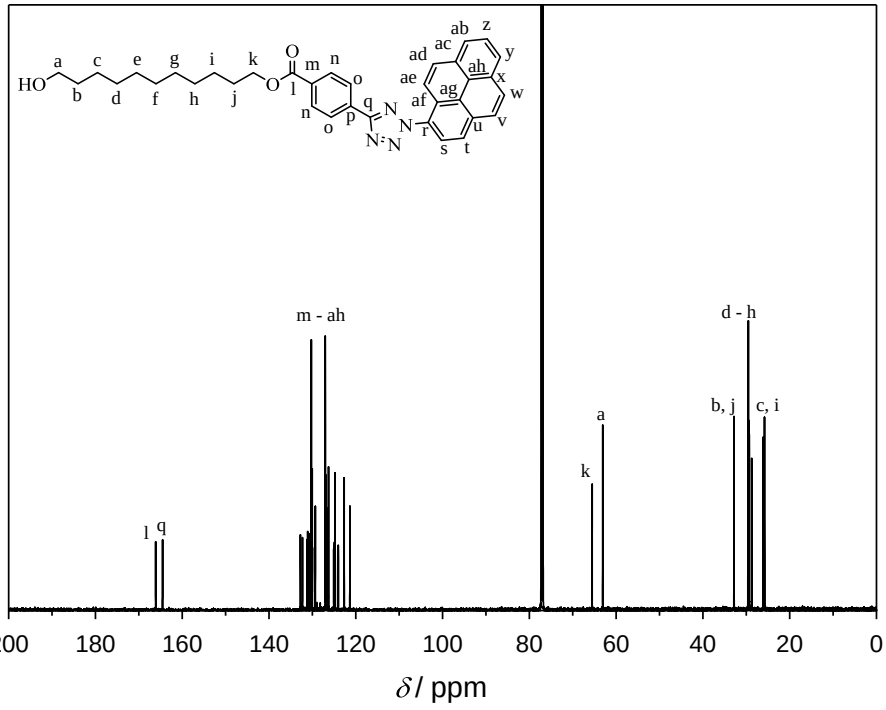

Figure S8. ^{13}C NMR spectrum (600 MHz, 1024 scans, $CDCl_3$) of 11-hydroxyundecyl 4-(2-(pyren-1-yl)-2H-tetrazol-5-yl)benzoate (Tz-Vis precursor, 5)).

Synthesis of 11-(acryloyloxy)undecyl 4-(2-(pyren-1-yl)-2H-tetrazol-5-yl)benzoate (Tz-Vis monomer)

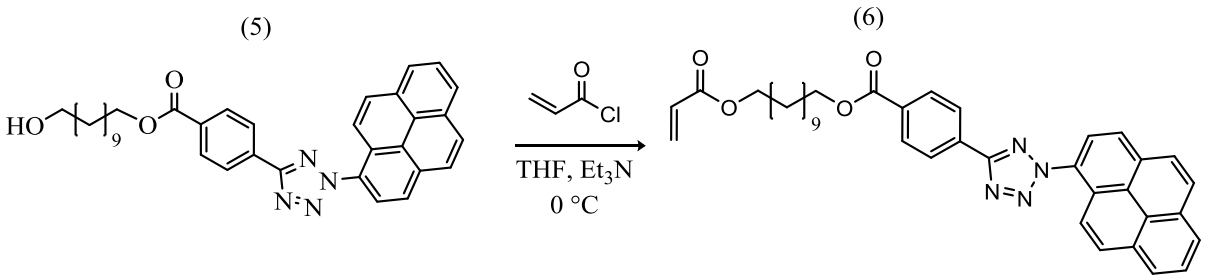

Scheme S6. General reaction scheme of the synthesis of 11-(acryloyloxy)undecyl 4-(2-(pyren-1-yl)-2H-tetrazol-5-yl)benzoate (Tz-Vis monomer).

In a flame dried schlenk flask, 1.38 g (2.47 mmol, 1.0 eq.) compound (**5**) and 5.3 mL (37.99 mmol, 15.4 eq.) triethylamine were dissolved in 150 mL of dry THF and subsequently cooled to 0 °C. 3.4 mL (41.69 mmol, 16.8 eq.) acryloyl chloride was slowly added under an inert atmosphere. The reaction was stirred for three hours at 0 °C and then over night at ambient temperature. The salt was filtered out and the solvent was evaporated under reduced pressure. The crude product was purified by flash chromatography (silica gel, cyclohexane/ethyl acetate, 70/30 v/v) to obtain 0.61 g of a pink powder (yield 40.2 %). ^{1}H NMR (600 MHz , $CDCl_3$) δ [ppm] = 8.39- 8.05 (m, 13 H), 6.34 – 6.31 (d/d, 1 H), 6.07 – 6.02 (d/d, 1 H), 5.75 – 5.73 (d/d, 1 H), 4.32 – 4.28 (t, 2 H), 4.09 – 4.07 (t, 2 H), 1.77 – 1.72 (m, 2 H), 1.62 – 1.58 (m, 2 H), 1.43 -1.38 (m, 2 H), 1.32 – 1.19 (m, 12 H); ^{13}C NMR (151 MHz , $CDCl_3$) δ [ppm] = 166.32, 164.5, 131.2, 130.4, 130.3, 130.1, 129.4, 128.7, 127.1, 126.9, 126.8, 126.4, 125.2, 125.1, 124.8, 124.2, 122.8, 121.5, 65.5, 64.7, 29.5, 29.3, 28.7, 28.6, 26.1, 25.9 (Figure S9). HRMS $[M+Na]^+$ m/z: calcd for $C_{38}H_{38}N_4O_4$, Na^+ 637.2792 found 637.2788.

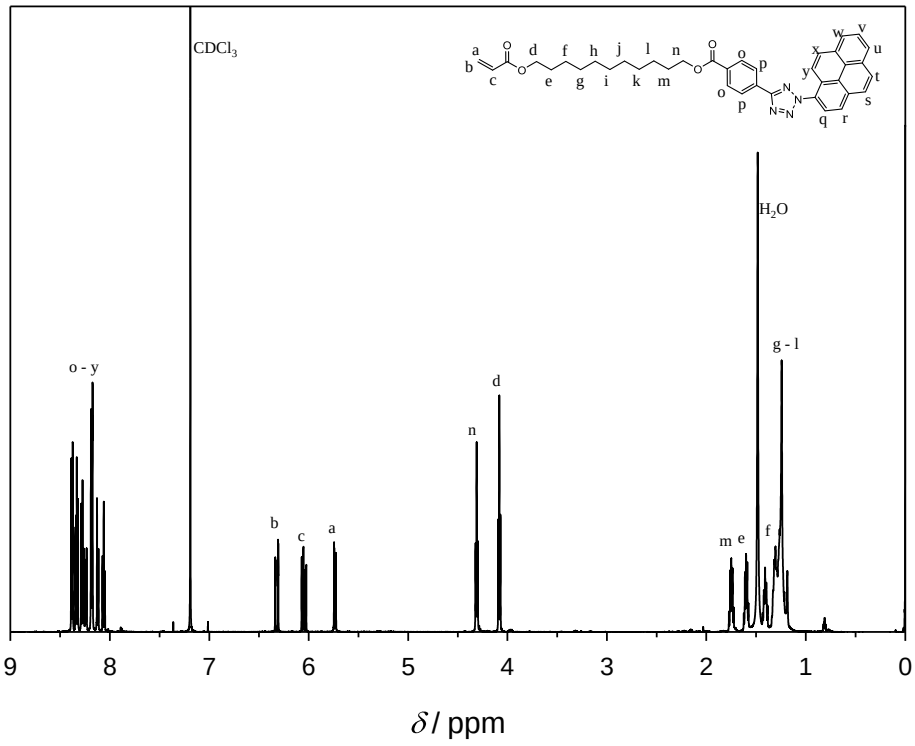

Figure S9. ^{1}H NMR spectra (600 MHz, 256 scans, $CDCl_3$) spectrum of of 11-(acryloyloxy)undecyl 4-(2-(pyren-1-yl)-2H-tetrazol-5-yl)benzoate (Tz-Vi**s** monomer, **6**): δ 8.50 – 8.12 (m, 11H), 6.35 (dd, J = 17.3, 1.6 Hz, 1H), 6.10 (dd, J = 17.3, 10.4 Hz, 1H), 5.79 (dd, J = 10.4, 1.6 Hz, 1H), 4.36 (t, J = 6.7 Hz, 2H), 4.12 (t, J = 6.7 Hz, 2H), 1.88 – 1.76 (m, 2H), 1.66 (p, J = 6.8 Hz, 2H), 1.53 (s, 10H), 1.29 (d, J = 23.4 Hz, 13H).

1.5. Miniemulsion

For a typical miniemulsion, the oil phase was prepared by adding MMA (0.9 g, 8.99 10^{-3} mole, 9 wt % rel. to water) , HD (0.072 g, 3.18 10^{-4} mole, 8 wt % rel. to monomer), 1,2-dichloroethane (0.1 g, 1.01 10^{-3} mole, 1 wt% rel. to water), AIBN (1.8 mg, 1.07 10^{-5} mole, 0.01 M rel. to the organic phase) and the tetrazole (Tz) monomer (variable weight, depending on recipe; 2.5 wt% up to 10 wt % rel. to monomer) to a small glass vial with a stirring bar. The vial was completely covered in aluminium foil and the Tz monomer was added as the last reagent. The solution was stirred at 300 rpm for 30 min at room temperature. Next, the oil phase was added to the water phase which was prepared in a vial (20 mL) covered with aluminium foil and consisted of Milli-Q water (10 g, 5.55 10^{-1} mole) and SDS (0.08 g, 2.70 10^{-4} mole, 8 wt % rel. to the organic phase) premixed at 300 rpm for 30 min. The mixture was homogenized by ultrasonication

(Branson Digital Sonifier) in an ice bath at 50% amplitude for 10 min. The miniemulsion was kept in the vial, with a stirring bar and sealed with a rubber septum, parafilm and steel wire. The vial was degassed for 30 min under nitrogen in an ice bath, and subsequently placed in a preheated oil bath (70 °C). Polymerization was conducted for 24 h under nitrogen atmosphere, completely shielded from light. After 24 h, the vial was taken out of the oil bath, opened to the air and the polymerization was stopped by placing the vial in liquid nitrogen. Conversion measurements were performed by taking a 2 mL aliquot from the vial immediately after stopping the polymerization.

1.6. NITEC/NICAL reaction

The latexes were irradiated in a *Luzchem* LZC-4V photoreactor using 6 LZC-UVB lamps, emitting at 300 nm (Figure S10) or 3 x 3W Blue LED emitting at 415 nm (Figure S11). The internal chamber was ventilated to maintain ambient temperature during the entire experiment. The samples were stirred employing the built-in LZC-D recessed magnetic stirrer.

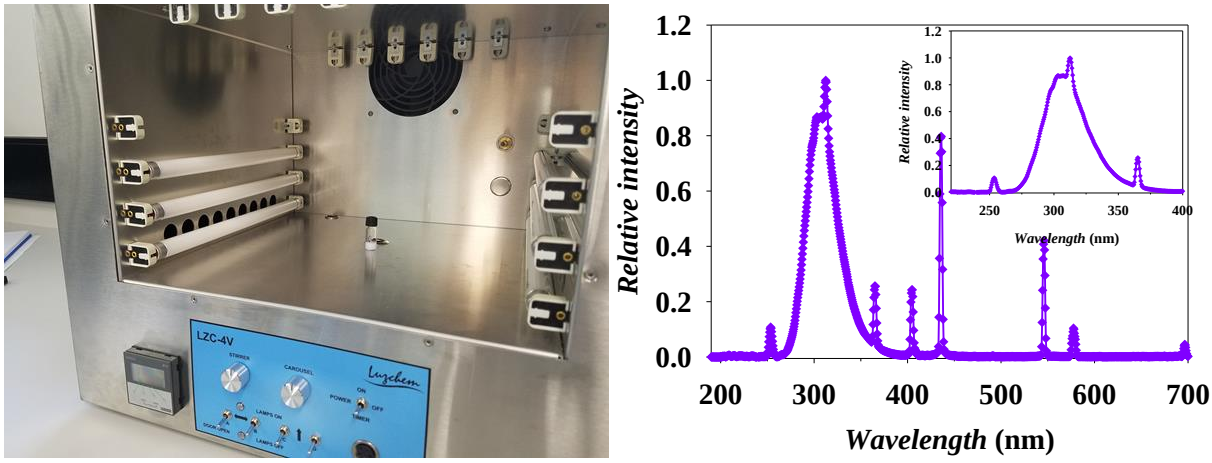

Figure S10. Picture of the set-up for the UV-B reaction (left) and emission spectrum (right)

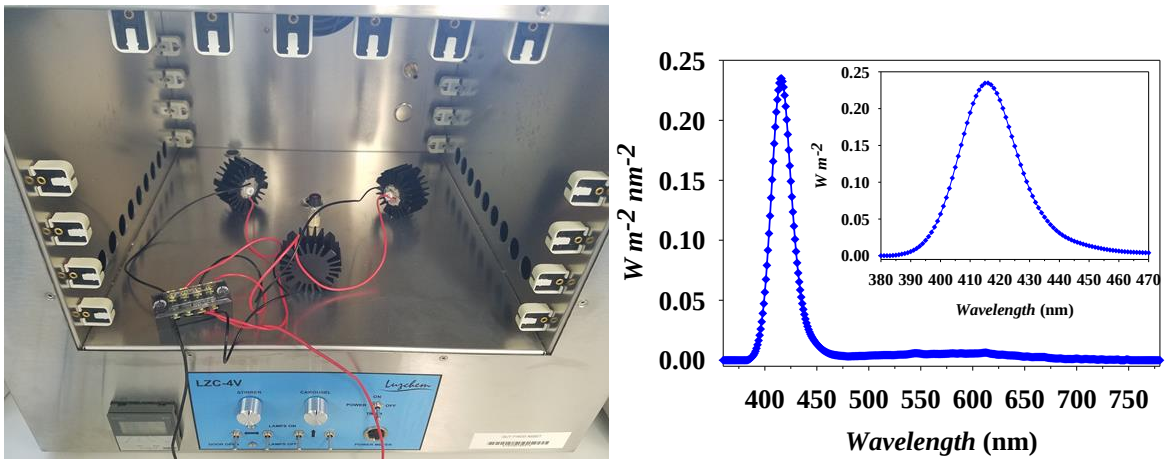

Figure S11. Picture of the set-up for the visible reaction (left) and emission spectrum of the 3 x 3W Blue LED (right)

UV-tetrazole

In a typical recipe, 0.0085 g N(-4-bromophenyl)-maleimide (0.0337 mmol, 1.0 eq.) was diluted in 2.00 mL of water. 2.00 mL (2.18 g) latex containing 10 wt% Tz-UV (0.0335 mmol Tz-UV, 1.0 eq.) was added and the mixture was stirred for 10 minutes. The stock solution was divided in 12 GPC vials (1.5 mL, 32 x 11.6 mm, clear glass, flat bottom, VWR) and exposed to UV-B light (300 nm) for preset time intervals (1 to 120 minutes). Following irradiation, a 10 µL aliquot of each sample was analyzed by UV and fluorescence spectroscopy after 250-fold dilution. Half of the latex was centrifuged (14 500 rpm, 5 minutes) and the precipitate washed with water twice. The precipitate was then dried under reduced pressure and pressed on Indium foil for XPS analysis. The rest of the sample was evaporated under reduced pressure and the dry latex was dissolved in CD_2Cl_2 for ^1H NMR analysis.

Visible tetrazole

In a typical recipe, 0.0074 g N(-4-bromophenyl)-maleimide (0.029 mmol, 1.0 eq.) was diluted in 2.00 mL of water. 2.00 mL (2.21 g) latex containing 10 wt% Tz-Vis (0.028 mmol Tz-Vis, 1.0 eq.) was added and the mixture was stirred for 10 minutes. The stock solution was divided in 12 GPC vials (1.5 mL, 32 x 11.6 mm, clear glass, flat bottom, VWR) and exposed to 3 x 3W

Blue LED (415 nm) for preset time intervals (1 to 120 minutes). Following irradiation, a 10 µL aliquot of each latex was analyzed by UV and fluorescence spectroscopy after 250-fold dilution. Half of the latex was centrifuged (14 500 rpm, 5 minutes) and the precipitate washed with water twice. The precipitate was then dried under reduced pressure and pressed on Indium foil for XPS analysis. The rest of the sample was evaporated under reduced pressure and the dry latex was dissolved in CD_2Cl_2 for ^1H NMR analysis.

Small test reaction

0.00993 g 11-hydroxyundecyl 4-(2-(pyren-1-yl)-2H-tetrazol-5-yl)benzoate - Tz-Vis precursor, **5 – (**0.017 mmol, 1.0 eq.) and 0.00449 g BVA (0.024 mmol, 1.4 eq.) were dissolved in 40 mL of DCM. The tetrazole stock solution was degassed with argon for 10 minutes. 5 mL was transferred into a vial and irradiated with 3 x 3W Blue LED (415 nm) for 60 minutes. Following irradiation, a 50 µL aliquot was analyzed by fluorescence spectroscopy after 100-fold dilution. The rest of the sample was evaporated under reduced pressure and the crude solid was dissolved in $CDCl_3$ for ^1H NMR analysis.

0.00137 g 11-hydroxyundecyl 4-(2-(pyren-1-yl)-2H-tetrazol-5-yl)benzoate - Tz-Vis precursor, **5 –** (0.002 mmol, 1.0 eq.) and 0.00135 g folic acid (0.003 mmol, 1.3 eq.) were dissolved in 1 mL of DMSO-d_6. The sample was then irradiated with 3 x 3W Blue LED (415 nm) for 60 minutes. Following irradiation, a 10 µL aliquot was analyzed by fluorescence spectroscopy after 300-fold dilution in DMSO. ^1H NMR spectra were recorded on the crude sample.

2. Analysis results of the polymer latexes prepared using varying UV light Tz amounts.

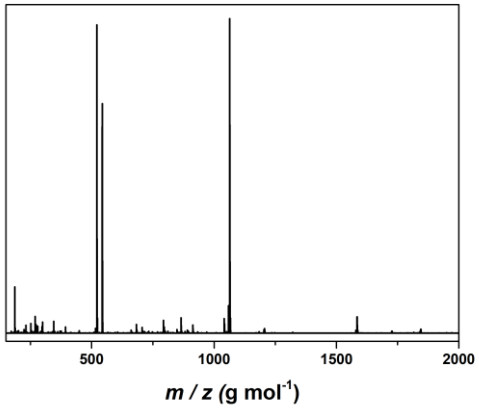

Figure S12. ESI-MS of Tz-UV monomer in THF / MeOH (3/2 v/v%) after 10 min of ultra sonication at 50 % intensity using a high shear probe.

Table S1. ESI-MS masses of Tz-UV monomer in THF / MeOH (3/2 v/v%) after 10 min of ultra sonication at 50 % intensity using a high shear probe.

Theoretical m/z	Experimental m/z	Δ m/z	Peak
521.2719	521.2750	0.0031	$[M+H]^+$
543.2592	543.2579	0.0013	$[M+Na]^+$
1063.5244	1063.5254	0.001	$[2M+Na]^+$

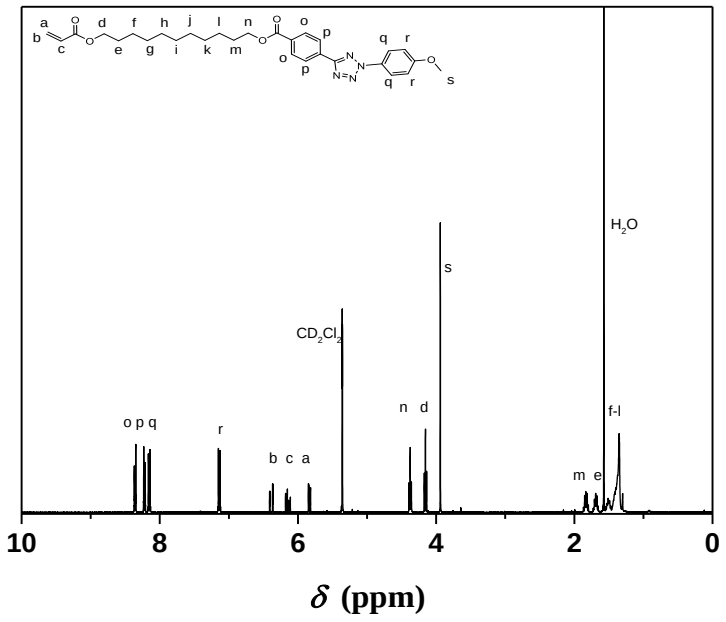

Figure S13. ^{1}H NMR spectrum (400 MHz, CD_2Cl_2) of Tz-UV monomer. NMR was taken after treatment of the monomer for 10 min of ultra-sonication at 50 % intensity using a high shear probe. δ 8.39 – 8.32 (m, 2H), 8.26 – 8.11 (m, 4H), 7.18 – 7.10 (m, 2H), 6.39 (dd, J = 17.3, 1.6 Hz, 1H), 5.83 (dd, J = 10.4, 1.6 Hz, 1H), 4.38 (t, J = 6.7 Hz, 2H), 4.15 (t, J = 6.7 Hz, 2H), 3.94 (s, 3H), 1.88 – 1.77 (m, 2H), 1.73 – 1.65 (m, 2H), 1.57 (s, 7H), 1.51 (p, J = 6.8 Hz, 2H), 1.35 (s, 7H), 1.32 (d, J = 18.1 Hz, 1H).

Table S2. Miniemulsion droplet diameter data (DLS; before polymerization) after 10 min ultra sonication at 50 % intensity using a high shear probe. Each run consisted of 10 measurements with 5 runs in total of which the average of each measurement is displayed below.

	$Z_{average}$ nm	$I_{average}$ nm	$V_{average}$ Nm	$N_{average}$ nm	*PDI*
PMMA	98 ± 3	105 ± 4	85 ± 3	67 ± 1	0.1 ± 0.01
2.5 wt% Tz-UV	48 ± 2	97 ± 37	39.5 ± 14	20 ± 7	0.257 ± 0.022
5 wt% Tz-UV	39 ± 1	93 ± 38	49 ± 7	21 ± 1	0.249 ± 0.038
7.5 wt% Tz-UV	71 ± 20	90 ± 40	36 ± 9	30 ± 3	0.340 ± 0.02
10 wt% Tz-UV	234 ± 40	191 ± 11	60 ± 30	30 ± 2	0.400 ± 0.028

Table S3. Polymer particle diameter data (DLS) after 24 h of polymerization at 70 °C. Each run consisted of 10 measurements with 5 runs in total of which the average of each measurement is displayed below.

	$Z_{average}$ nm	$I_{average}$ nm	$V_{average}$ nm	$N_{average}$ nm	*PDI*
PMMA	88 ± 3	184 ± 10	192 ± 12	55 ± 3	0.17 ± 0.01
2.5 wt% Tz-UV	115 ± 1	134 ± 2	108 ± 4	73 ± 3	0.125 ± 0.013
5 wt% Tz-UV	120 ± 3	155 ± 6	98 ± 10	47 ±11	0.208 ± 0.021
7.5 wt% Tz-UV	171 ± 15	232 ± 25	166 ± 45	60 ± 12	0.240 ± 0.024
10 wt% Tz-UV	167 ± 4	198 ± 21	174 ± 50	75 ± 10	0.22 ± 0.013

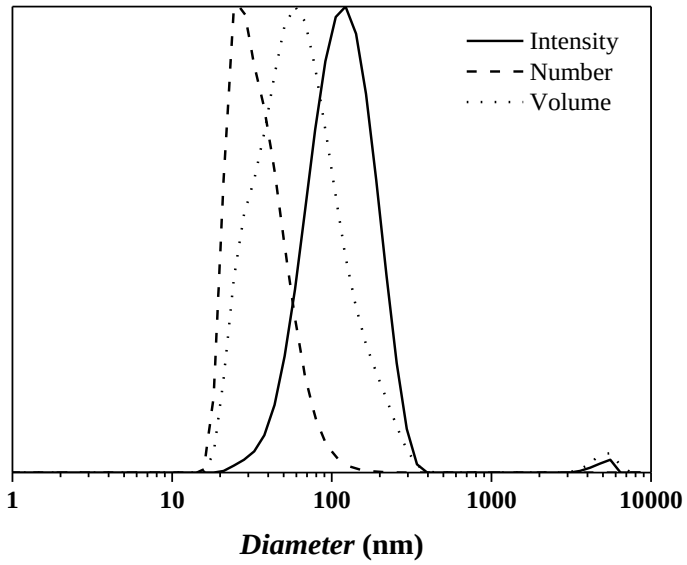

Figure S14. Particle size distributions based on intensity, number and volume for PMMA-Tz-UV (containing 2.5 wt % Tz) particles formed after 24 h of polymerization at 70 °C.

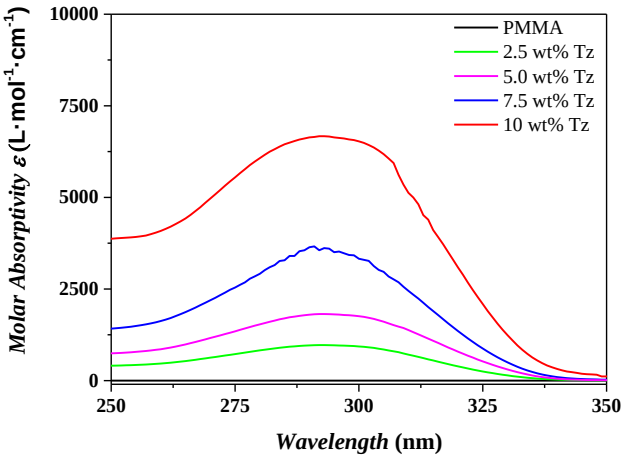

Figure S15. UV-Vis measurements of the PMMA latex (black lines) and PMMA Tz-UV latexes (colored lines) of highly diluted translucent latex solutions with a maximum absorbance of 293 nm.

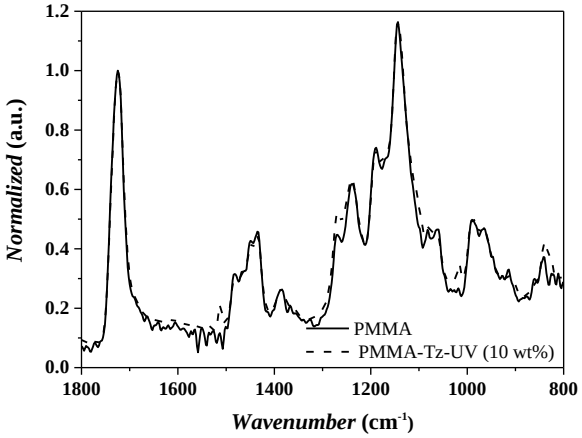

Figure S16. FT-ATR of dried PMMA latex (black line) and PMMA-Tz-UV (10 wt %) latex (dashed line). The carbonyl peak (C=O at 1700 cm^{-1}) is taken as a reference peak.

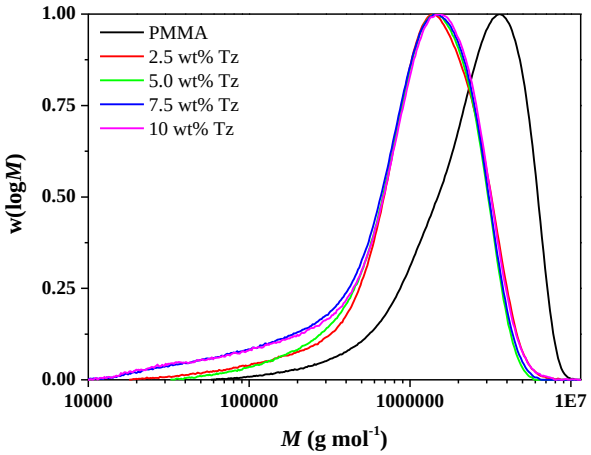

Figure S17. SEC distributions of dried PMMA latex (black line) and PMMA-Tz-UV latexes (colored lines) measured in THF against PMMA calibration standards.

Table S4. SEC and conversion results of dried PMMA latex and PMMA-Tz-UV latexes. SEC traces are shown in Figure S17.

	M_n	M_w	$Đ$	Conversion
	g mol^{-1}	g mol^{-1}		%
PMMA	1 420 300	2 806 000	2.0	91
2.5 wt% Tz-UV	625 700	1 402 900	2.34	93
5 wt% Tz-UV	706 600	1 390 800	1.97	90
7.5 wt% Tz-UV	339 400	2 007 800	3.34	94
10 wt% Tz-UV	330 500	1 348 600	4.08	94

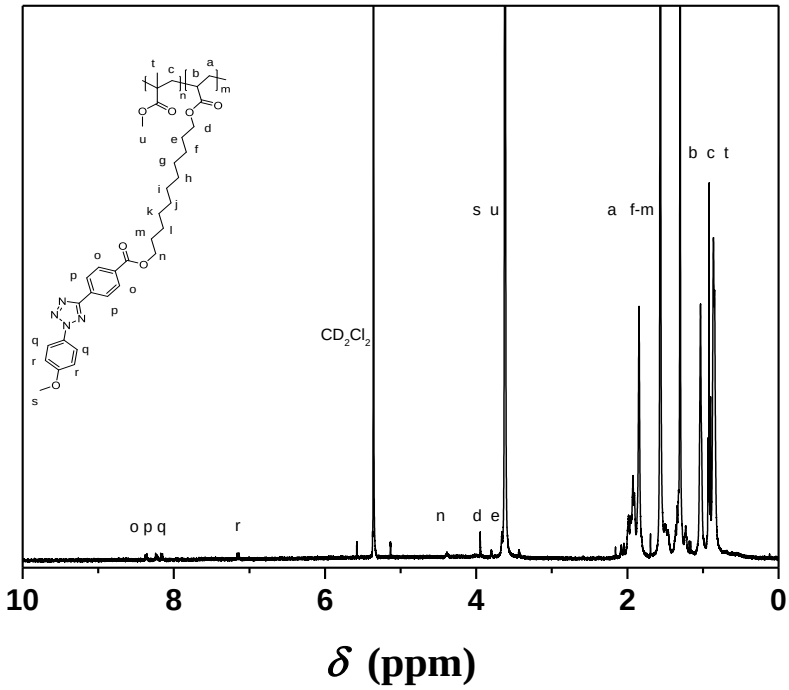

Figure S18. ^{1}H NMR spectrum of dried PMMA-Tz-UV (containing 2.5 wt% Tz-UV) latex recorded in CD_2Cl_2 by using 64 scans and 12 s delay on a 400 MHz Bruker.

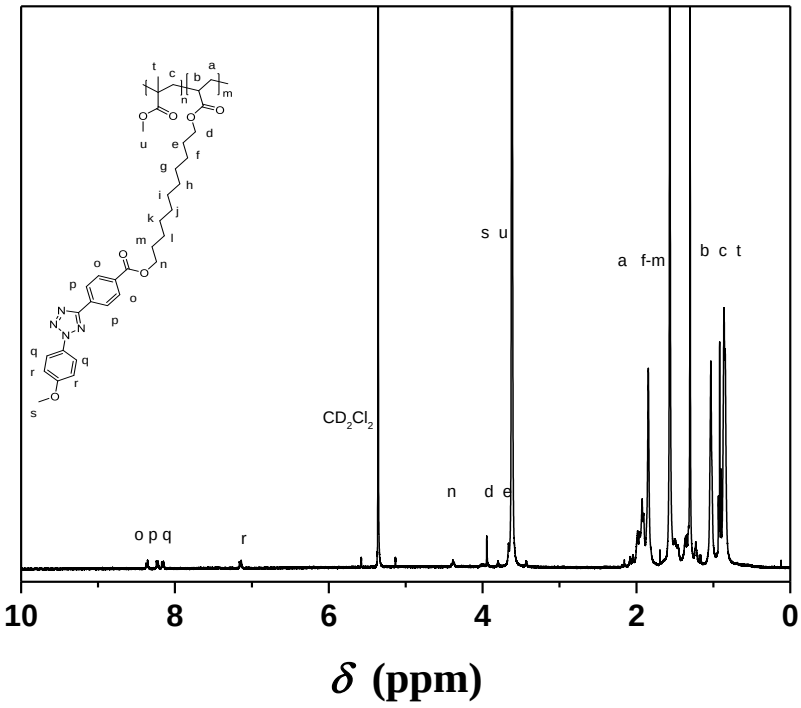

Figure S19. ^{1}H NMR spectrum of dried PMMA-Tz-UV (containing 5 wt% Tz-UV) latex recorded in CD_2Cl_2 by using 64 scans and 12 s delay on a 400 MHz Bruker.

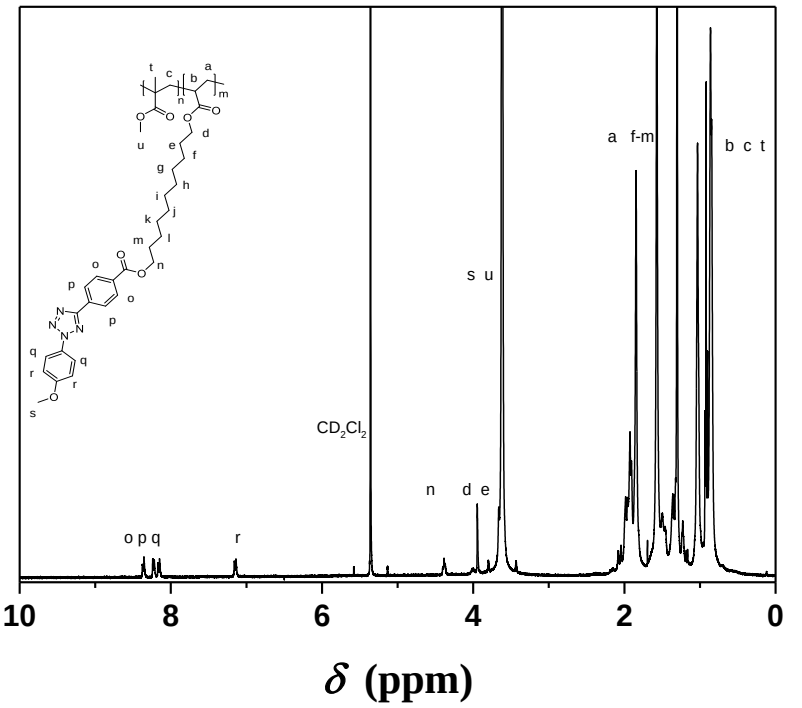

Figure S20. ^{1}H NMR spectrum of dried PMMA-Tz-UV (containing 7.5 wt% Tz-UV) latex recorded in CD_2Cl_2 by using 64 scans and 12 s delay on a 400 MHz Bruker.

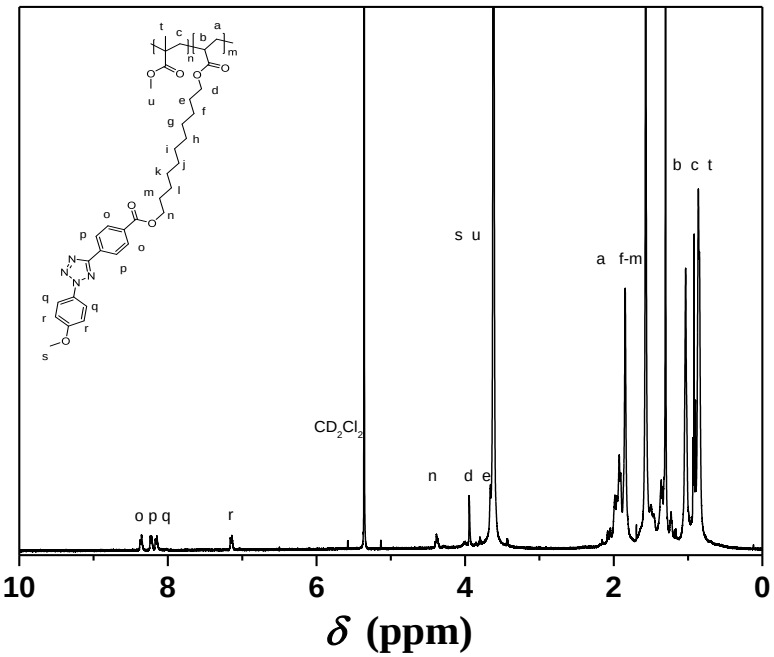

Figure S21. ^{1}H NMR spectrum of dried PMMA-Tz-UV (containing 10 wt% Tz-UV) latex recorded in CD_2Cl_2 by using 64 scans and 12 s delay on a 400 MHz Bruker.

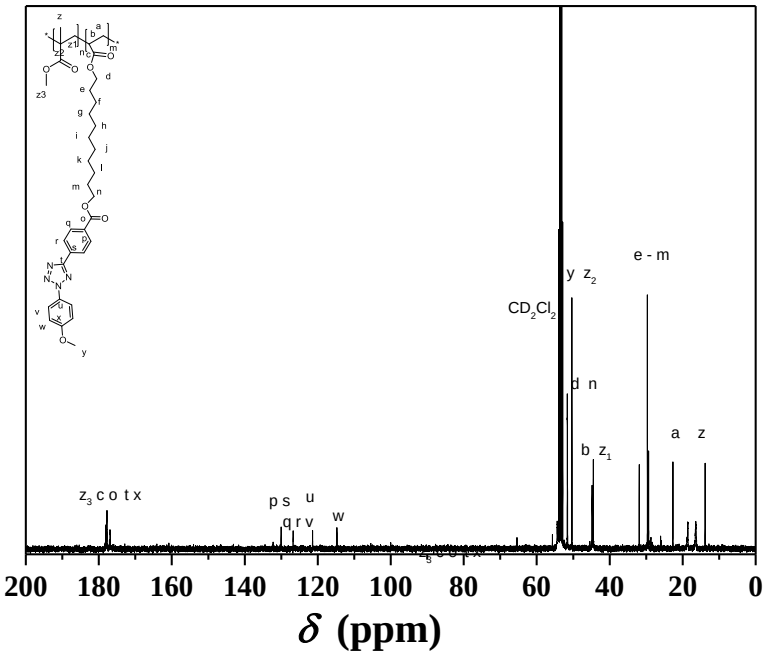

Figure S22. ^{13}C NMR spectrum of dried PMMA-Tz-UV latex (containing 10 wt% Tz-UV) recorded in CD_2Cl_2 by using 256 scans on a 400 MHz Bruker.

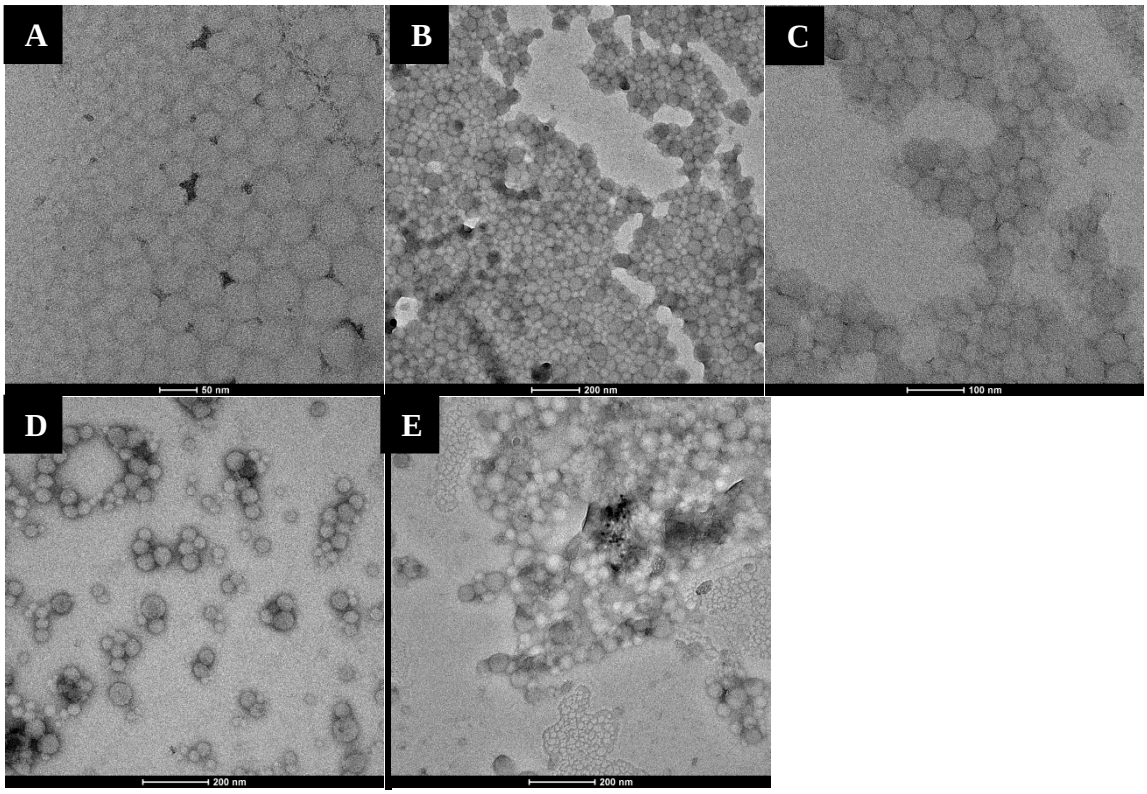

Figure S23. TEM images of PMMA latex (A) and PMMA-Tz-UV latexes (2.5 wt% B; 5.0 wt% C; 7.5 wt% D; 10 wt% E) using 2 wt% osmium vapor (OsO_4) staining.

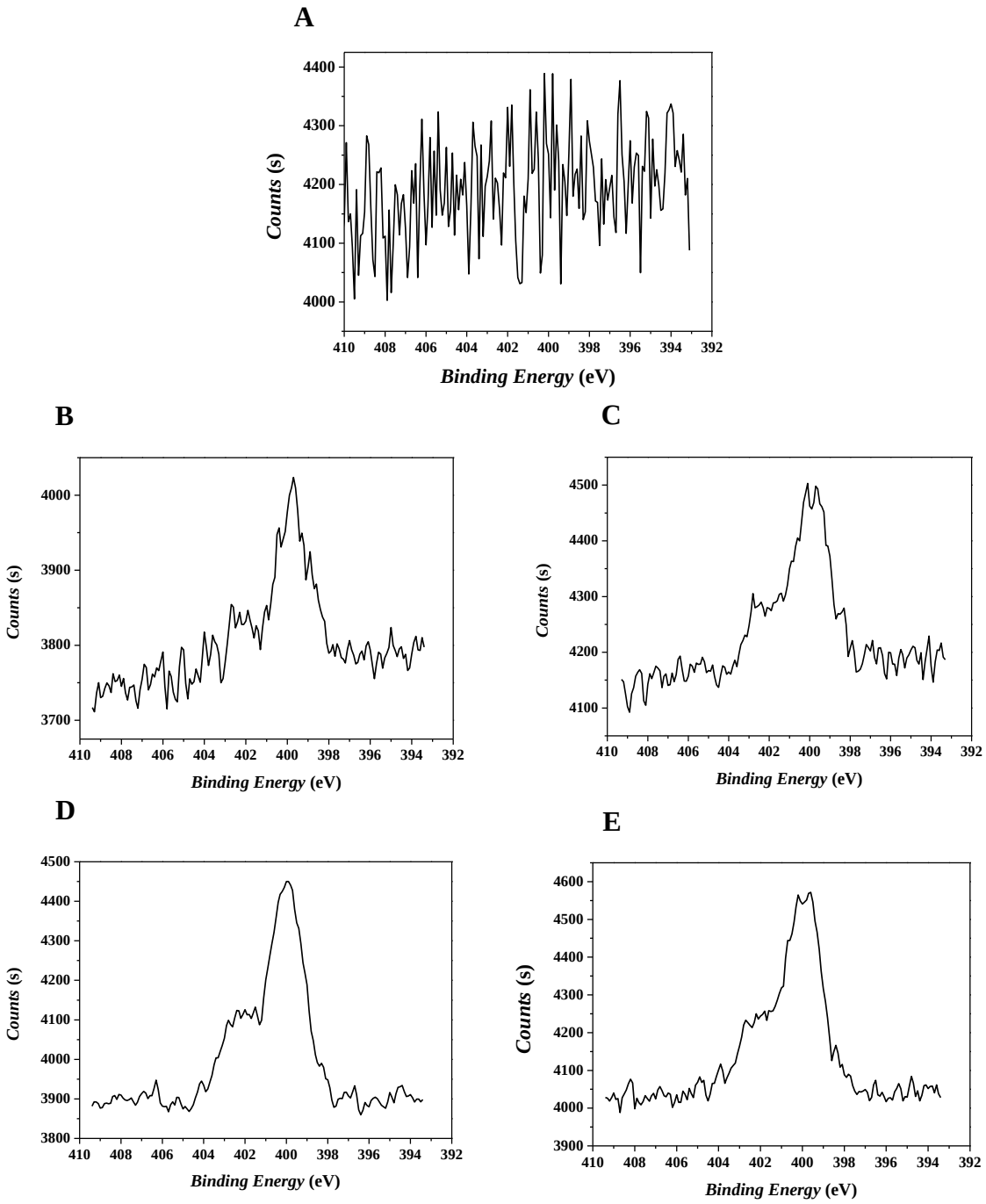

Figure S24. High resolution XPS scans of Nitrogen (N1*s*) of the dried PMMA reference samples (A) and PMMA-Tz-UV latexes (2.5 wt% B; 5.0 wt% C; 7.5 wt% D; 10 wt% E). The atomic percentage of nitrogen at the surface of each sample was calculated by integration of the raw peaks, without mathematical treatment. The reference peak for charge compensation is the C-C peak at 284 eV.

3. Analysis results of the polymer latexes using 10 wt% UV light Tetrazole and varying amounts of SDS.

Table S5. Miniemulsion droplet diameter data (DLS; before polymerization) after 10 min ultra sonication at 50 % intensity using a high shear probe. Each run consisted of 10 measurements with 5 runs in total of which the average of each measurement is displayed below.

	$Z_{average}$	$I_{average}$	$V_{average}$	$N_{average}$	*PDI*
	nm	**nm**	**nm**	**nm**	
PMMA	98 ± 3	105 ± 4	85 ± 3	67 ± 1	0.1 ± 0.01
6 wt % SDS	48 ± 2	136 ± 5	57 ± 2	27 ± 1	0.185 ± 0.01
8 wt% SDS	62 ± 3	128 ± 5	45 ± 2	20 ± 1	0.263 ± 0.02
10 wt% SDS	45 ± 2	142 ± 6	53 ± 3	26 ± 1	0.181 ± 0.02

Table S6. Polymer particle diameter data (DLS) after 24 h of polymerization at 70 °C. Each run consisted of 10 measurements with 5 runs in total of which the average of each measurement is displayed below.

	$Z_{average}$	$I_{average}$	$V_{average}$	$N_{average}$	*PDI*
	nm	**nm**	**nm**	**nm**	
PMMA	88 ± 3	184 ± 10	192 ± 12	55 ± 3	0.170 ± 0.01
6 wt % SDS	297 ± 8	815 ± 20	1355 ± 120	85 ± 2	0.564 ± 0.10
8 wt% SDS	167 ± 4	198 ± 21	174 ± 50	75 ± 8	0.220 ± 0.013
10 wt% SDS	524 ± 11	356 ± 25	189 ± 47	81 ± 7	0.321 ± 0.02

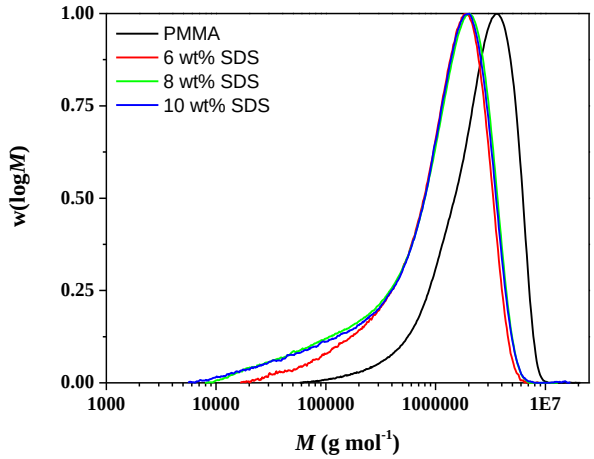

Figure S25. SEC of dried PMMA latex (black line) and PMMA-Tz-UV latexes (colored lines) measured in THF against PMMA calibration standards.

Table S7. SEC and conversion results of dried PMMA latex and PMMA-Tz-UV latexes. SEC traces are shown in Figure S25.

	M_n	M_w	$Đ$	Conversion
	g mol^{-1}	g mol^{-1}		%
PMMA	1 420 300	2 806 000	2.0	91
6 wt % SDS	491 200	1 450 800	2.9	99
8 wt% SDS	281 600	2 358 000	5.1	98
10 wt% SDS	258 100	1 438 000	5.5	94

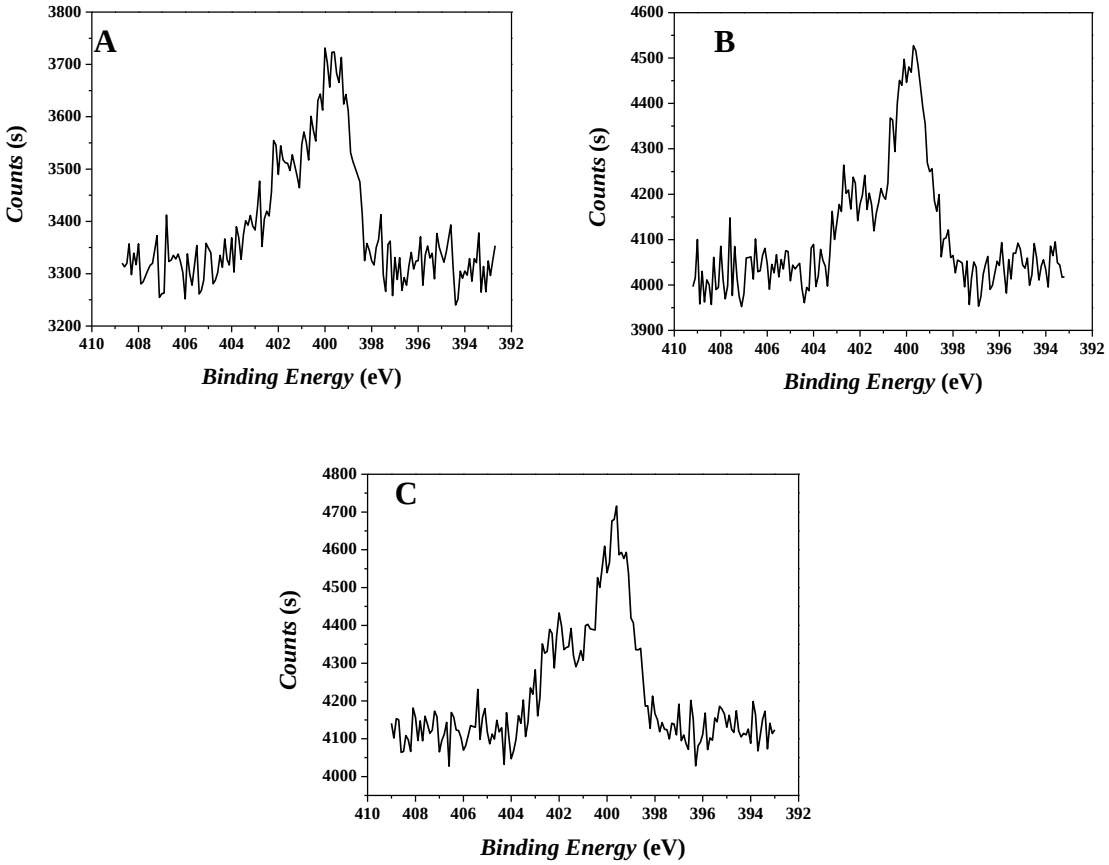

Figure S26. High resolution XPS scans of nitrogen (N1*s*) of the PMMA-Tz-UV latexes (6 wt% SDS A; 8 wt% SDS B; 10 wt% SDS C). The atomic percentage of nitrogen at the surface of each sample was calculated by integration of the raw peaks, without mathematical treatment. The reference peak for charge compensation is the C-C peak at 284 eV.

3. Analysis results of the polymer latexes prepared using varying Visible light Tz amounts.

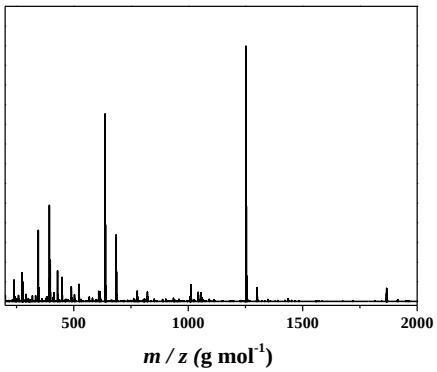

Figure S27. ESI-MS of Tz-Vis monomer in THF / MeOH (3/2 v/v%) after 10 min of ultra sonication at 50 % intensity using a high shear probe.

Table S8. ESI-MS masses of Tz-Vis monomer in THF / MeOH (3/2 v/v%) after 10 min of ultra sonication at 50 % intensity using a high shear probe.

Theoretical m/z	Experimental m/z	Δ m/z	Peak
637.2750	637.2763	0.0013	$[M+Na]^+$
1251.5621	1251.5636	0.0015	$[2M+Na]^+$

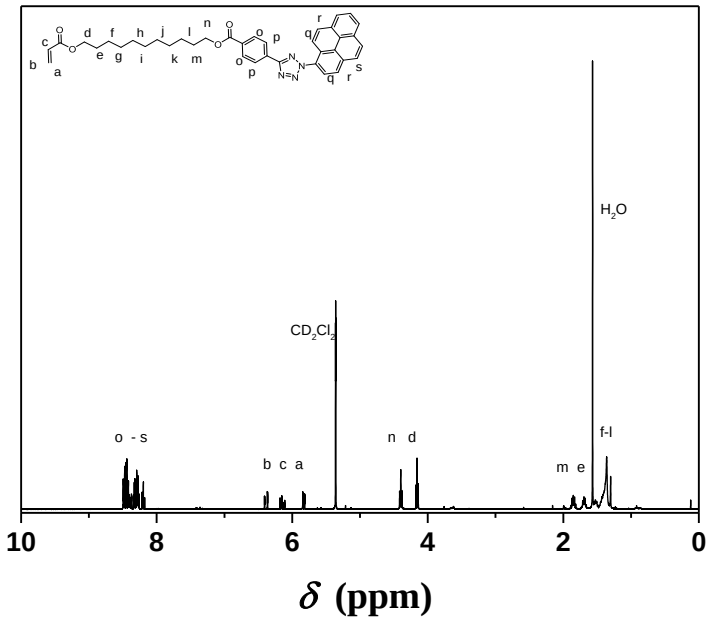

Figure S28. ^{1}H NMR spectrum (400 MHz, CD_2Cl_2) of Tz-Vis monomer. NMR was taken after treatment of the monomer for 10 min of ultra-sonication at 50 % intensity using a high shear probe. δ 8.50 – 8.12 (m, 11H), 6.35 (dd, J = 17.3, 1.6 Hz, 1H), 6.10 (dd, J = 17.3, 10.4 Hz, 1H), 5.79 (dd, J = 10.4, 1.6 Hz, 1H), 4.36 (t, J = 6.7 Hz, 2H), 4.12 (t, J = 6.7 Hz, 2H), 1.88 – 1.76 (m, 2H), 1.66 (p, J = 6.8 Hz, 2H), 1.53 (s, 10H), 1.29 (d, J = 23.4 Hz, 13H).

Table S9. Miniemulsion droplet diameter data (DLS; before polymerization) after 10 min ultra sonication at 50 % intensity using a high shear probe. Each run consisted of 10 measurements with 5 runs in total of which the average of each measurement is displayed below.

	$Z_{average}$	$I_{average}$	$V_{average}$	$N_{average}$	*PDI*
	nm	**nm**	**nm**	**nm**	
PMMA	98 ± 3	105 ± 4	85 ± 3	67 ± 1	0.1 ± 0.01
2.5 wt% Tz-Vis	43 ± 2	193 ± 5	54 ± 2	20 ± 1	0.228 ± 0.02
5 wt% Tz-Vis	56 ± 2	206 ± 4	45 ± 2	22 ± 1	0.355 ± 0.1
7.5 wt% Tz-Vis	58 ± 1	316 ± 7	127 ± 5	32 ± 2	0.322 ± 0.08
10 wt% Tz-Vis	89 ± 2	104 ± 2	46 ± 3	27 ± 2	0.249 ± 0.04

Table S10. Polymer particle diameter data (DLS) after 24 h of polymerization at 70 °C. Each run consisted of 10 measurements with 5 runs in total of which the average of each measurement is displayed below.

	$Z_{average}$	$I_{average}$	$V_{average}$	$N_{average}$	*PDI*
	nm	**nm**	**nm**	**nm**	
PMMA	88 ± 3	184 ± 10	192 ± 12	55 ± 3	0.17 ± 0.01
2.5 wt% Tz-Vis	149 ± 8	187 ± 11	209 ± 15	74 ± 4	0.204 ± 0.02
5 wt% Tz-Vis	106 ± 7	159 ± 11	135 ± 8	37 ± 2	0.215 ± 0.01
7.5 wt% Tz-Vis	164 ± 9	251 ± 14	320 ± 21	74 ± 3	0.228 ± 0.03
10 wt% Tz-Vis	111 ± 6	200 ± 10	130 ± 7	31 ± 2	0.289 ± 0.03

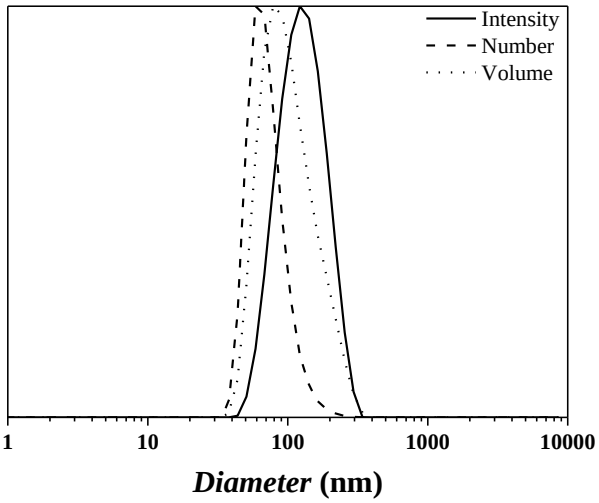

Figure S29. Particle size distributions based on intensity, number and volume for PMMA-Tz-Vis (containing 2.5 wt % Tz) particles formed after 24 h of polymerization at 70 °C.

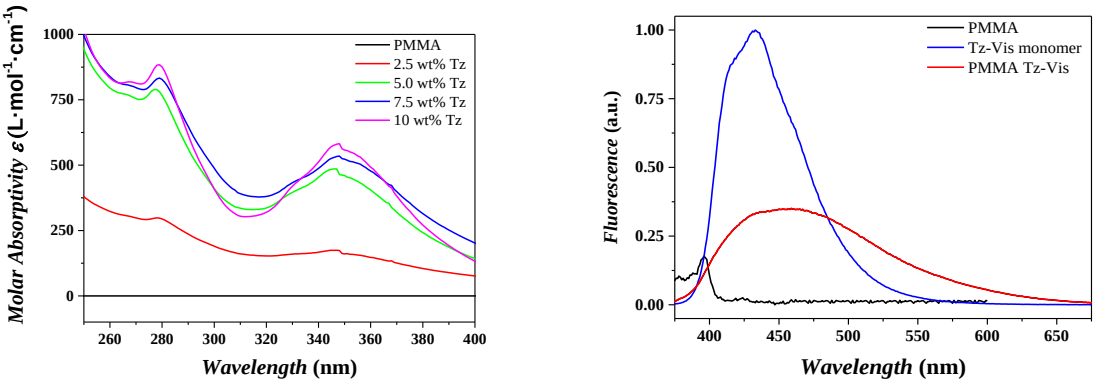

Figure S30. UV-Vis (left) and Fluorescence (right) measurements of the PMMA latex (black line) and PMMA-Tz-Vis latexes (colored lines) of highly diluted translucent latex solutions with a maximum absorbance and emission of 348 nm and 432 nm respectively.

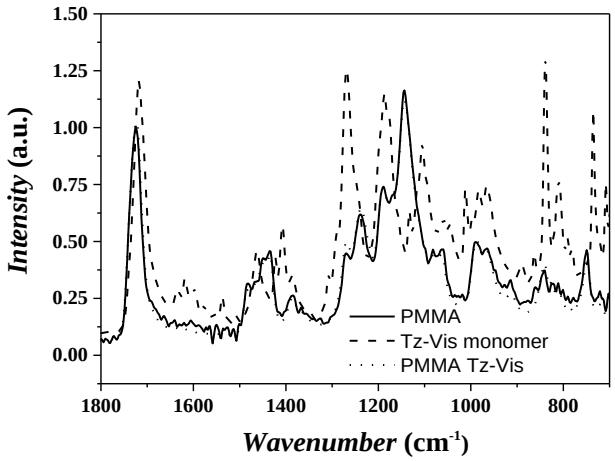

Figure S31. FT-ATR of dried PMMA latex (solid line), Tz-Vis monomer (dashed line) PMMA-Tz-Vis (10 wt %) latex (dotted line). De carbonyl peak (C=O at 1700 cm^{-1}) is taken as a reference peak.

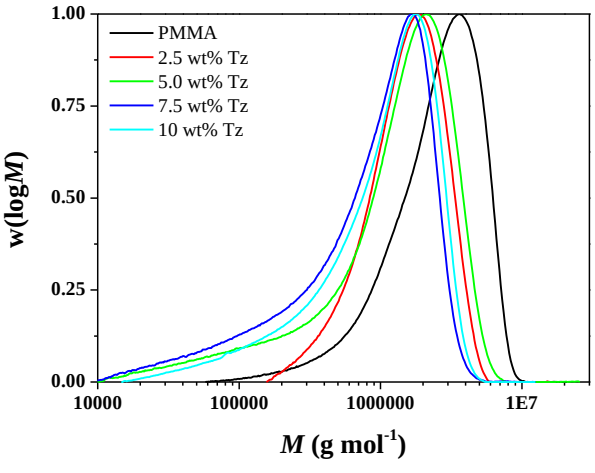

Figure S32. SEC of dried PMMA latex (black line) and PMMA-Tz-Vis latexes (colored lines) measured in THF against PMMA calibration standards.

Table S11. SEC and conversion results of dried PMMA latex and PMMA-Tz-Vis latexes. SEC traces are shown in Figure S32.

	M_n	M_w	$Đ$	Conversion
	g mol^{-1}	g mol^{-1}		%
PMMA	1 420 300	2 806 000	2.0	91
2.5 wt% Tz-Vis	1 126 000	1 694 000	1.6	95
5.0 wt% Tz-Vis	345 600	1 618 000	4.7	98
7.5 wt% Tz-Vis	258 800	1 090 000	4.2	99
10 wt% Tz-Vis	420 400	1 280 000	3.0	92

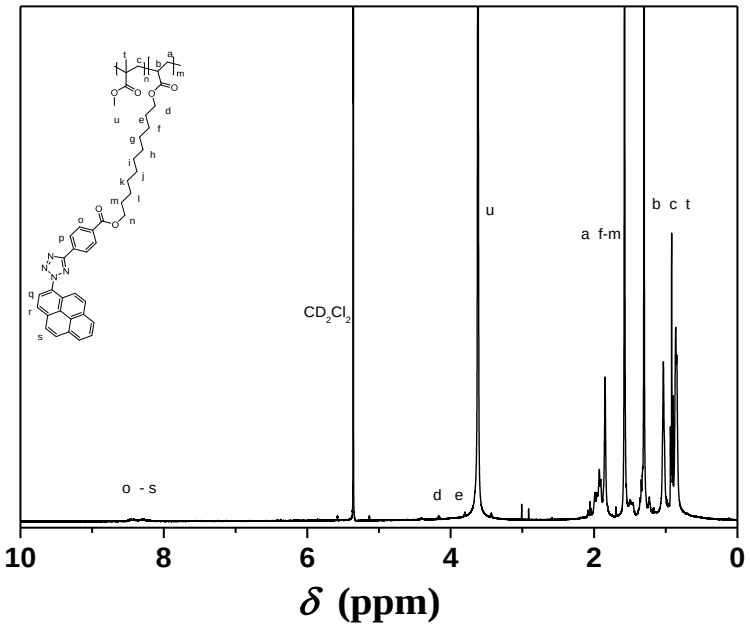

Figure S33. ^{1}H NMR spectrum of dried PMMA-Tz-Vis (containing 2.5 wt% Tz-Vis) latex recorded in CD_2Cl_2 by using 64 scans and 12 s delay on a 400 MHz Bruker.

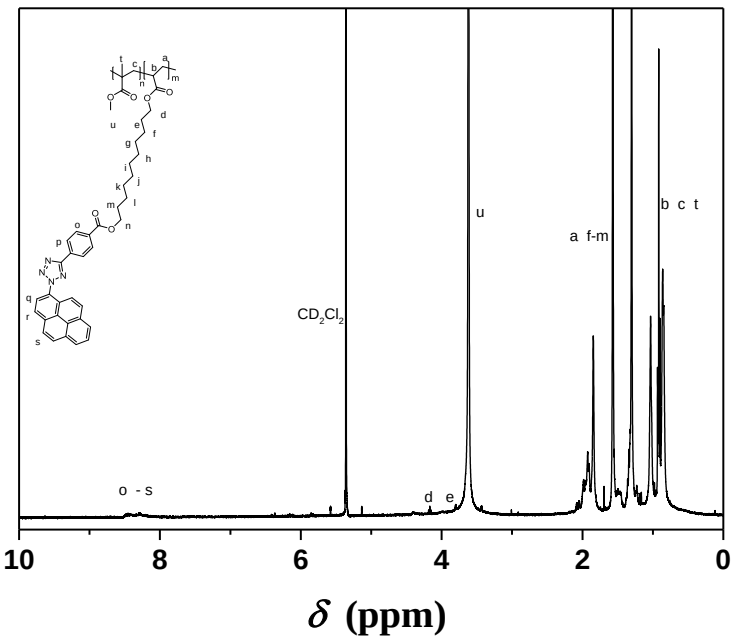

Figure S34. [1]H NMR spectrum of dried PMMA-Tz-Vis (containing 5 wt% Tz-Vis) latex recorded in CD_2Cl_2 by using 64 scans and 12 s delay on a 400 MHz Bruker.

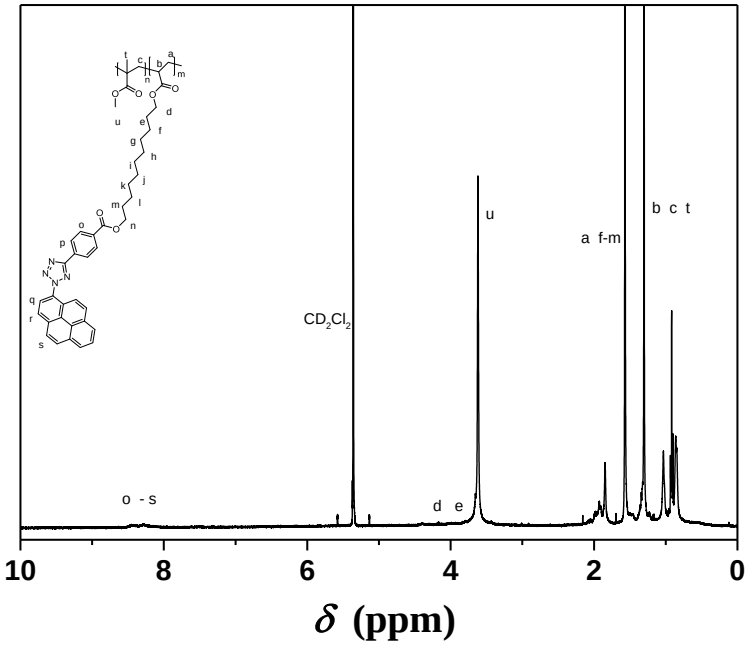

Figure S35.[1]H NMR spectrum of dried PMMA-Tz-Vis (containing 7.5 wt% Tz-Vis) latex recorded in CD_2Cl_2 by using 64 scans and 12 s delay on a 400 MHz Bruker.

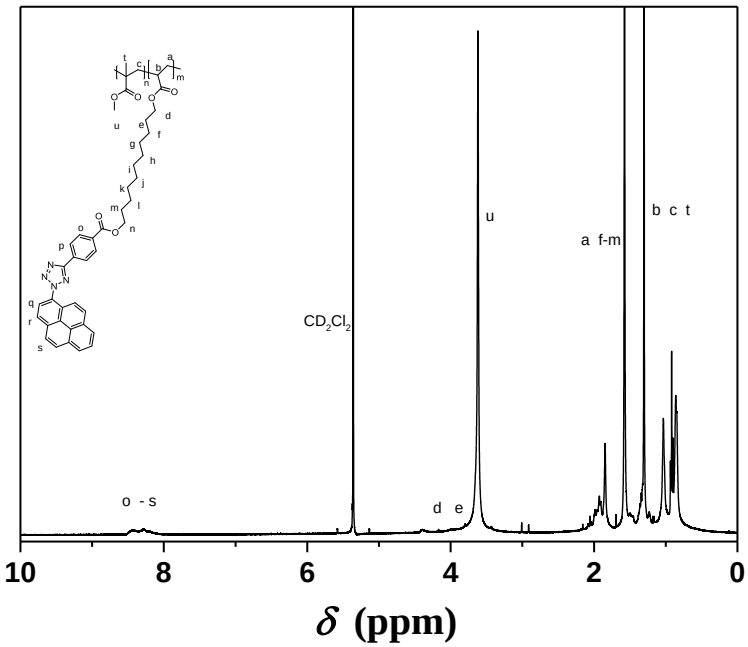

Figure S36. ^{1}H NMR spectrum of dried PMMA-Tz-Vis (containing 10 wt% Tz-Vis) latex recorded in CD_2Cl_2 by using 64 scans and 12 s delay on a 400 MHz Bruker.

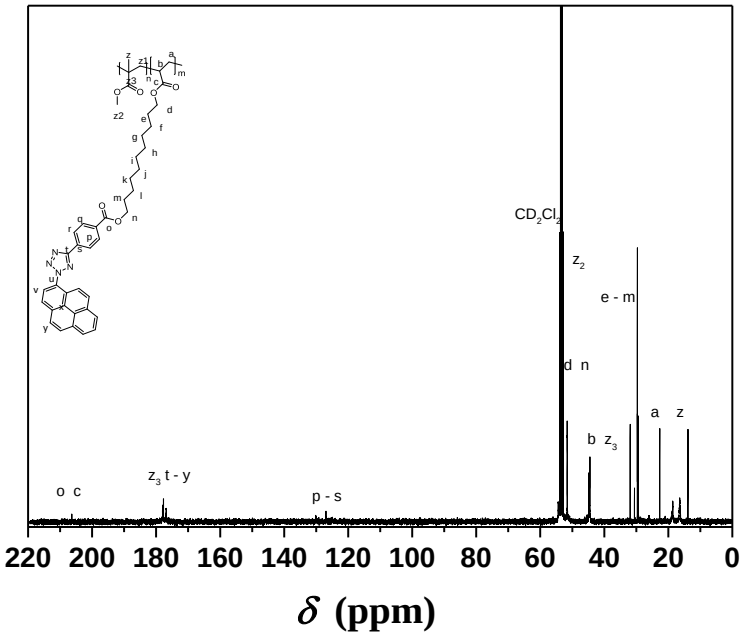

Figure S37. ^{13}C NMR spectrum of dried PMMA-Tz-Vis (containing 10 wt% Tz-Vis) latex recorded in CD_2Cl_2 by using 64 scans and 12 s delay on a 400 MHz Bruker.

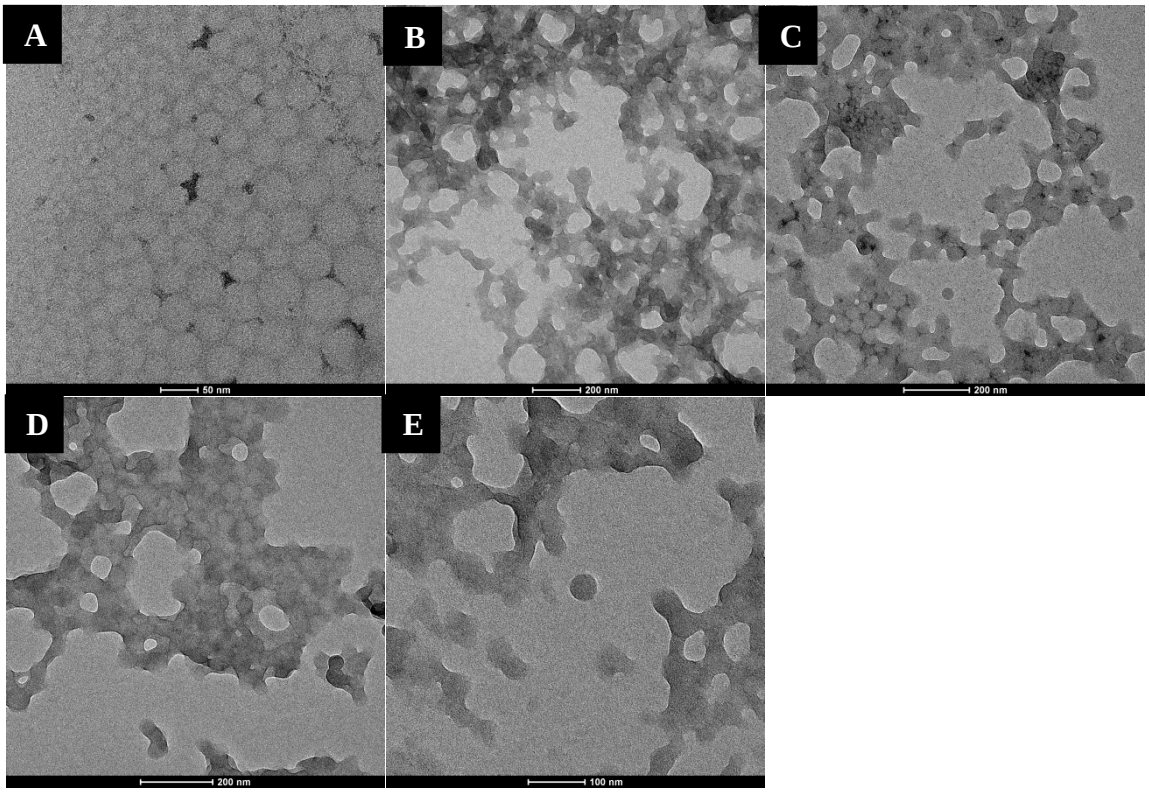

Figure S38. TEM images of PMMA latex (A) and PMMA-Tz-Vis latexes (2.5 wt% B; 5.0 wt% C; 7.5 wt% D; 10 wt% E) using a 2 wt% osmium vapor (OsO_4) staining for each sample.

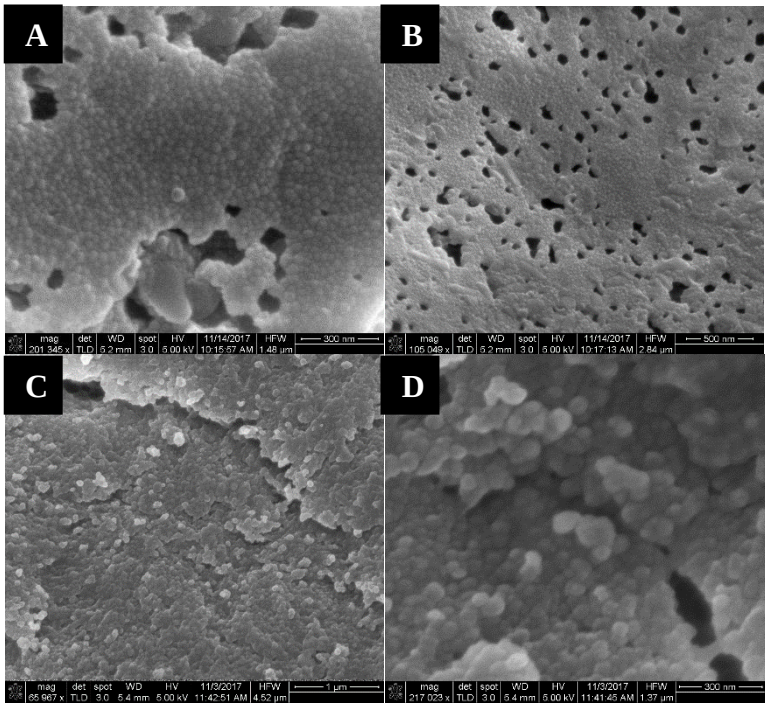

Figure S39. SEM images of dried PMMA-Tz-Vis latexes (2.5 wt% B; 5.0 wt% C; 7.5 wt% D; 10 wt% E) using double sided carbon tape and a 5 nm platinum coating for each sample.

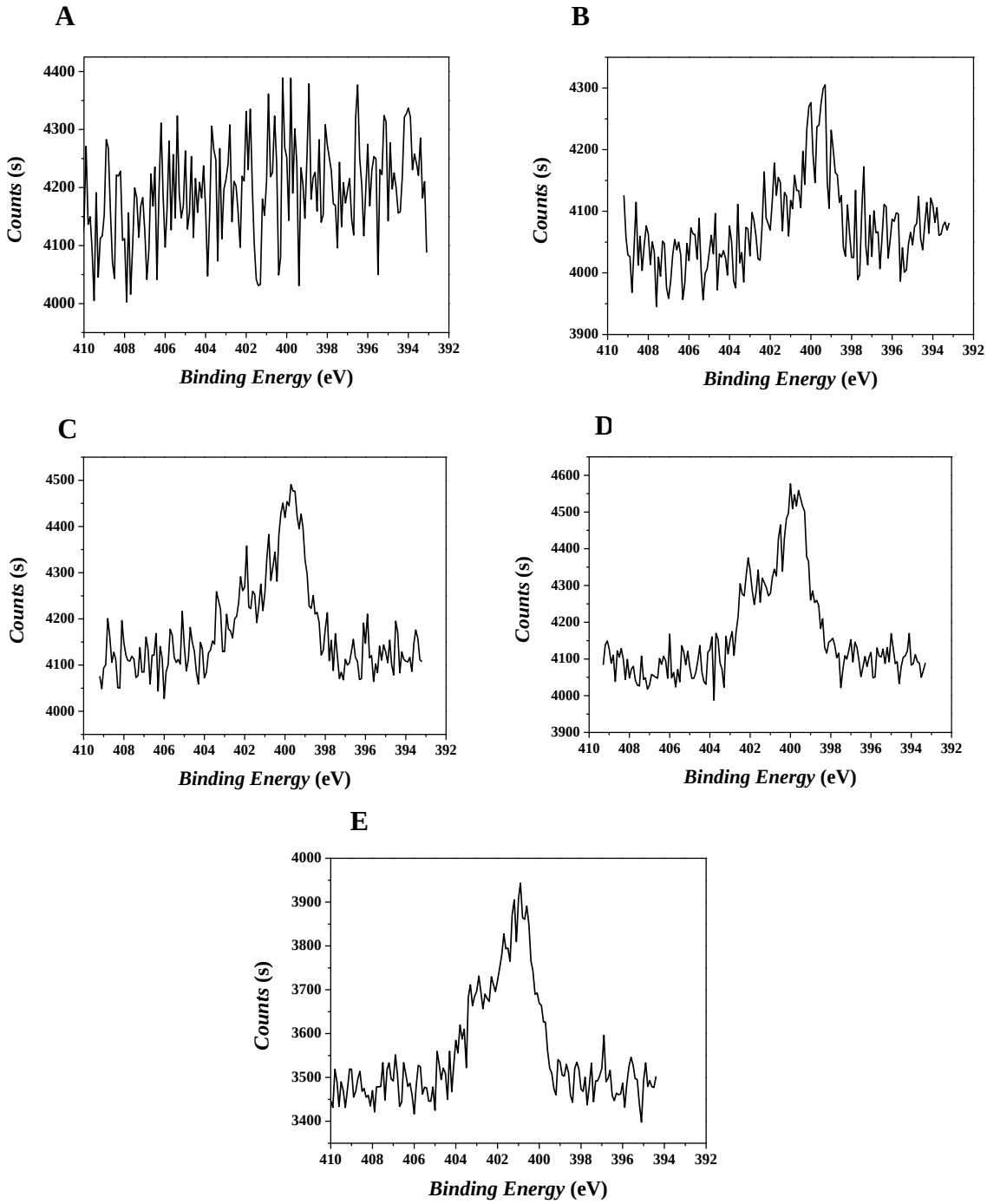

Figure S40. High resolution XPS scans of Nitrogen (N1s) of the dried PMMA reference samples (A) and PMMA-Tz-Vis latexes (2.5 wt% B; 5.0 wt% C; 7.5 wt% D; 10 wt% E) are presented. The atomic percentage of nitrogen at the surface of each sample was calculated by integration of the raw peaks, without mathematical treatment. The reference peak for charge compensation is the C-C peak at 284 eV.

4. Analysis results of the PMMA-Tz-UV after irradiation under UV-B light

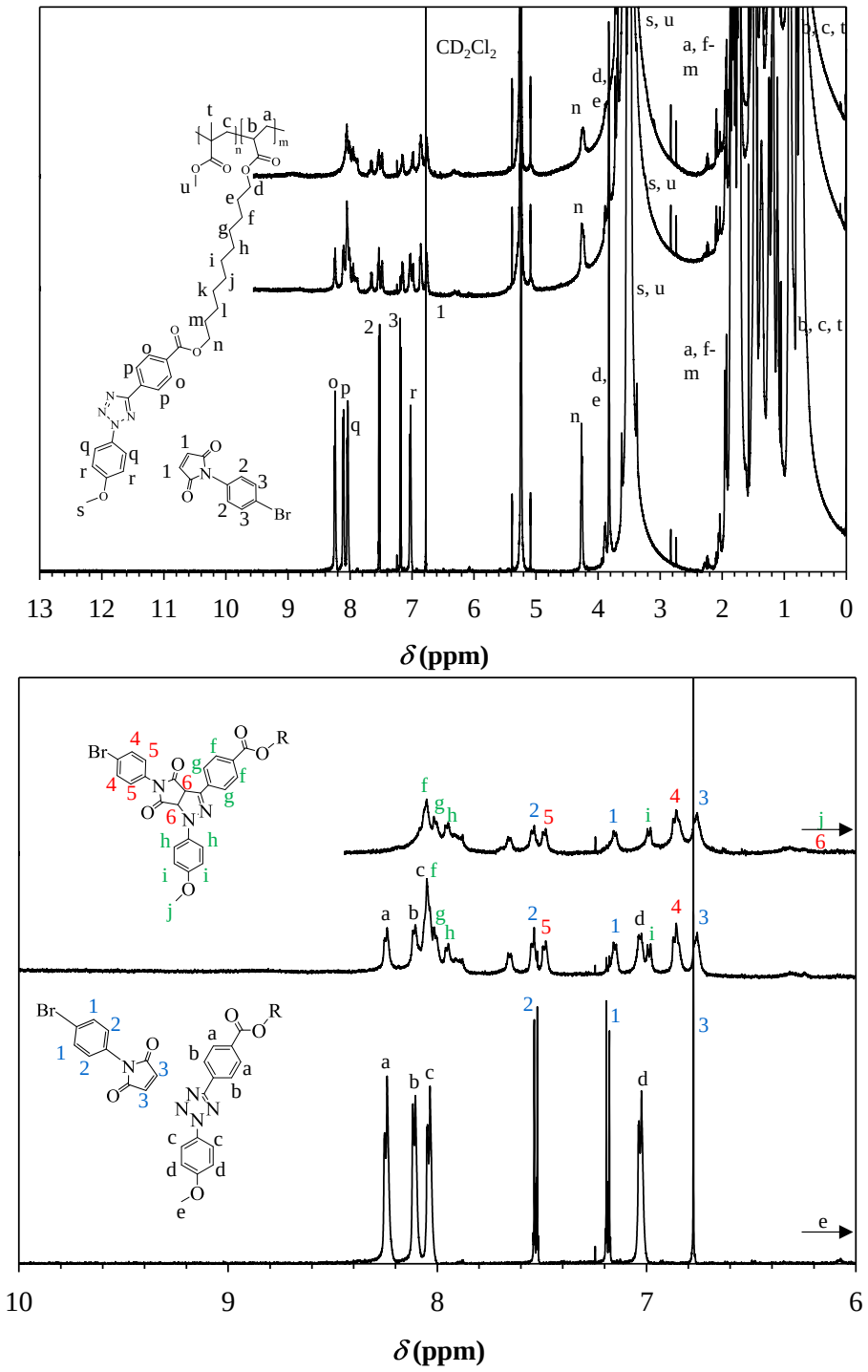

Figure S41. ^{1}H NMR of the PMMA-Tz-UV (10 wt%, UV4) copolymer after the NITEC reaction with N-BPM at 0 (bottom), 10 (middle) and 120 minutes (top) with the corresponding labels. Zoom in the aromatics region (6 to 10 ppm) below (600 MHz, 128 scans, 12 s delay, CD_2Cl_2)

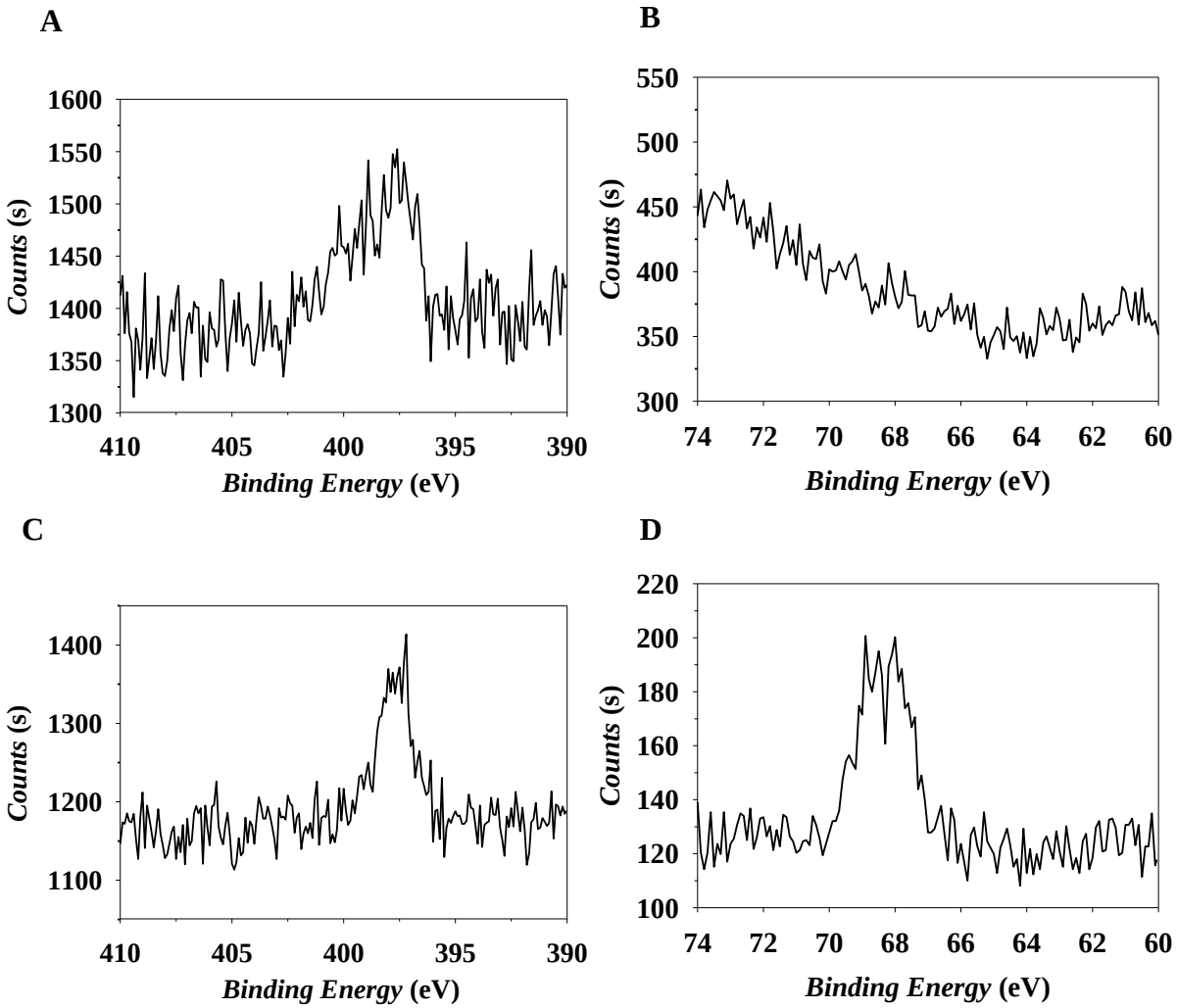

Figure S42. High resolution XPS scans of Nitrogen (N1*s*) and Bromine (Br3*d*) of the dried and washed PMMA-Tz-UV latexes (10 wt%, UV4) before (A – B) and after NITEC reaction with N-BPM (C – D) (120 minutes of irradiation) are presented.

Table S12. Atomic percentage measured by XPS of the washed and dried PMMA-Tz-UV latexes (10 wt%, UV4) after NITEC reaction with N-BPM at different time reaction. The atomic percentage at the surface of each sample was calculated by integration of the raw peaks, without mathematical treatment. The average of two measurements on different location of the same sample and standard deviation are presented.

Time (min) / atom%	0	10	60	120
Br3*d*	0.00 ± 0.00	0.16 ± 0.06	0.27 ± 0.01	0.22 ± 0.01
C1*s*	73.68 ± 0.22	74.75 ± 0.16	74.05 ± 0.07	76.05 ± 0.39
N1*s*	1.04 ± 0.05	0.90 ± 0.04	0.86 ± 0.06	0.74 ± 0.00
O1*s*	25.26 ± 0.20	23.72 ± 0.58	23.62 ± 0.60	22.99 ± 0.38
S1*s*	0.00 ± 0.00	0.36 ± 0.36	0.05 ± 0.05	0.00 ± 0.00

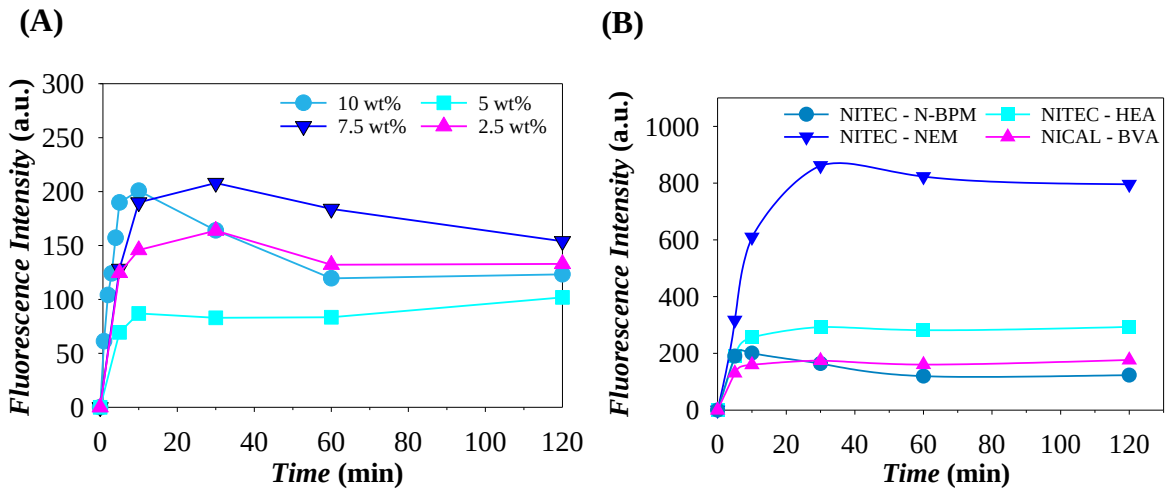

Figure S43. (A) Kinetic plots displaying the fluorescence emission *vs.* reaction time for the NITEC reaction of N-BPM and latexes containing 2.5 wt% (triangle up, UV1), 5 wt% (square, UV2), 7.5 wt% (triangle down, UV3) and 10 wt% (circle, UV4) of Tz-UV (λ_{ex} = 390 nm). (B) Fluorescence emission spectra of highly diluted PMMA-Tz-UV (10 wt%) latex after the NITEC reaction with N-BPM, HEA and NEM at different reaction times (λ_{ex} = 390 nm).

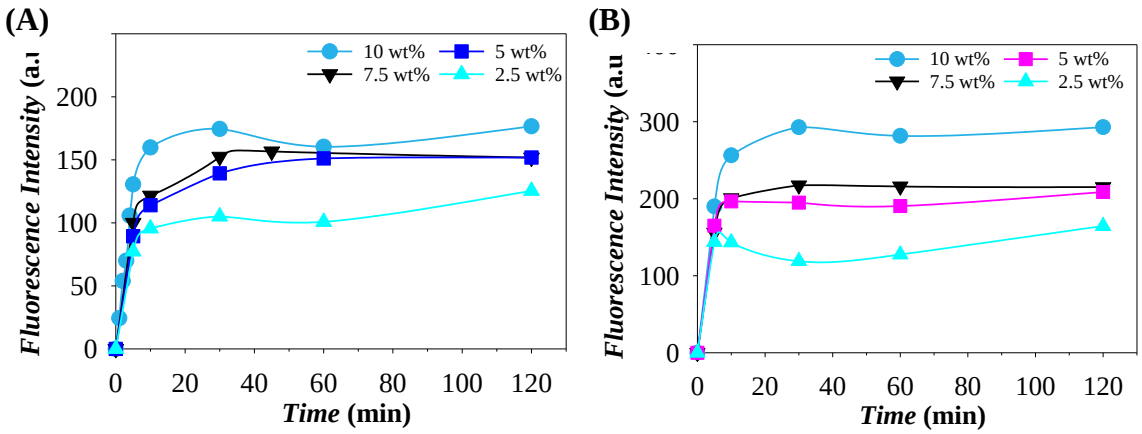

Figure S44. Kinetic plots displaying the fluorescence emission *vs* reaction time for the NICAL reaction with BVA (A) or the NITEC of HEA (B) and latexes containing 2.5 wt% (triangle up, UV1), 5 wt% (square, UV2), 7.5 wt% (triangle down, UV3) and 10 wt% (circle, UV4) of Tz-UV (λ_{ex} = 390 nm).

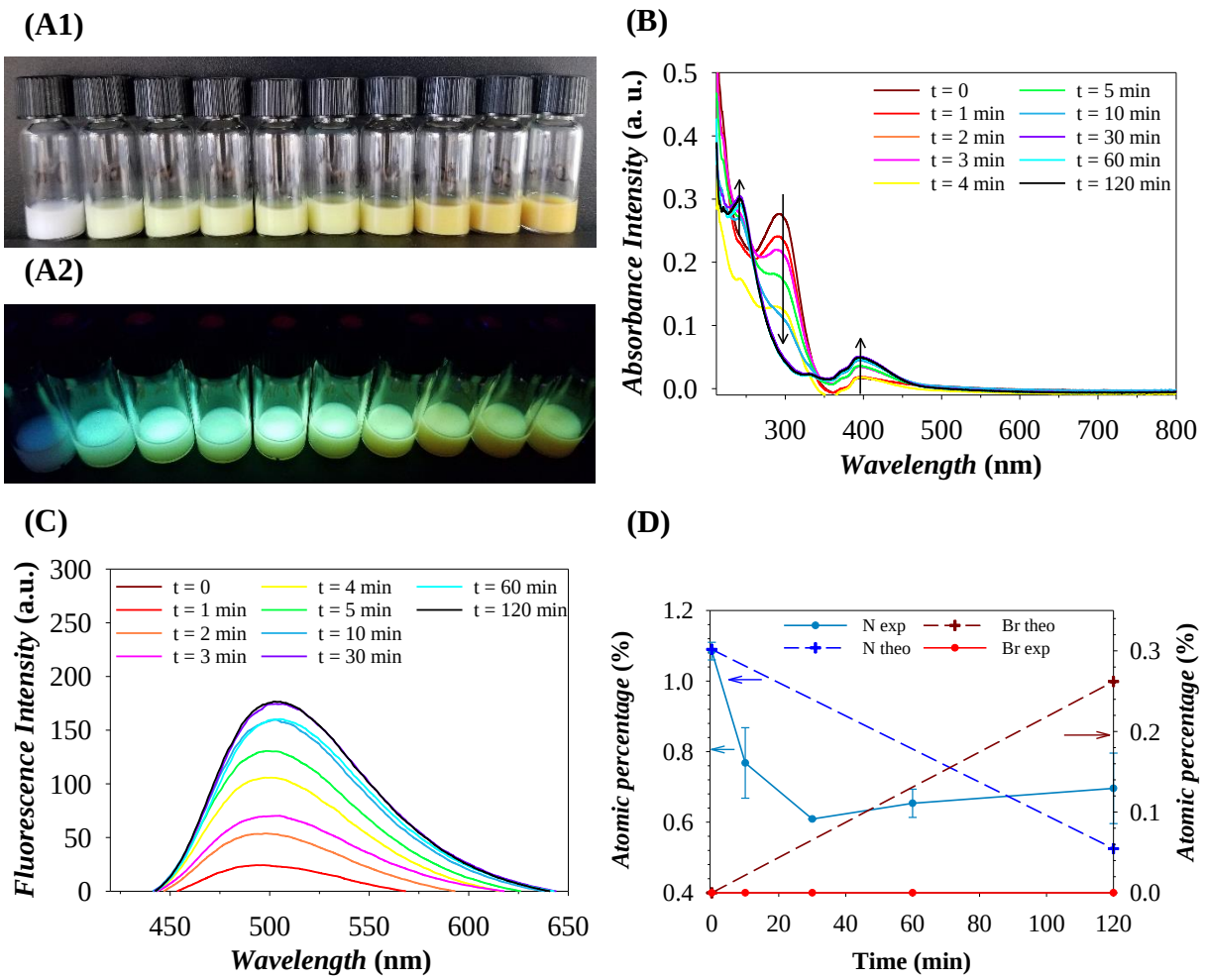

Figure S45. (A) Photographs of the PMMA-Tz-UV (10 wt%, UV4) latex after the NICAL reaction with BVA at different reaction times (from left to right: 0, 1, 2, 3, 4, 5, 10, 30, 60 and 120 min) under white light (A1) and under a hand-held UV lamp (λ_{ex} = 365 nm) (A2). (B) UV-vis absorbance spectra of highly diluted PMMA-Tz-UV (10 wt%, UV4) latex after the NICAL reaction with BVA at different reaction times. (C) Fluorescence emission spectra of highly diluted PMMA-Tz-UV (10 wt%, UV4) latex after the NICAL reaction with BVA at different reaction times (λ_{ex} = 390 nm). (D) Atomic percentage of Nitrogen (left y-axis) and Bromine (right y-axis) measured by XPS on the surface of the dried copolymer after purification and theoretical content (Equation S1 and S2).

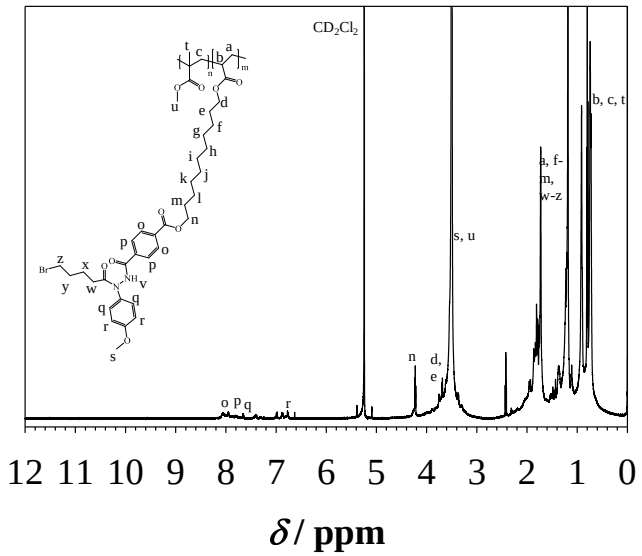

Figure S46. ^{1}H NMR of the PMMA-Tz-UV (10 wt%, UV4) copolymer after the NICAL reaction with BVA at 60 minutes with the corresponding labels (600 MHz, 128 scans, 12 s delay, CD_2Cl_2)

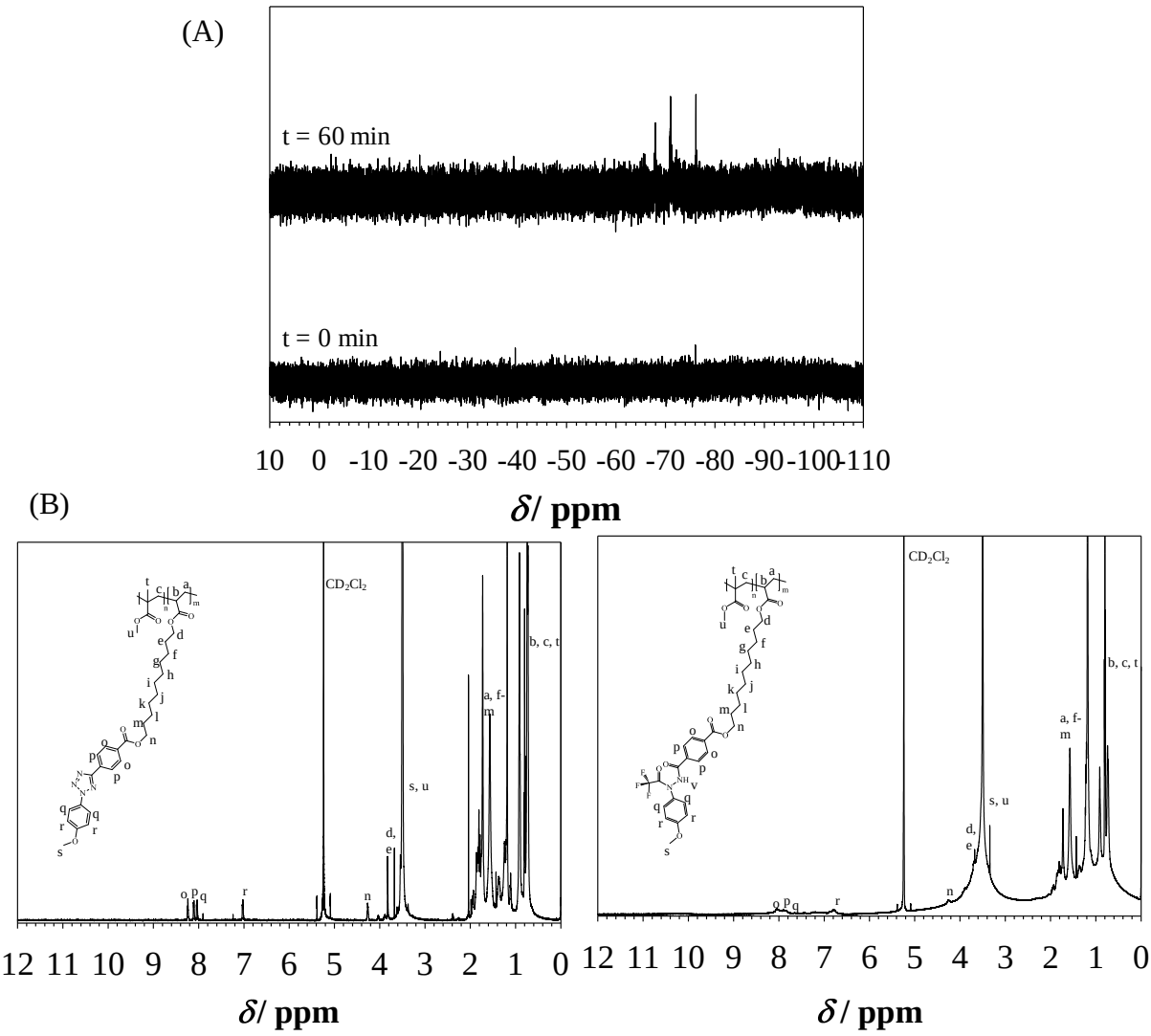

Figure S47. (A) ^{19}F NMR of the PMMA-Tz-UV (10 wt%, UV4) copolymer after the NICAL reaction with TFA at 0 (bottom), and 60 minutes (top) after purification of the copolymer (600 MHz, 12 s delay, 128 scans, CD_2Cl_2). (B) ^{1}H NMR of the PMMA-Tz-UV (10 wt%, UV4) copolymer after the NICAL reaction with TFA at 0 (left) and

60 minutes (right) after purification of the copolymer with the corresponding labels (600 MHz, 12s delay, 128 scans CD_2Cl_2).

Table S13. Atomic percentage measured by XPS of the washed and dried PMMA-Tz-UV latexes (10 wt%, UV4) after NICAL reaction with BVA at different time reaction. The atomic percentage at the surface of each sample was calculated by integration of the raw peaks, without mathematical treatment. The average of two measurements on different location of the same sample and standard deviation are presented.

Time (min) / atom%	0	10	30	60	120
Br3*d*	0.00 ± 0.00	0.00 ± 0.00	0.00 ± 0.00	0.00 ± 0.00	0.00 ± 0.00
C1*s*	64.24 ± 0.65	73.55 ± 2.1	74.77 ± 0.08	76.26 ± 0.24	74.19 ± 0.12
N1*s*	1.09 ± 0.02	0.77 ± 0.10	0.61 ± 0.00	0.65 ± 0.04	0.70 ± 0.10
O1*s*	34.66 ± 0.62	25.68 ± 1.98	24.61 ± 0.09	23.08 ± 0.29	25.10 ± 0.02
S1*s*	0.00 ± 0.00	0.00 ± 0.00	0.00 ± 0.00	0.00 ± 0.00	0.00 ± 0.00

Table S14. Atomic percentage measured by XPS of the washed and dried PMMA-Tz-UV latexes (10 wt%, UV4) after NICAL reaction with TFA at different time reaction. The atomic percentage at the surface of each sample was calculated by integration of the raw peaks, without mathematical treatment. The average of two measurements on different location of the same sample and standard deviation are presented.

Time (min) / atom%	0	60
F*1s*	0.00 ± 0.00	0.18 ± 0.01
C1*s*	73.66 ± 0.00	74.11 ± 0.34
N1*s*	1.00 ± 0.00	0.48 ± 0.01
O1*s*	25.34 ± 0.00	25.23 ± 0.34
S1*s*	0.00 ± 0.00	0.00 ± 0.00

Table S15. Atomic percentage measured by XPS of the dried PMMA-Tz-UV latexes (10 wt%, UV4) after NICAL reaction with BVA at different time reaction (no purification). The atomic percentage at the surface of each sample was calculated by integration of the raw peaks, without mathematical treatment.

Time (min) / A(%)	0	10	30	60	120
Br3*d*	0.26	0.09	0.14	0.09	0.28
C1*s*	75.59	76.18	75.80	75.80	72.60
N1*s*	0.89	0.53	0.37	0.30	0.32
O1*s*	22.49	22.53	23.39	23.11	26.08
S1*s*	0.78	0.67	0.66	0.697	0.721

5. Analysis results of the PMMA-Tz-Vis after irradiation under visible light

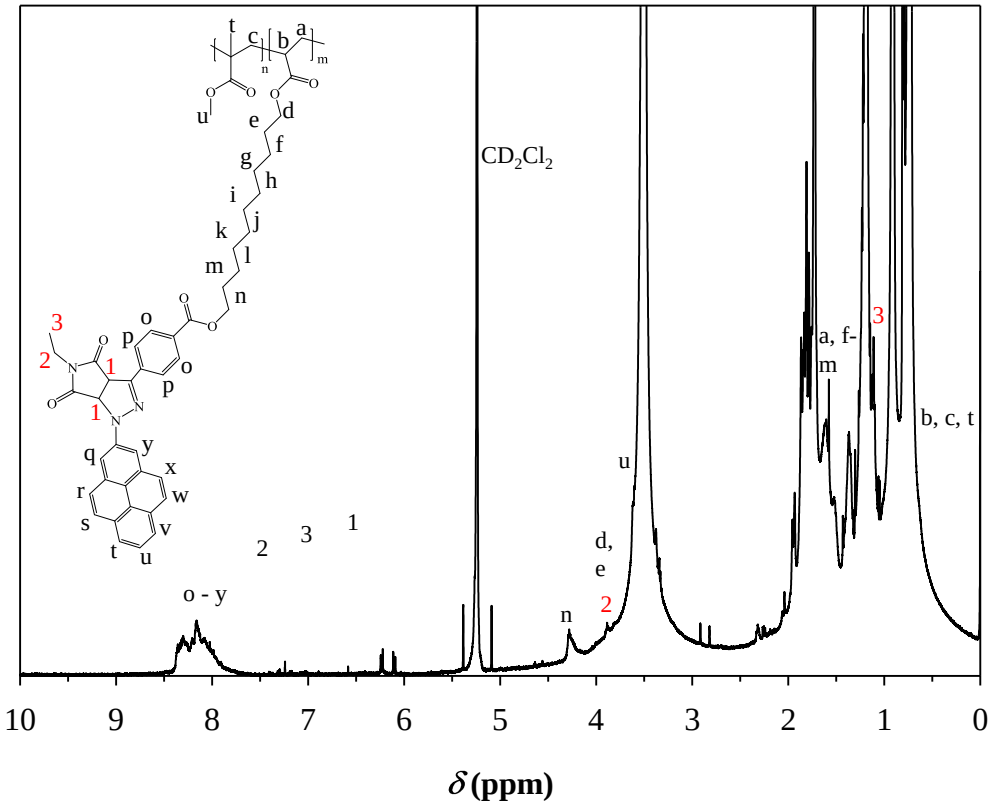

Figure S48. ^{1}H NMR spectrum of dried PMMA-Tz-Vis (containing 10 wt% Tz-Vis) latex recorded in CD_2Cl_2 by using 128 scans and on a 600 MHz Bruker with the corresponding labels.

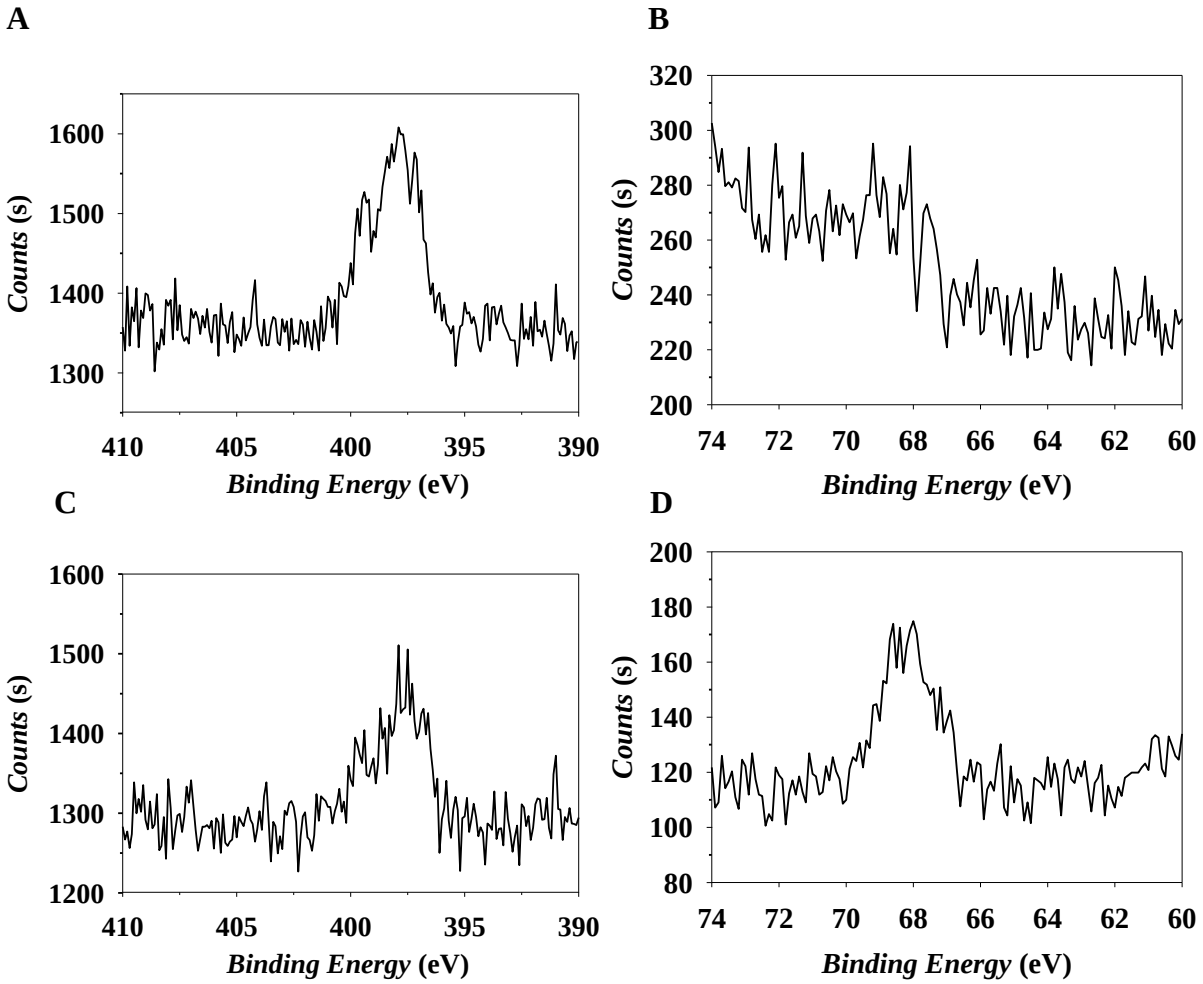

Figure S49. High resolution XPS scans of Nitrogen (N1*s*) and Bromine (Br3*d*) of the dried and washed PMMA-Tz-Vis latexes (10 wt%, Vis4) before (A - B) and after NITEC reaction with N-BPM (C - D) (120 minutes of irradiation) are presented.

Table S16. Atomic percentage measured by XPS of the washed and dried PMMA-Tz-V**is** latexes (10 wt%, Vis4) after NITEC reaction with N-BPM at different time reaction. The atomic percentage at the surface of each sample was calculated by integration of the raw peaks, without mathematical treatment. The average of two measurements on different location of the same sample and standard deviation are presented.

Time (min) / atom%	0	30	60	120
Br3*d*	0.00 ± 0.00	0.13 ± 0.01	0.14 ± 0.1	0.16 ± 0.01
C1*s*	75.69 ± 0.40	75.72 ± 0.14	75.72 ± 0.14	75.59 ± 0.46
N1*s*	1.07 ± 0.01	1.14 ± 0	0.97 ± 0.04	0.80 ± 0.05
O1*s*	23.24 ± 0.42	22.71 ± 0.98	23.12 ± 0.22	23.24 ± 0.38
S1*s*	0.00 ± 0.00	0.00 ± 0.00	0.04 ± 0.04	0.21 ± 0.03

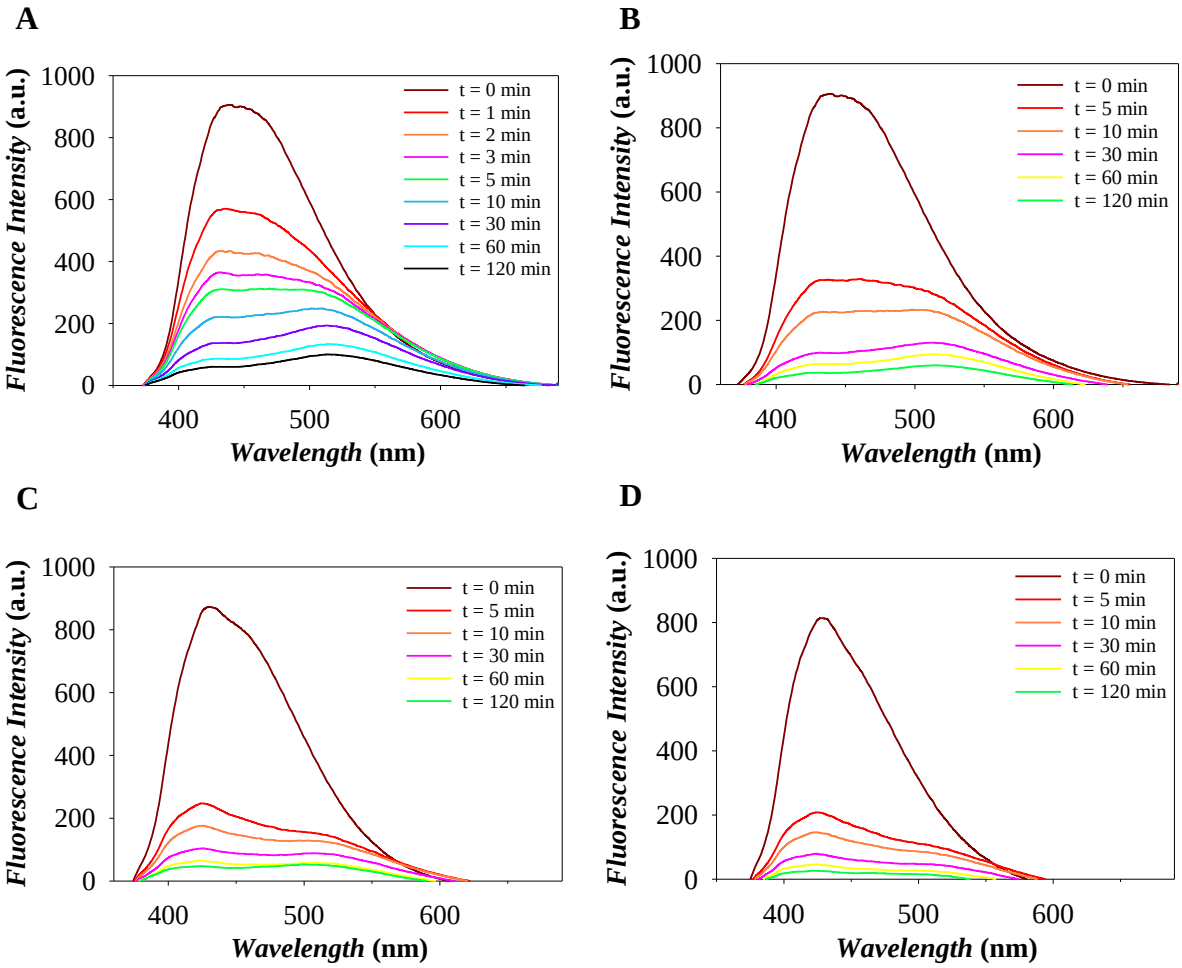

Figure S50. Fluorescence intensity of **P**MMA-Tz-Vi**s** latexes (A - 10 wt%, B - 7.5 wt%, C - 5.0 wt% and D - 2.5 wt%) after NITEC reaction with NEM at different times reactions are presented (λ_{ex} = 350 nm).

Table S17. Atomic percentage measured by XPS of the washed and dried PMMA-Tz-Vis latexes (10 wt%, Vis4) after NICAL reaction with BVA after 120 minutes of irradiation. The atomic percentage at the surface of each sample was calculated by integration of the raw peaks, without mathematical treatment. The average of two measurements on different location of the same sample and standard deviation are presented.

Time (min)	0	120
Atom%a		
Br3*d*	0.00 ± 0.00	0.00 ± 0.00
C1*s*	74.04 ± 2.05	74.03 ± 2.05
N1*s*	0.94 ± 0.07	0.73 ± 0.07
O1*s*	31.11 ± 4.89	25.12 ± 1.99
S1*s*	0.00 ± 0.00	0.06 ± 0.06

Table S18. Atomic percentage measured by XPS of the dried PMMA-Tz-Vis latexes (10 wt%, Vis4) after NICAL reaction with BVA after 120 minutes of irradiation (no purification). The atomic percentage at the surface of each sample was calculated by integration of the raw peaks, without mathematical treatment. The average of two measurements on different location of the same sample and standard deviation are presented.

Time (min) / atom%	0	10	60	120
Br3*d*	0.11 ± 0.02	0.12 ± 0.00	0.11 ± 0.0	0.12 ± 0.01
C1*s*	75.97 ± 0.18	75.83 ± 0.42	75.83 ± 0.45	75.72 ± 0.11
N1*s*	0.80 ± 0.03	0.78 ± 0.06	0.68 ± 0.07	0.64 ± 0.07
O1*s*	22.25 ± 0.16	22.38 ± 0.30	22.43 ± 0.52	22.59 ± 0.06
S1*s*	0.86 ± 0.03	0.89 ± 0.06	0.95 ± 0.00	0.92 ± 0.09

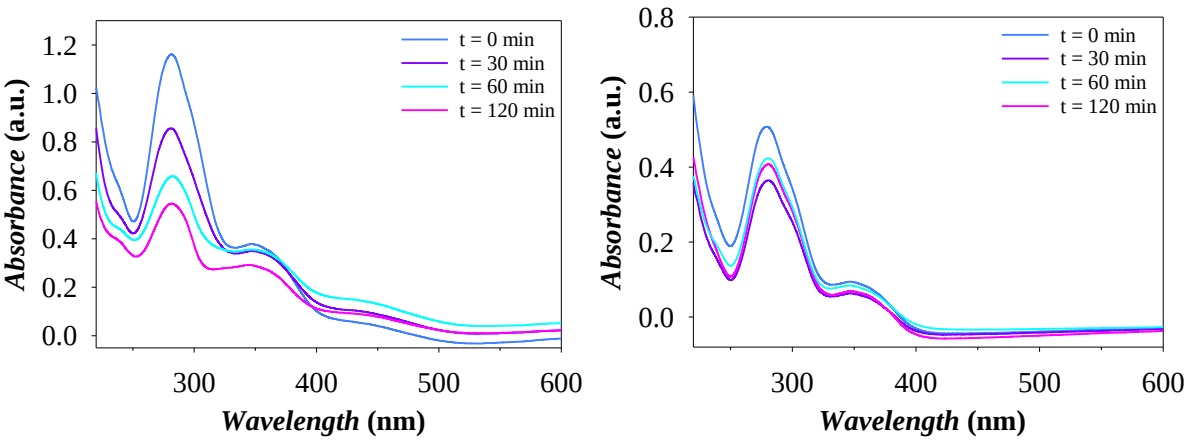

Figure S51. UV-vis absorbance of a folic acid solution (7.2 g L^{-1}) after 2 h irradiation under UV-B light (300 nm) (left) and under visible light (415 nm) (right).

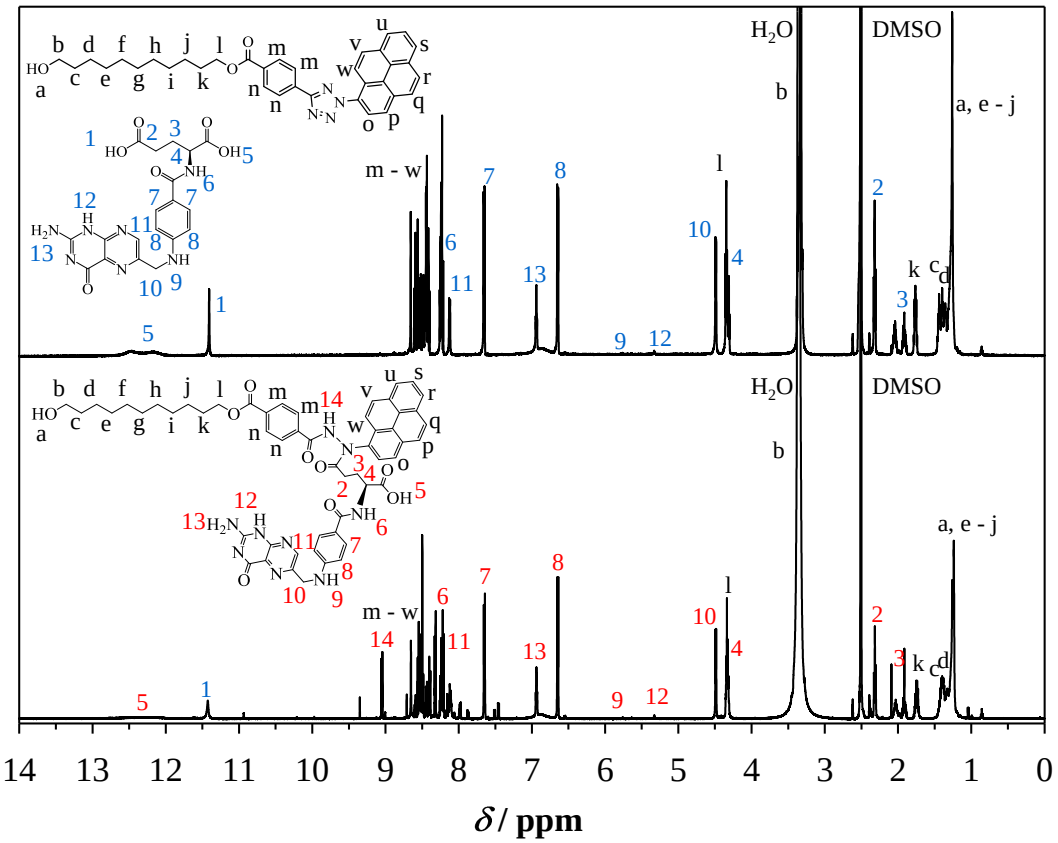

Figure S52. ^{1}H NMR spectrum of the Visible-Tet precursor with folic acid before and after 1 h irradiation under visible light with the corresponding labels (600 MHz, 12 s delay, 128 scans, DMSO-d_6)